EFFECT OF NANOSCALE CONFINEMENT ON THE PHYSICAL PROPERTIES OF POLYMER THIN FILMS

A Thesis

Presented to

The Academic Faculty

by

Lovejeet Singh

In Partial Fulfillment

of the Requirements for the Degree

Doctor of Philosophy in Chemical Engineering

Georgia Institute of Technology

October 2004

EFFECT OF NANOSCALE CONFINEMENT ON THE PHYSICAL PROPERTIES OF POLYMER THIN FILMS

Approved:

Dr. Clifford L. Henderson, Chair

Dr. Peter J. Ludovice

Dr. Laren Tolbert

Dr. Carson J. Meredith

Dr. William J. Koros

DATE APPROVED: October 7, 2004

ACKNOWLEDGEMENTS

I would first like to gratefully acknowledge funding support for this work from the Semiconductor Research Corporation (SRC) and DARPA. I would also like to thank several people who helped me and with whose support I was able to complete this work. First I would like to thank my advisors Prof. Clifford L. Henderson and Prof. Peter J. Ludovice, both of them guided me at every step when I needed their advice. They were always available with their suggestions on conducting experiments and useful discussions. I would also like to thank my thesis committee members Dr. Laren Tolbert, Dr. William J. Koros and Dr. J. Carson Meredith for spending time in reading my thesis. I would also like to thank all the group members in Henderson and Ludovice research group who provided support by being good friends and providing many valuable suggestions. I would also like to thank Jeff in ChE Machine shop for fabricating hot stage. Finally, I would like to thank my parents, my brother and my niece for providing love and encouragement to work hard towards my goals. And above all I thank God for providing me will power and motivation to work hard towards my goals.

TABLE OF CONTENTS

LIST OF FIGURES

LIST OF TABLES

SUMMARY

The behavior of polymeric systems confined into thin films is a situation that has numerous practical consequences. One particular application in which the properties of thin polymer films is becoming crucially important is in the design, formulation, and processing of photoresists for semiconductor microlithography. As devices continue to be scaled down into the nano-regime, the microelectronics industry will ultimately rely upon a molecular understanding of materials for process development. The majority of these devices are now confined in planar geometries; thus, thin films have played an ever-increasing role in manufacturing of modern electronic devices. This movement towards thinner resist films creates larger surface to volume ratios, and hence thin films can exhibit thermodynamic, structural, and dynamic properties that are different from those of the bulk material. Resist materials can behave differently simply due to applications with thinner films. These changes in material behavior could result in problems as current resist materials are used at thinner film thicknesses. It is thus extremely important to understand the properties of polymers when confined in such confined geometries for various applications including resists for lithographic patterning. In present work, the influence of a variety of factors including film thickness, molecular weight, and substrate interactions on the polymer thin film physical properties such as the glass transition temperature, coefficient of thermal expansion, dissolution rate, and diffusion coefficient was studied in detail using a combination of experimental characterization and molecular modeling simulation techniques.

It was shown that nano-confinement of polymer thin films influences number of their bulk physical properties including glass transition temperature, coefficient of thermal expansion, dissolution rate, and diffusion behavior. This study supports the idea that there is spatially dependent polymer physical properties within the ultra-thin film, with deviations from bulk behavior occurring near the film interfaces. Further, the data suggests that the length scales over which these deviations occur are proportional to polymer chain dimensions as is shown in the ability to uniformly describe the thin film behavior when the film thickness is rescaled by the polymer radius of gyration. It was found that the T_g of supported polymer thin films can be modeled using a "master" curve based on reduced thickness and reduced T_g, and a single equations have been generated that describes the dependence of T_g on molecular weight and film thickness for variety of systems.

The influence of initial polymer film thickness and substrate on the dissolution behavior of photoresist polymers was studied using quartz crystal microbalance methods. Vapor sorption and desorption studies using quartz crystal microbalance methods were used to study the effect of film thickness, polymer type, substrate and polymer molecular weight on the diffusion coefficients of small molecules in model photoresist polymers. Finally, molecular dynamics simulations were used to understand anisotropic nature of physical properties in ultra-thin polymer films. Simulations show that surface of resist films becomes key contributor to physical properties for ultra-thin polymer films.

CHAPTER 1

INTRODUCTION TO SEMICONDUCTOR PROCESSING AND MICROLITHOGRAPHY

1.1 Introduction

Polymer thin films play an increasingly important role in a range of technological applications including: coatings, adhesives, lithography, organic electronics, and sensors. These applications require polymers to meet diverse performance criteria that range from electronic and optical performance to adhesive and mechanical performance. The major advantage of using polymer thin films over non-polymeric materials in *some* technologies is that polymers are inexpensive and easy to fabricate. Polymers of a virtually "limitless" range of chemistries and thus physical and chemical properties can be synthesized. One particular application in which the properties of such thin polymer films is becoming crucially important is in the design, formulation, and processing of photoresists used for semiconductor microlithography [1.1-1.3].

The electronics industry has grown rapidly in the last four decades. This growth has been driven by a revolution in microelectronics. In the early 1960s, putting more than one transistor on a piece of semiconductor was considered cutting edge. Integrated circuits (ICs) containing tens of devices were the most advanced integrated electronics available. Digital computers were large, slow, and extremely costly. Bell Labs, which had invented the transistor a decade earlier, rejected the concept of ICs. They reasoned

that in order to achieve a working circuit that all of the integrated devices must work. Therefore, it was deemed impossible to get even 50% of simple 20 transistor circuits to function since that would demand each transistor device must have a 96.6% probability of working successfully (required individual device probability of function for 50% function of 20 element circuit is $(0.5)^{1/20}$=0.966, or 96.6%). This was considered to be ridiculously optimistic at the time, yet today integrated circuits are built with tens of millions of transistors [1.4]. Fortunately others persisted and today the semiconductor industry is both a technological and economic driver for the world.

To chart the progress of microelectronics it is easiest to follow one type of chip. Memory chips have had essentially the same function for many years, making this type of analysis meaningful. Furthermore, they are extremely regular in their structure and fabrication and can be sold in large volumes, making technology customized for the chip design and fabrication economical. As a result, memory chips have the highest transistor density of all ICs. Figure 1.1 shows the density of dynamic random access memories (DRAMs) as a function of time. The vertical axis is logarithmic [1.4]. The density of these circuits increase by increments of 4X, and each of these increments takes three to four years. One of the most fundamental changes in the fabrication process that allows this technology evolution is the minimum feature size that can be printed on each chip generation. Not only does this increase IC density, the shorter distances that electrons and holes have to travel across the smaller transistor gates improve the transistor speed. Part of the IC performance improvement comes from this increased transistor performance, and part of it comes from being able to pack the transistors closer together,

decreasing the parasitic capacitance and increasing DRAM capacity. The left-hand side of Figure1.1 shows that ICs have progressed from possessing feature sizes of 10 microns in the 1970's to well under 1 micron today.

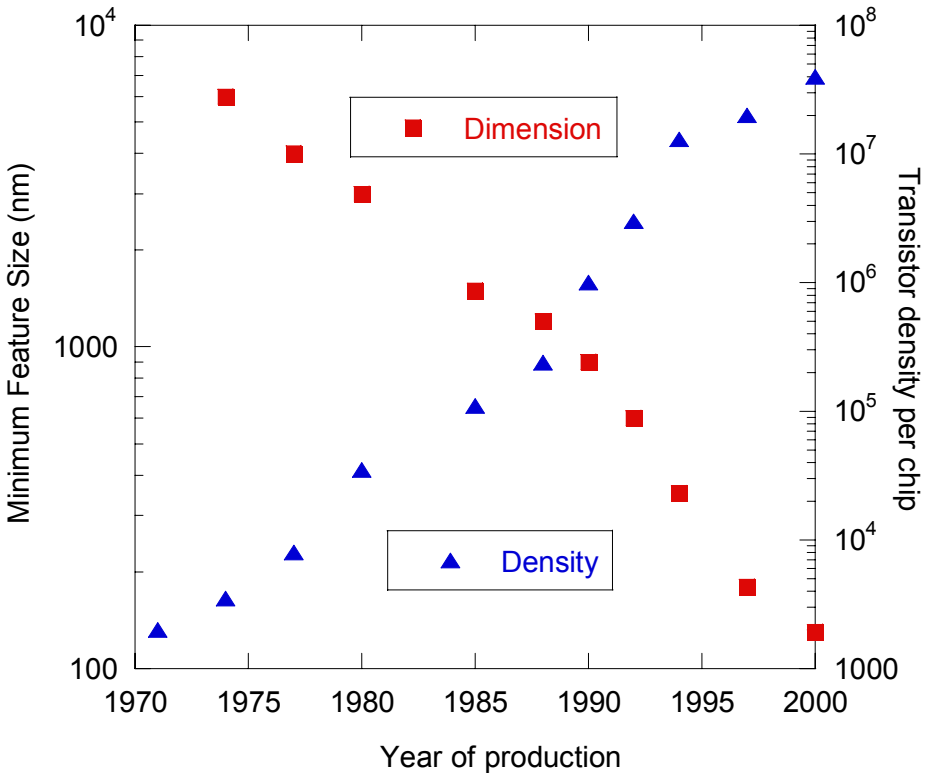

Figure 1.1 Plot illustrating the relationship in semiconductor manufacturing between minimum feature size and transistor density of integrated circuits in Intel microprocessor units.

1.2 Device Fabrication

Transistors are the basic elements in integrated circuits (ICs), which consist of very large numbers of transistors interconnected with other circuitry on a single silicon microchip or "chip". The transistor, invented by three scientists at Bell Laboratories in

1947, rapidly replaced the vacuum tube as an electronic signal regulator. A transistor regulates current flow or voltage and thus acts as a switch or gate for electronic signals. A transistor fundamentally consists of three regions of a semiconductor material, each capable of carrying a current. A semiconductor is a material, such as germanium or silicon, that conducts electricity in a "semi-enthusiastic" way. The conductivity of the semiconductor lies somewhere between a real conductor such as copper and an insulator such as a metal oxide or plastic.

The semiconductor material is given special properties by a chemical process called doping. The doping results in a material that either adds extra electrons to the material (which is then called N-type for the extra negative charge carriers) or creates "holes", electron vacancies in the bonding structure of the material, in the material's crystal structure (which is then called P-type because it results in more positive charge carriers). The transistor's three-region structure contains an N-type semiconductor layer sandwiched between P-type layers (a PNP configuration) or a P-type layer between N-type layers (an NPN configuration).

A small change in the voltage applied at the inner semiconductor layer (which acts as the control electrode) produces a large, rapid change in the current passing through the entire component. The component can thus act as a current switch. Today's computers use circuitry made with complementary metal oxide semiconductor (CMOS) technology. CMOS uses two complementary transistors per gate (one with N-type material; the other with P-type material).

Monolithic IC fabrication can be illustrated by studying the basic cross section of a MOS transistor as shown in Figure 1.2 [1.5-1.6]. The n-channel MOS transistor is formed in a p-type substrate. Source and drain regions are formed by selectively converting shallow regions at the surface of the p-type substrate to n-type material using methods such as ion implantation. Thin and thick silicon dioxide regions on the surface form the gate insulator of the transistor and serve to isolate one device from another. A thin film of polysilicon is used to form the gate of the transistor, and a metal such as aluminium is used to make contact to the source and drain. Interconnections between devices can be made using layers of conductive polysilicon, metal, and insulator.

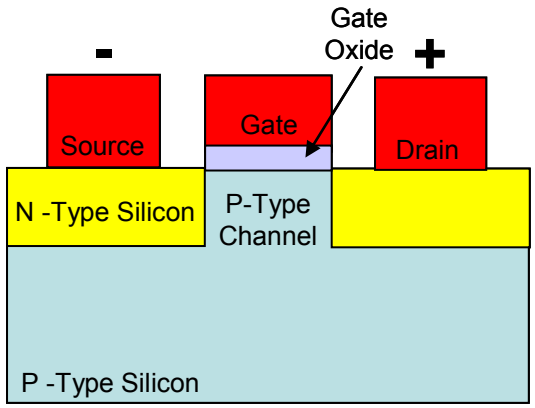

Figure 1.2 The basic structure of an n-channel metal-oxide-semiconductor (NMOS) transistor structure.

MOS structures are fabricated through the repeated application of a number of basic processing steps including oxidation, photolithography, etching, diffusion,

evaporation or sputtering, chemical vapor deposition, ion implantation, epitaxy and annealing [1.5-1.6].

Silicon dioxide can be formed by heating a silicon wafer to a high temperature (1000 to 1200^{o}C) in the presence of oxygen. This process is called oxidation. Metal films can be deposited through evaporation by heating the metal to its melting point in a vacuum. Thin films of silicon nitride, silicon dioxide, polysilicon, and metal can all be formed through a process knows as chemical vapor deposition, in which the material is deposited out of a gaseous mixture onto the surface of the wafer. Metals and insulators may also be deposited by a process called sputtering.

Shallow n- and p- type layers are formed by high temperature (1000 to 1200^{o}C) diffusion of donor or acceptor impurities into silicon or by ion implantation, in which the wafer is bombarded with high-energy donor or acceptor ions generated in a high-voltage particle accelerator.

In order to build devices and circuits, the various materials used to build up each device must be patterned into the required shapes and sizes. For example, the n- and p-type regions that make up the source and drain must be formed selectively in the surface of the wafer. A variety of masking materials including silicon dioxide, silicon nitride, polysilicon, and photoresist can all be used to mask areas of the wafer surface to prevent penetration of dopants into undesired regions of the substrate during ion implantation or

diffusion. However, this masking pattern itself must be formed initially, and is accomplished through a process known as microlithography.

1.3 Microlithography

The dramatic increase in performance and cost reduction in the electronics industry are attributable to innovations in the integrated circuit and packaging fabrication processes. The speed and performance of the chips, their associated packages, and, hence, the computer systems built based on these devices are in general dictated by the lithographic minimum printable size. Microlithography, often referred to simply as lithography, is the process of transferring a pattern into a reactive polymer film (termed a photoresist or resist) which will subsequently be used to replicate that pattern into an underlying thin film or conductor. Microlithography involves defining a pattern in a radiation sensitive polymer film coated onto a substrate and subsequently transferring that pattern into the substrate by etching, deposition, or ion implantation through the polymer pattern. Today's small, powerful hand held devices, such as cell phones and personal digital assistants, are a result of this ever increasing circuit density and speed. Device feature sizes have continued to shrink allowing large numbers of more powerful devices to be fabricated on each wafer. Lithography replicates a pattern rapidly from chip to chip, wafer to wafer, or substrate to substrate, and determines in large part the throughput and the cost of microelectronic systems. A lithographic system includes an exposure tool, a mask, a photoresist, and all of the accessory processing equipment required to accomplish pattern transfer from the mask to the photoresist. [1.6].

From the late 1960s, when integrated circuits possessed linewidths of 5 μm, to 1997, when minimum linewidths reached 0.35 μm in 64Mb DRAM circuits, optical microlithography was used ubiquitously for manufacturing. This dominance of optical lithography in production is the result of a worldwide effort to improve optical exposure tools and resists over the past four decades. Although lithography system costs (which are typically more than one third the costs of processing a wafer to completion) increase as minimum feature sizes on a semiconductor chip decreases, optical lithography remains attractive and the technology of choice because of its high wafer throughput.

Fabrication of the device consists of a repeated cycle of steps consisting of film deposition, lithography, etching, and cleaning. First, a material is deposited onto the substrate using one of a variety of techniques such as thermal oxidation, chemical vapor deposition, physical vapor deposition, etc. Next, the substrate is covered with a photosensitive polymer film, the photoresist, which is then patterned using microlithography (see Figure 1.3). The patterned photoresist layer serves as a pattern transfer layer or protective mask for the subsequent process steps such as plasma etching. The substrate is etched or processed in other manners in the areas that remain unprotected by the resist film. Finally, the patterned photoresist layer is then stripped away and the substrate is cleaned. This cycle is repeated numerous times in order to build up the various layers of the IC. Advancements in lithographic technology have been the key driver for increases in the speed and density of microchips, and account for about one-half of the chip productivity improvements each year through steady decreases in minimum feature size.

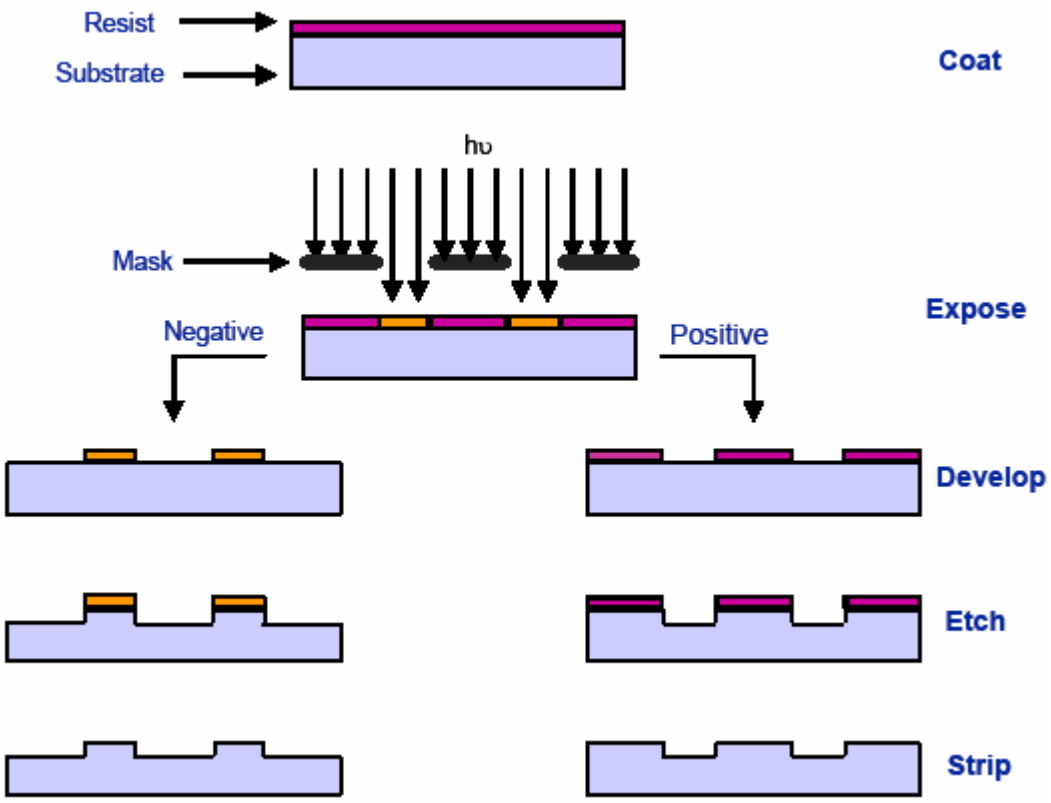

Figure 1.3 Microlithography processing sequence.

There are two primary attributes of a lithography system that control the minimum printable feature size. The first is the resolution of the system. In the early 1970s, Wilczynski of IBM assembled a small group to address the resolution limits of optical lithography. The resolution is essentially the minimum possible size that one can print a crisp, discernable image of a line or other feature. It is the minimum feature size possible. The second attribute of a lithography system that limits the feature size is the depth of focus. The depth of focus is the distance on either side of the image focal plane

that the projected image will remain in focus (i.e. of the correct size) within a specified tolerance. In order to have a well defined and correctly sized pattern after development of the resist film, it is important that the projected image remain in focus throughout the entire thickness of the photoresist. The resolution and depth of focus are described by the following equations [1.6].

$$resolution = \frac{k\lambda}{NA} \tag{1}$$

$$Depth\ of\ \ focus = \pm \frac{\lambda}{2(NA)^2} \tag{2}$$

Here λ refers to the wavelength of the exposure source and NA refers to its numerical aperture. In 1975, Wilczynski's group, using an exposure wavelength of 405 nm (the Hg emission H-line) at an NA of 0.32, succeeded in demonstrating a step-and-repeat optical projection camera at a linewidth of 1 μm. This pivotal demonstration led optical tool vendors to make continued improvements in optical lithography that have sustained the technology since that time. The strategy to meet the continued demands for higher resolution and larger depth of focus has been to migrate from visible light at 436 nm (the Hg emission G-line), to 365 nm (the Hg emission I-line), to deep-UV (248-nm) wavelengths for resist exposure. This trend is now continuing by using wavelengths of 193 nm and possibly beyond [1.6].

As the wavelength becomes shorter, the light source becomes more complex and expensive. Initially, the light source was a mercury lamp filtered for the G and H emission lines, and later for the I-line (365 nm). Lithography at a wavelength of 248 nm

spurred the development of a reliable and line narrowed KrF laser, though mercury lines near 250 nm have been used in catadioptric lithography systems (a combination of mirrors and lenses). 193-nm ArF excimer laser sources have now been developed and 193 nm lithopgraphy exposure tools are currently the cutting edge in microelectronics manufacturing.

In equation 1, which describes the resolution of a projection optical lithography system, the constant *k* is primarily a material parameter that accounts for the ability of the photoresist material to resolve a particular aerial image pattern (typically in the range of 0.4 to 0.8, although today manufacturing at a k of approximately 0.3 is performed) depending upon the contrast and other attributes of the photoresist. Thus, for any particular wavelength exposure generation and numerical aperture, there are generally improvements in resist materials that also reduce the minimum printable feature size by reducing this *k* factor [1.6]. Unfortunately, reducing the wavelength or increasing the numerical aperture also reduces the depth of focus, requiring thinner resist films that are more difficult to create and have lower plasma etch resistance. Because the depth of focus decreases proportionally to the square of the numerical aperture, it has been more desirable to reduce resolution by reducing exposure wavelength. This has been the trend in recent years and the reason for moving into the deep - UV exposure region (240 - 260 nm light) from the mid - UV region (300-365 nm). The industry is now moving to 193 nm lithography for this same reason. Figure 1.4 shows the historical progression of lithographic exposure technologies in terms of DRAM production. Also shown on this figure are the two principle types of photoresists that have been used and the

corresponding feature size generations that have been produced with each. These photoresist technologies will be discussed in more detail in the next section.

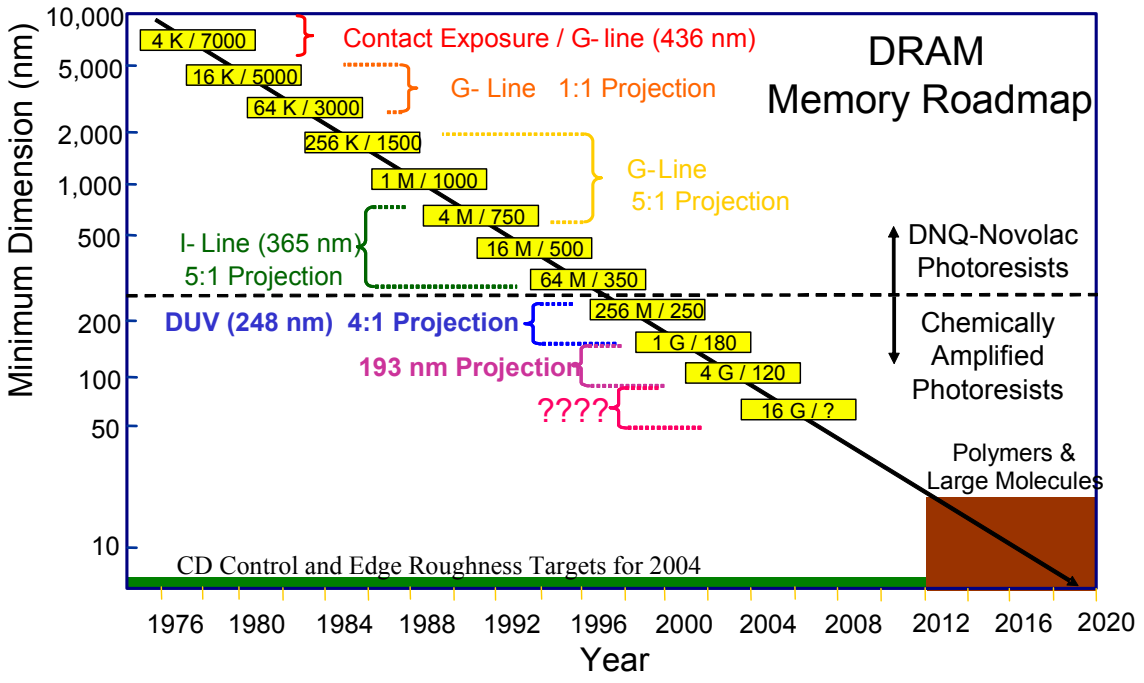

Figure 1.4 DRAM technology progression shown with the corresponding lithographic exposure tool and photoresist technology used to produce each device generation.

As mentioned above, this decrease in wavelength will reduces depth of focus, which means that thinner resist films must be used. It is clear that for certain future lithographic technologies resist film thicknesses well below 200 nm may be required. Table 1.1 shows the projected near term and long term resist thickness requirements for future lithography according to the International Technology Roadmap for Semiconductors (ITRS) [1.7].

Table 1.1 Resist Requirements – Near-term & Long Term.

Year of Production	2003	2005	2007	2010	2016
Resist Thickness (nm)	200-400	170-320	150-280	120-160	50-80

1.4 Photoresists

The continuing advances in optical lithography depend not only on tool design and improvements, but also on the concomitant development of innovative resist materials and associated processing which defines the chip circuitry. Even with the highest-resolution stepper available, the aerial image projected through the mask is degraded because of diffraction effects and lens aberrations. The resist must compensate for this pattern distortion by converting a "blurred" aerial image back into a "sharp" binary stencil so that closely packed circuitry features can be defined. This can be accomplished by designing "high-contrast" resist systems that respond over a narrow range of exposure intensity to eliminate the blurred edges of the aerial image. In addition to providing high contrast to achieve resolution, the resist exposure sensitivity must be optimized for the amount of energy available at the exposure wavelength of the optical tool. The high absorption of the photoresists (diazonaphthoquinone-novolac or DNQ-novolac based systems) developed for the G-, H-, and I-line exposure tools would have required such a large increase in exposure dose at 248 nm that wafer throughput would

have ultimately been too low. In addition, high resist absorption degraded the profile of the final developed resist images. Therefore, beginning with the 248 nm exposure tools, chemically amplified photoresists have been utilized to overcome these problems.

Resist systems must also provide etch resistance, thermal stability during processing, ease of developing, and adhesion to the substrate. There are many synthetic paths to UV-sensitive polymers that will cross-link, degrade, or undergo molecular rearrangement when irradiated. This irradiated or exposed area can be either rendered more soluble (positive resists) or less soluble (negative resists) in an appropriate developer relative to the unexposed area. Both positive and negative systems combining all of the attributes described above have been necessary to achieve the small dimensions and linewidth control required for increased speed and circuit density. The development of resist materials to meet these demanding requirements is a significant challenge. Over the past forty years, scientists have been able to provide a wide variety of materials and processes to answer the resolution, sensitivity, and processing needs of each succeeding chip generation.

Beginning in the early 1960s, Eastman Kodak was the first to provide resists specifically designed for the electronics industry. These were negative-resist systems which cross-linked upon exposure to light. Their resolution was limited because of pattern swelling in solvent-based developers. They were replaced in the 1970s by positive resists developed by Azoplate which utilized diazoketones and novolak resins that could be exposed using "near-UV" optical tools and developed in water-based solutions. Improvements in the chemistry and processing of these systems have provided

the DNQ-novolac resists that are still widely used to fabricate half-micron devices and the larger scale wiring levels in modern IC devices.

Key in the development of deep-UV lithography was the revolutionary work of Ito, Willson, and Frechet at IBM in the early 1980s [1.8]. These workers recognized very early that if DUV lithography was to become a reality, a new imaging mechanism with very high efficiency (fast photospeed) was required, due to limited output of mercury lamps at 250 nm. The new resist design, termed chemical amplification (used here as CA) involved the preparation of an acid-reactive polymer, formulated with an 'onium salt' photoacid-generator (PAG). The critical feature in these CA resists is that the acid-labile group (attached to the polymer) reacts with the photogenerated acid from the PAG to render the polymer soluble. This reaction occurs in such a way that a new molecule of acid is generated in the process, and thus the process is catalytic. This catalytic nature is responsible for the high sensitivity of these materials [1.9]. Figure 1.5 shows a schematic example of a chemically amplified resist.

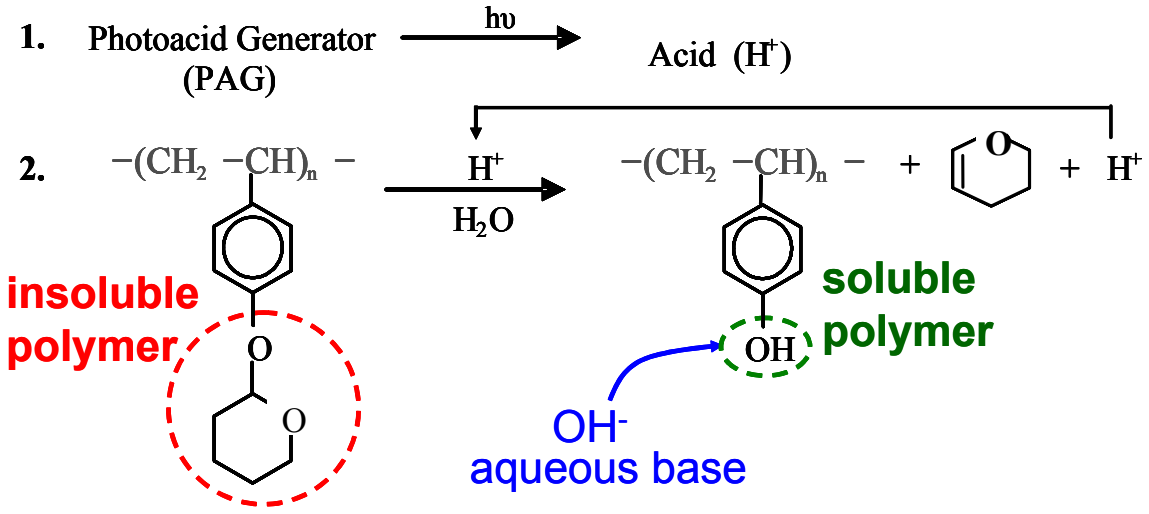

Figure 1.5 Diagram of the basic function of a chemically amplified photoresist. A photoacid generator is formulated with an insoluble "protected" polymer resin. Exposure of the mixture produces photoacid which subsequently deprotects the polymer resin rendering the exposed regions soluble in developer.

Concerted research in the early-to-mid 1980s uncovered much promise, as well as many problems with this new mode of lithography. A variety of acid-catalyzed chemical reactions were incorporated into the basic resist design [1.9], and CA resists were extended into negative imaging [1.10]. The contrast of these new resists was extremely high compared with traditional DNQ-novolac positive photoresists. Problems initially arose, however, in gaining aqueous development in these early CA resists. As a result, the first commercial resist process implemented into manufacturing was the IBM TBOC resist developed with organic solvents in the negative-tone [1.11]. The second generation of CA resist technology was the result of a breakthrough in the development of aqueous developing positive-tone materials. IBM APEX resist is the best known of this class of materials [1.12]. AT&T developed a conceptually different material (CAMP) which behaved similarly. [1.13]

APEX resist was the first relatively large scale, commercially available DUV (positive-tone) photoresist. Several sub-generations of this resist were developed in the late-1980s and early 1990s, including dyed versions [1.14]. It is well suited for manufacturing 0.35 μm devices with DUV exposure tools with moderate numerical apertures. It was discovered that such chemically amplified resists were very sensitive to airborne base contamination, and thus modern chemically amplified resist formulations are formulated to contain a variety of small molecule additives to combat this and other inherent problems with the CA resist design.

As devices continue to be scaled down into the nano-regime, the microelectronics industry will ultimately rely upon a molecular understanding of materials for process development. The majority of these devices are now confined in planar geometries; thus, thin films have played an ever-increasing role in manufacturing of modern electronic devices. Optical lithography continues to be the cornerstone of modern integrated circuit manufacturing by providing the enabling technology for patterning device structures. One of the critical challenges in the future progression of lithographic technologies will be the ability to design and produce resist systems that are capable of manufacturing these sub-100 nm features. As polymer film dimensions approach within an order of magnitude or two of the radius of gyration (R_g) of the polymer, there can be significant departures from bulk physical behavior. It is thus extremely important to understand the properties of polymers when confined in such thin films for various applications including resists for lithographic patterning. It is the objective of this work to design techniques to measure the physical properties for ultra-thin polymer films and to determine the magnitude and length scales at which nanoscale confinement effects are

observed in polymer thin films. Molecular dynamics simulations will also be used to provide a better fundamental insight into the underlying phenomena which give rise to these thin film effects.

1.5 References

[1.1] Rao, V.; Hutchinson, J.; Holl, S.; Langtom, J.; Henderson, C.; Wheeler, D. R.; Cardinale, G.; O' Connell, D.; Goldsmith, J.; Bohland, J.; Taylor, G.; Sinta, R. *J. Vac. Sci. Technol. B* 1988, *16*, 3722.

[1.2] Solak, H. H.; He, D.; Li, W.; Cerrina, F. J. Vac. Sci. Technol. B 1999, 17, 3052.

[1.3] C. G. Willson, R. A. Dammel, A. Reiser, "Photoresist Materials: A Historical Perspective," *Proc. SPIE*, **3049**, 28–41, (1997).

[1.4] S. A. Campbell, The Science and Engineering of Microelectronics Fabrication, Oxford University Press, New York, 1996.

[1.5] R. Jaeger, "Introduction to Microelectronic Fabrication," Vol. 5, Addison-Wesley, 1993.

[1.6] L. F. Thompson, C. G. Willson, and M. J. Bowden, *Introduction to Microlithography*, American Chemical Society, Washington, DC, 1983.

[1.7] http://public.itrs.net/

[1.8] H. Ito, C. G. Willson, Technical Papers of SPE Regional Technical Conference on Photopolymers, 331 (1982); H. Ito, C.G. Willson, J.M.J.Frechet, U.S. Patent 4,491,628 (1985).

[1.9] A. A. Lamola, C. R. Szmanda, and J. W. Thackeray, Solid State Technol., 34(8), 53 (1991).

[1.10] W. Feely, J. Imhof, C. Stein, T. Fisher and M. Legenza, Polym. Engin. Sci., 16, 1101 (1986), W. Feely, Proc. SPIE, 631, 48 (1986).

[1.11] J. Maltabes, et al., Proc. SPIE, 1262, 2 (1990).

[1.12] R. Wood, C. Lyons, J. Conway, R. Mueller, Proc. KTI Inteface '88, 341 (1988).

[1.13] R. Tarascon, et al., Polym. Eng. Sci., 29, 850 (1989); O. Nalamasu, et al., Proc. SPIE, 1262, 32 (1990).

[1.14] W. Conley, et al., Proc. SPIE, 2195, 461 (1994).

CHAPTER 2

GLASS TRANSITION BEHAVIOR OF POLYMER THIN FILMS

2.1. Introduction

Numerous studies have shown that the physical properties of ultrathin polymer films may deviate substantially from that of the bulk polymer. One particular physical property that has been extensively studied in a variety of polymer films is the glass transition temperature (T_g) [2.1]. The glass transition temperature is a particularly important physical property for thin film applications since it marks the temperature at which a number of physical properties of the polymer change such as the coefficient of thermal expansion, mechanical modulus and loss (and their dielectric and acoustical equivalents), rate of diffusion through the polymer, as well as other properties. Thus, it is clear that a better fundamental understanding of the glass transition temperature of ultrathin polymer films would be useful in a variety of fields.

The T_g for thin polymer films has previously been shown to be a function of both the film thickness and, in the case of supported films, the type of substrate [2.2-2.6]. A variety of techniques have been demonstrated in the literature for measuring the T_g of thin polymer films including ellipsometry, Brillouin light scattering (BLS), local AFM thermal probes, AFM lateral force methods, x-ray reflectivity, and positron annihilation [2.2,2.7-2.10]. In this work, the influence of film thickness, molecular weight and substrate on the observed glass transition temperature for polymer thin films is

investigated using variable angle spectroscopic ellipsometry. Beaucage and co-workers were the first to use single wavelength ellipsometry to measure the glass transition of thin (~300 nm) polystyrene (120,000 M_n) films cast on silicon wafers [2.11]. T_g was determined by measuring the temperature dependence of the film refractive index, and the change in film thickness with temperature was used to calculate the linear and bulk thermal expansion coefficients of the material. The coefficient of thermal expansion (α) at ambient pressure of the polystyrene films was found to be in reasonable agreement with values reported for bulk polystyrene. It is important to note that in their work significant shifts in the T_g were reported between heating and cooling cycles for thin polystyrene films, creating some uncertainty in their measured T_g values. Perhaps most importantly, their work points out the importance of controlling the thermal history of a sample when making such measurements. Keddie and Jones measured the glass transition temperature of thin polystyrene films cast on silicon substrates as a function of film thickness using spectroscopic ellipsometry [2.2]. It was found that the glass transition temperature decreased as the film thickness was reduced below approximately 100 nm. Measurements were made for three different polystyrene molecular weights (M_w=120,000 ; 500,800 ; 2,900,000) and it was reported that the T_g of the thin films was not strongly affected by molecular weight. Fukao and co-workers measured the glass transition temperature for polystyrene films supported on glass substrates as function of film thickness using a capacitance measurement method [2.12]. A decrease in T_g was again observed with decreasing film thickness below 110 nm. Fryer et. al. reported the development of local differential thermal analysis and ellipsometry to measure the glass transition temperature of thin photoresist films [2.10]. They applied these techniques to

measure the glass transition temperature as a function of the film thickness for both polystyrene and poly(methyl methacrylate) (PMMA). Measurement of the T_g as a function of film thickness for polystyrene showed that the maximum depression in T_g was approximately 20^{o}C for a film thickness of 35 nm. Films of PMMA cast on native silicon oxide also showed a similar depression in the T_g of approximately 10^{o}C for film thickness below 70 nm. Tsui and co-workers studied the depression in T_g with decreasing film thickness for polystyrene on native oxide coated silicon substrates using two different molecular weight polymers (Mw=13,700 and 550,000) [2.13]. Their data suggests that molecular weight has little or no influence on the T_g behavior of ultrathin polymer films. However, Hartmann and co-workers studied glass transition phenomena in thin isotactic poly(methyl methacrylate) supported films of two different molecular weights (M_w=44,900 and 164,700) using dielectric spectroscopy [2.15]. Their dielectric spectroscopy data exhibits a molecular weight dependence in the T_g depressions for isotactic poly(methyl methacrylate) supported films, with the lower molecular weight polymer deviating from the bulk behavior only at lower values of the film thickness as compared to the higher molecular weight sample.

Keddie and Jones performed the first study of the relative influence of the two substrates, gold and silicon oxide, on the T_g of ultrathin films of poly(methyl methacrylate) (PMMA) [2.23]. By measuring thermal expansion of PMMA films with spectroscopic ellipsometry, they found that the T_g increases by 5 ^{o}C on SiO_x but decreases by 15 ^{o}C on gold in films less than 40 nm thick. Prucker et al. used optical waveguide spectroscopy to monitor the temperature dependence of the refractive index

and of the thermal (linear) expansivity for thin poly(methyl methacrylate) (PMMA) films independently from each other [2.24]. The PMMA films of different thicknesses were prepared by three different techniques; by spin casting from solution, by grafting-from approach and by the Langmuir/Blodgett/Kuhn technique. They found that all these films prepared on hydrophobic substrates show the expected decrease of T_g for ultrathin samples. However, this behavior is independent of the strongly varying intramolecular architecture and organization of the macromolecular chains in the various films.

All of these experiments support the fact that the T_g values of polymer thin films may be strongly influenced by film thickness. As a result of these experimental investigations, there have been a number of different mechanisms and models proposed to describe this T_g behavior. Thus far, no fundamental model is successfully able to accurately capture all of the observed phenomena. In attempting to develop our own comprehensive model that can be used to explain the behavior of such ultrathin polymer films, it was found that the effect of polymer dimensions (i.e. molecular weight and architectural effects) had still been investigated in only a very limited sense. The original study by Keddie and co-workers displayed some scatter in the T_g versus film thickness data for the three different molecular weights used. In light of the relatively strong M_w dependence reported for freely standing films [2.3], the molecular weight dependence and effect of substrate on the T_g of ultrathin supported films has been investigated in this work.

2.2. Experimental Section

2.2.1 Materials

Five different polystyrene samples that vary in both molecular weight and polydispersity index (M_w/M_n) were used to investigate the variation in glass transition temperature with film thickness and molecular weight. These polystyrene samples are hence forth referred to as samples PS-1 through PS-5. PS-5 (M_w=239,700; M_w/M_n=2.00) and PS-2 (M_w=212,400; M_w/M_n=1.05) were purchased from Aldrich Chemical Co., while PS-1 (M_w= 31,600 M_w/M_n=1.09), PS-4 (M_w=1,571,000 M_w/M_n=1.03) and PS-3 (Mw=560,900 M_w/M_n=1.04) were purchased from Scientific Polymers. Four different poly(methyl methacrylate) samples that vary in molecular weight were used to investigate the variation in glass transition temperature with film thickness and molecular weight. These samples are hence forth referred to as samples PMMA-1 through PMMA-4. PMMA-1 (M_w=52,700; M_w/M_n=1.08), PMMA-2 (M_w=298,000; M_w/M_n=1.02), PMMA-3 (M_w=838,300; M_w/M_n=1.04) and PMMA-4 (M_w=1,554,000; M_w/M_n=1.05) were purchased from Scientific Polymers. Toluene (99.9% pure, Fisher Scientific Chemicals) was used as a casting solvent in these experiments. 1, 1, 1, 3, 3, 3 – Hexamethyl – disilazane (99.9 % pure, Aldrich Chemical Co. Inc., termed as HMDS henceforth) was used to modify nature of substrate used in experiments. Single side polished silicon <100> test grade wafers purchased from Nova Electronic Materials were used as substrates for film preparation. All polymer materials and solvents were used as received.

2.2.2 Sample Preparation

Polystyrene thin films were cast from toluene solutions onto cleaned native oxide coated silicon wafers using a CEE 100 CB spin coat and bake system from Brewer Science (Rolla, MO). The water contact angle on the silicon substrates was measured as a test of the substrate surface condition using a VCA 2500 XE contact angle system (AST Products, Inc.). In all cases, the water contact angle was measured to be approximately 15º which supports the presence of a hydrophilic native oxide surface. Spectroscopic ellipsometry measurements also indicated a silicon native oxide thickness of approximately 25 Å. Spin speeds (1000 rpm to 5000 rpm) and polymer concentrations (0.1% to 8% polymer by weight) were tightly controlled to achieve polymer film thicknesses ranging from approximately 20 nm to 700 nm. All polystyrene films were baked at 90°C for 4 minutes using the CEE Model 100 CB hot plate to remove the majority of the casting solvent, and then transferred into a vacuum oven at 135°C (above the measured T_g for all films used in this study) and 20 inches Hg vacuum for 20-48 hrs, depending on polymer weight, to anneal the films and remove additional residual casting solvent.

Nonpolar surfaces were prepared by coating HMDS on silicon wafers using a CEE 100 CB spin coat and bake system from Brewer Science (Rolla, MO) using spin speed of 3000 rpm and baking 4 minutes at 90°C. . The water contact angle on HMDS covered surface was approximately 69-70°. Poly(methyl methacrylate) thin films,

thicknesses ranging from approximately 30 nm to 650 nm, were cast from toluene solutions onto these HMDS covered surfaces using spin speeds of 1000 rpm to 5000 rpm and polymer concentrations of 0.1% to 6% polymer by weight. All PMMA films were baked at 90°C for 4 minutes using the CEE Model 100 CB hot plate to remove the majority of the casting solvent, and then transferred into a vacuum oven at 150°C (above the measured T_g for all films used in this study) and 20 inches Hg vacuum for 15-40 hrs, depending on polymer weight, to anneal the films and remove other residual casting solvent.

2.2.3 Film Surface Roughness Measurements and Defect Metrology

Atomic force microscopy (AFM) using a Digital Instruments (Santa Barbara, CA) Dimension 3100 system with a Nanoscope III controller was used to quantify film roughness and to inspect for film defects. The RMS roughness for the films was found not to exceed approximately 1 nanometer for any of the films used in this study. Any films with observed defects were discarded and recast.

2.2.4 Ellipsometry Measurements

The thickness and refractive index of the polymer films as a function of temperature were determined from ellipsometry measurements made on a V-VASE variable angle spectroscopic ellipsometer (J.A. Woollam Co., Inc.) The samples were held at a

constant, controlled temperature during each measurement using a hot stage that was custom designed and constructed for the V-VASE ellipsometer. The temperature of the hot stage and samples located on the silicon wafers were calibrated using a Tempilstik temperature indicator and an Omega thermocouple. The temperatures reported here are as measured for a sample on the surface of a silicon wafer loaded onto the hot stage. For each measurement, the hot stage controller temperature was set to the appropriate value and the stage was allowed to equilibrate to the desired temperature. The polymer film sample was held at the desired temperature for 10 minutes before ellipsometry measurements were made. This 10 minute time scale was determined to be sufficient based upon measurements of the ellipsometry parameters Ψ and Δ for the various samples made during isothermal holds at temperatures in the range of interest (30ºC to 145ºC). No significant changes in Ψ and Δ were measured in the films after only a few minutes at temperature. Ψ and Δ were measured for each sample over the wavelength range from 500 nm to 1000 nm at incident angles of 65º, 70º, and 75º (with respect to normal to the plane of the substrate). The Ψ and Δ data were analyzed and fit to determine the film thickness and refractive index using the WVASE-32 software package (J.A. Woollam, Inc.). Film thicknesses reported for each sample are at 25ºC unless otherwise specified. Sample refractive indices are for 630 nm light at 25ºC unless otherwise specified.

2.2.5 Determination of T_g from Ellipsometry Data

The T_g of each sample was determined using the ellipsometry data in a variety of ways. Using only the raw ellipsometry data, the T_g can be determined from the

discontinuity in either of the ellipsometry parameters, Ψ or Δ, at a particular wavelength as a function of temperature as described previously in the literature [2.2]. The basic method is to fit the appropriate response variable versus temperature using two linear least squares regression lines and solve for the temperature location of the intersection point at the discontinuity. The raw Ψ and Δ data can also be fit to yield the film thickness and refractive index as a function of temperature. The discontinuity in either the film thickness or refractive index versus temperature can also be used as a measure of T_g. All of these data analysis methods were used in this work, and it was generally found that the four methods yielded glass transition temperatures that were in agreement to within one degree Celsius. The most sensitive method for locating the T_g (i.e. the one that showed the largest change in slope of the response variable versus temperature) was using the discontinuity in film thickness versus temperature. Therefore, the T_g measurements reported in this work are determined in this manner unless otherwise specified. Measurements were made in which the temperature of the sample was both successively increased for each measurement (referred to as a heating cycle) and decreased (referred to as a cooling cycle). T_g measurements using both heating and cooling cycle data agreed to within 1.5ºC or less, with the cooling cycle data being consistently above that measured using heating cycle data. Unless otherwise specified, T_g measurements reported here are based on heating cycle data. It should also be noted that changes in the optical properties of silicon and other substrates materials with temperature can have a significant impact on the accurate measurement of the thickness of ultrathin films on these substrates. Therefore, in this work, control experiments were performed in which the optical properties and thickness of the native oxide coated silicon

substrates were measured as a function of temperature. This data was used to rigorously model the full film stack thicknesses and optical properties as a function of temperature. Using such methods, temperature dependent substrate models were used which eliminated such confounding effects.

2.3. Results

Figure 2.1 shows representative thickness versus temperature data obtained for the PS-2 sample on native silicon oxide with an initial thickness of 78 nm. As can be seen from the figure, there is a significant change in the slope of the two linear fits to the thickness versus temperature data, and in this work the temperature intersection of the two fit lines is defined as glass transition temperature. For this particular example, slopes of two fit lines were found to be 0.456 and 0.119 with an R^2 value of approximately 0.99 for both lines. Figure 2.2 shows an independently obtained refractive index versus temperature data set for the same film using a new set of ellipsometry data. It can be seen that the T_g values obtained from both data sets and measurement methods differ by only 0.6 ^oC, which indicates the good reproducibility of the T_g data obtained via these methods.

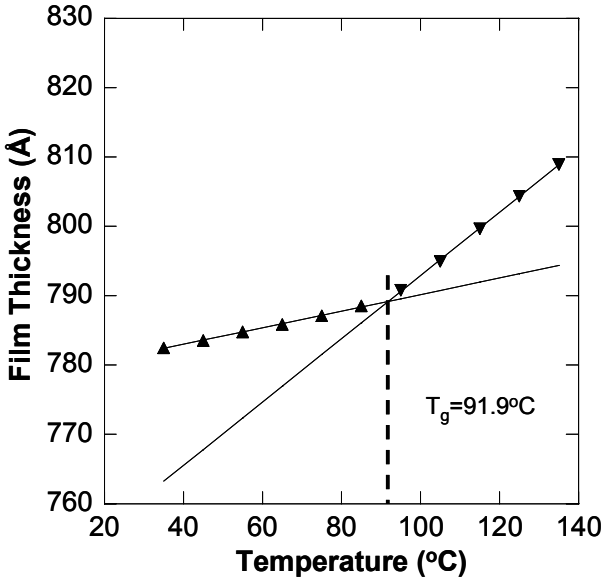

Figure 2.1 Typical thickness versus temperature data for PS-2 film on native silicon oxide, initial thickness of the film is 78 nm. ▲ = glass , ▼ = melt.

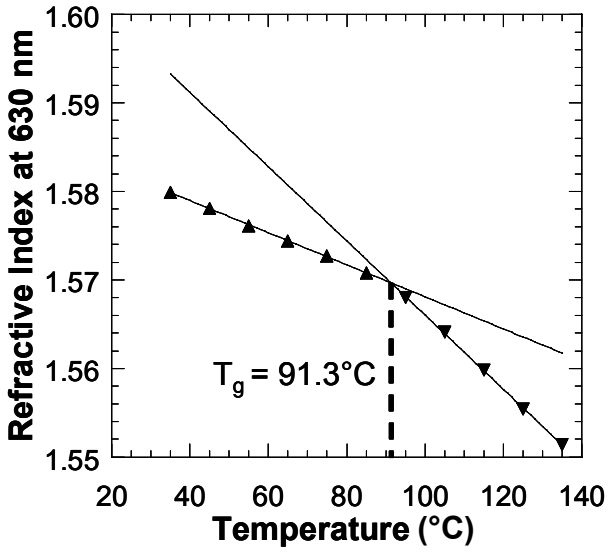

Figure 2.2 Refractive index at 630 nm versus temperature for a PS-2 film on native silicon oxide (same film used to collect data shown in Figure 1). ▲ = glass , ▼ = melt.

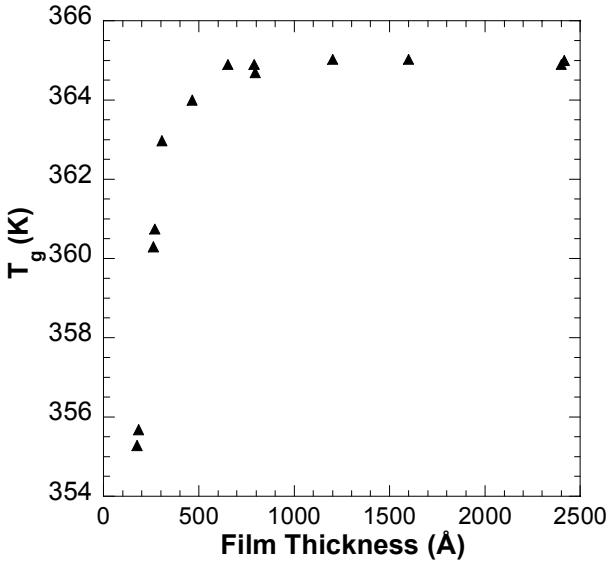

Figure 2.3 Effect of film thickness on T_g for PS-2 on native silicon oxide (M_w=212,400, M_w/M_n=1.05).

Figure 2.3 shows a representative plot of the glass transition temperature versus initial film thickness. For this particular polymer, PS-2 (M_w=212,400), the T_g begins to show deviation from the bulk value at a film thickness of approximately 65 nm and the highest measured deviation was approximately 10ºC. Similar trends of decreasing T_g with decreasing film thickness were observed for all five PS samples on native silicon oxide substrate studied in this work. This result is in agreement with the other published results.

As mentioned previously, in order to verify that the length of time at which the sample was held at temperature did not influence the measurements and thus the reported T_g, a series of experiments at different isothermal hold temperatures was conducted. Figure 2.4 shows one representative data set from these measurements in which a film was held at 20ºC above its T_g and the thickness of the film as a function of time was

monitored. As can be seen, there is no significant change in film thickness observed over time scales of three hours, a period longer than that required for measurement of an entire heating or cooling cycle for a film. No significant confounding effects were observed in any of the experiments.

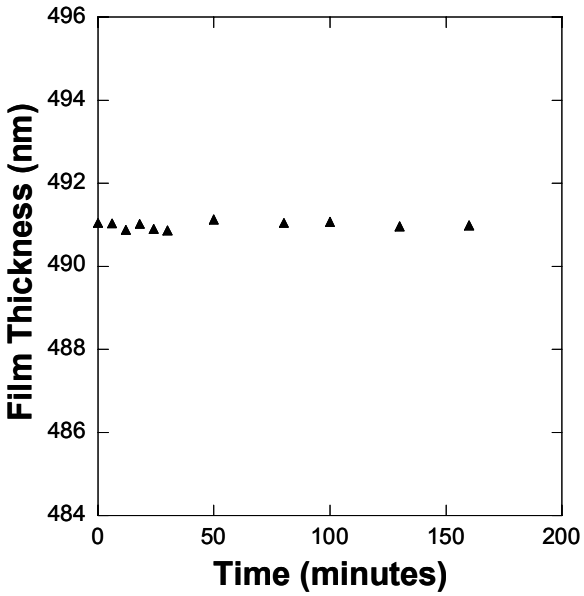

Figure 2. 4 Effect of time on film thickness at constant temperature (~20^{o}C above T_g).

Since a series of narrow polydispersity samples of different molecular weights were measured, it is possible to compare the bulk thermophysical properties of polystyrene as measured using ellipsometry against reported literature values obtained via other methods. One important property that can be verified is the scaling of bulk T_g for polystyrene as a function of molecular weight. Figure 2.5 shows the dependence of bulk T_g on molecular weight as determined from the thin films used in this work. For these measurements, the bulk T_g is reported using film thicknesses well above the thickness at

which any T_g suppression was observed (nominally >350nm in thickness). Reding and co-workers [2.16] proposed the following molecular weight dependence for bulk T_g,

$$T_g^{\infty}(K) = 373 - \left(\frac{100000}{M_w}\right). \qquad (2.1)$$

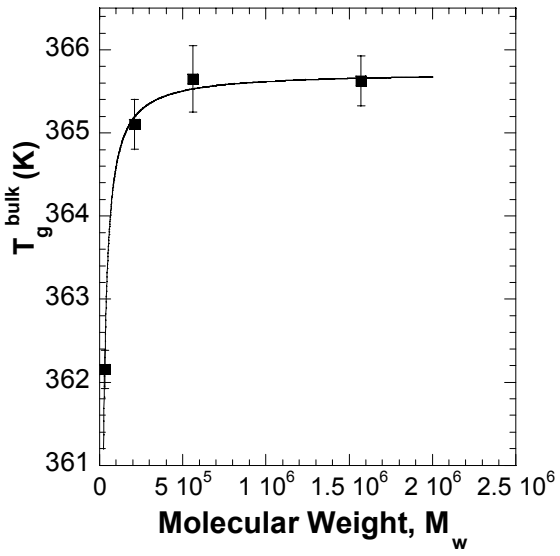

Figure 2.5. Effect of molecular weight on bulk T_g. Error bars represent the 90% confidence limits calculated using 4 measurements at each molecular weight.

The thin film data shown in Figure 5 was fit using the same functional form as equation (2.1), which yields

$$T_g^{\infty}(K) = 366 - \left(\frac{113000}{M_w}\right). \qquad R^2=0.993 \qquad (2.2)$$

One of the main goals for this work was to investigate the influence of molecular weight on the T_g of ultrathin polymer films. Figure 2.6 shows the T_g versus film thickness for three of the different molecular weight polystyrene samples on native silicon oxide. It can clearly be seen from this data that the T_g of each of the different molecular weights begin to deviate from their bulk T_g values at different thickness values. Measurements were also made on the PS-1 sample (M_w=31,600), but no substantial deviations in the glass transition temperature were observed for that sample down to film thicknesses on the order of 60 nm, and below this thickness it was difficult to obtain defect free, stable thin films. Therefore, based on this study, it is observed that there exists a dependency of T_g on both M_w and film thickness for polystyrene films on native oxide coated silicon substrates. This result does not agree with previous conclusions drawn by other researchers, who stated that there was no appreciable influence of molecular weight on the T_g versus film thickness behavior of ultrathin polymer films [2.2,2.13].

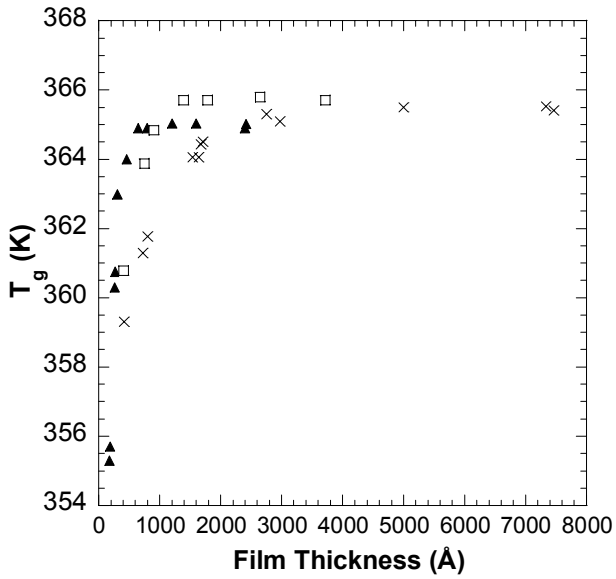

Figure 2.6 Effect of Molecular Weight on T_g as a function of film thickness for PS on native silicon oxide substrate. ▲ M_w=212,400, □ M_w=560,900, × M_w=1,571,000.

However, if one looks more closely at the data obtained by Keddie and coworkers [2.2], it is observed that a majority of the scattering in their data which makes the observation of any molecular weight effect difficult was produced by only the highest molecular weight (2,900,000) sample. In an effort to compare their data with the data obtained in this work, the two lower molecular weight data sets (120,000 and 500,800) were replotted (see Figure 2.7). After replotting the data, it was found that the two lower molecular weight samples did indeed appear to show a molecular weight dependence similar to the one reported in the present work. Therefore, also shown as an inset in Figure 2.7 is a plot showing the same T_g data for the two lower molecular weight samples studied by Keddie and coworkers on a rescaled axis in terms of the polymer radius of

gyration. As observed in the present work, both samples begin to display deviations from bulk T_g behavior at approximately 10 times the polymer radius of gyration. This also is in agreement with the present experiments.

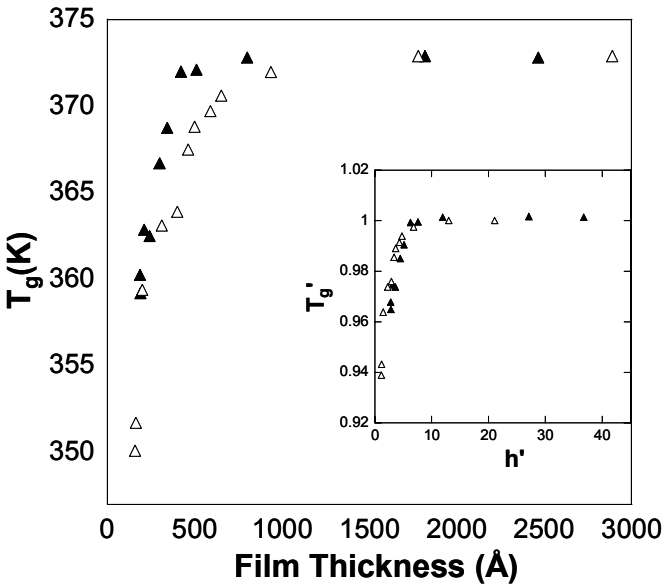

Figure 2.7. The glass transition temperature (T_g) as a function of film thickness as reported by Keddie and coworkers for polystyrene thin films on native silicon oxide substrate [2.2]. The inset plot shows the reduced glass transition temperature (T_g') as a function of reduced thickness (h') for the data shown in main plot. ▲ M_w = 120,000 Δ M_w= 500,800

Figure 2.7 also shows that the data obtained by Keddie and coworkers display relatively little scatter in the data for the two lower molecular weight samples. Thus, it does appear that it was principally only the higher molecular weight data set in their work which added sufficient scatter to the overall data set to hide the molecular weight dependence of the glass transition behavior of the films. It is worth pointing out that using these additional data sets that five different molecular weight samples (three in

present work and two from Keddie and coworkers), show a consistent molecular weight dependence. It should also be noted that for the higher molecular weight sample (1,500,000) used in this work, that 48 hours at a temperature of 135°C was found to be a minimal set of annealing conditions that could be used to obtain consistent and reproducible results. A significantly longer annealing time should be required for the highest molecular weight sample analyzed by Keddie and co-workers (2,900,000 g/mole). Assuming the annealing time for a film has the same dependence on M_w as the polymer reptation time, which scales with $M_w^{3.4}$, then the proper annealing time for a 2,900,000 M_w sample will be approximately 480 hrs at 135°C [2.14]. However, Keddie and coworkers annealed their 2,900,000 M_w sample for only 48 hours. This may explain some of the rather large scattering observed in their original 2,900,000 M_w sample data. Further support for this molecular weight dependence of the thickness dependent glass transition temperature for polymer thin films is supplied by the fact that a similar molecular weight dependence was also observed by Hartmann and co-workers in thin isotactic poly(methyl methacrylate) supported films [2.15].

Figure 2.8 shows the T_g versus film thickness for three of the different molecular weight poly(methyl methacrylate) samples on HMDS coated substrate. It can clearly be seen from this data that the T_g of each of the different molecular weights begin to deviate from their bulk T_g values at different thickness values. It is observed that there exists a strong dependency of T_g on both M_w and film thickness at film thicknesses ranging from 30 nm to approximately 250 nm (depending on molecular weight).

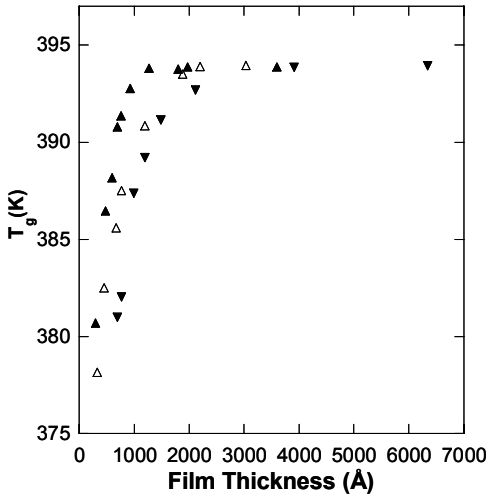

Figure 2.8. Effect of Molecular Weight on T_g as a function of film thickness on HMDS coated substrate. ▲ M_w=298,000, Δ M_w=838,300, ▼ M_w=1,554,000.

In an attempt to investigate the influence of substrate on T_g of ultrathin polymer films, we compared results of PMMA films prepared on HMDS coated silicon surfaces and on silicon native oxide surfaces, Figure 2.9 shows results for one molecular weight. It was observed that for PMMA on silicon native oxide surfaces, T_g start increasing below a critical thickness of around 70 nm, while for PMMA on HMDS coated substrate T_g start decreasing below a critical thickness of around 130 nm. This result supports the idea that by controlling interaction between polymer and substrate, we can have a situation where there will be no change in T_g value with film thickness. This result is also supported by recent simulation work reported by Chow [2.25].

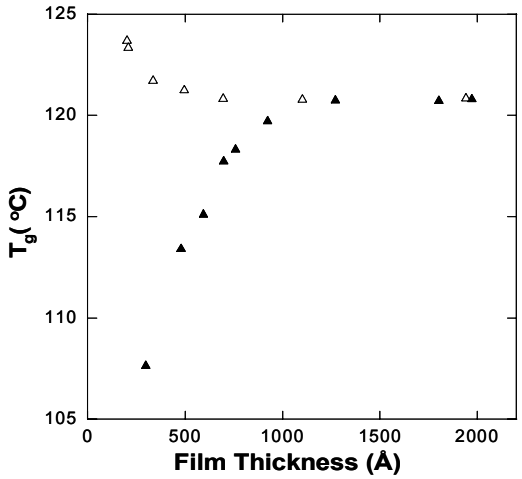

Figure 2. 9. Effect of substrate on T_g as a function of film thickness M_w=298,000. Δ PMMA on SiO_2/Si, ▲ PMMA on HMDS/Si.

Figure 2.10 shows the T_g versus film thickness for three of the different molecular weight poly(methyl methacrylate) samples on silicon native oxide substrates. It can be seen from this data that the T_g of each of the different molecular weights begin to increase from their bulk T_g values at different thickness values. It is observed that there exists a strong dependency of T_g on both M_w and film thickness at film thicknesses ranging from 30 nm to approximately 130 nm (depending on molecular weight).

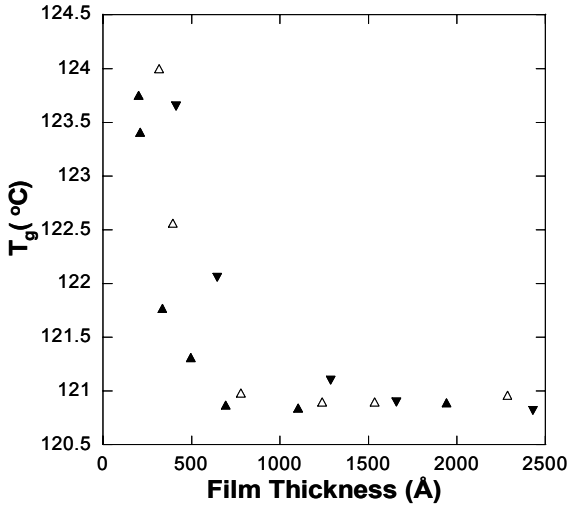

Figure 2.10. Effect of molecular weight on the T_g of PMMA as a function of film thickness on silicon native oxide substrate. ▲ M_w=298,000, Δ M_w=838,300, ▼ M_w=1,554,000.

As a first attempt to investigate the influence of polydispersity on the behavior of the T_g of polymer thin films, a polydisperse polystyrene sample was measured and compared with the monodisperse data shown previously. In this case, results for PS-5 (Mw=239,700; M_w/M_n=2.00) and the monodisperse sample most closely matching this average molecular weight, PS-2 (Mw=212,400; M_w/M_n=1.05), are shown plotted together in Figure 2.11. As can be seen from Figure 2.11, at low film thicknesses (< ~100 nm) the films behave in a nearly identical fashion. However, the polydisperse sample displays deviations from its bulk behavior at substantially larger thicknesses, on the order of 250 nm, as compared to the monodisperse sample. This may indicate a difference in the relative contributions to the T_g behavior of the films from the various molecular weight components in the polydisperse sample.

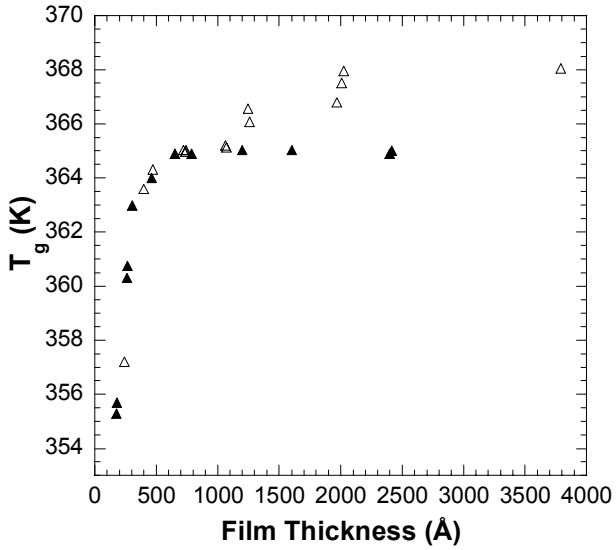

Figure 2.11. Effect of Polydispersity on T_g of PS films on native silicon oxide. ▲ M_w=212,400 and M_w/M_n = 1.05, Δ M_w=239,700 and M_w/M_n = 2.00.

2.4 Discussion

It was observed in this work that the T_g values for polymer thin films begin to deviate substantially from the bulk at different thickness values for different polymer molecular weights, with larger molecular weights showing deviations at larger film thicknesses. This supports the idea that the underlying controlling phenomena is dependent on, or related to, the polymer chain dimensions. Thus, it was hypothesized that it should be possible to develop a "master curve" that captures this molecular weight influence. In order to develop such a master curve, two reduced quantities were defined as follows:

$$T_g' = \frac{T_g(h)}{T_g^{\infty}} \tag{2.3}$$

$$h' = \frac{h}{\left\langle s^2 \right\rangle^{1/2}} \quad . \tag{2.4}$$

Here T_g^{∞} is the bulk glass transition temperature for the polymer and $\left\langle s^2 \right\rangle^{1/2}$ is the root-mean-square radius of gyration. In the first expression, the reduced T_g is generated by scaling the observed T_g by the bulk T_g^{∞} to eliminate the minor dependence of bulk polymer behavior on molecular weight. The second quantity, the "reduced film thickness" is used to express the film dimensions in terms of a scaled unit polymer chain dimension. The root-mean-square radius of gyration is calculated using,

$$\left\langle s^2 \right\rangle^{1/2} = \sqrt{\frac{C_{\infty} M_w l^2}{6 M_o}} \quad . \tag{2.5}$$

Here M_w is the weight average molecular weight of the polymer, M_o is the molecular weight of one repeat unit, C_{∞} is the polymer characteristic ratio, and l is the average bond length [2.17]. In this particular case, a characteristic ratio (C_{∞}) of 10 for a polystyrene random coil polymer was used in all calculations [2.18]. This value was chosen as representative of the literature values for polystyrene. Figure 2.12 shows this reduced glass transition temperature (T_g') plotted versus the reduced thickness (h') for PS films on native silicon oxide. It can be observed that using such a scaling reduces the various T_g versus film thickness curves into a single master curve regardless of molecular weight. In this system, deviations from bulk behavior for the glass transition temperature are observed for film thickness below approximately 10 times the polymer radius of gyration. Equation (2.6) can be obtained as an empirical fit to this master curve if one fits the reduced data to the same empirical form used by Keddie and co-workers.

$$T_g' = 1 - \frac{1}{14.4h'^{1.78}}. \qquad (2.6)$$

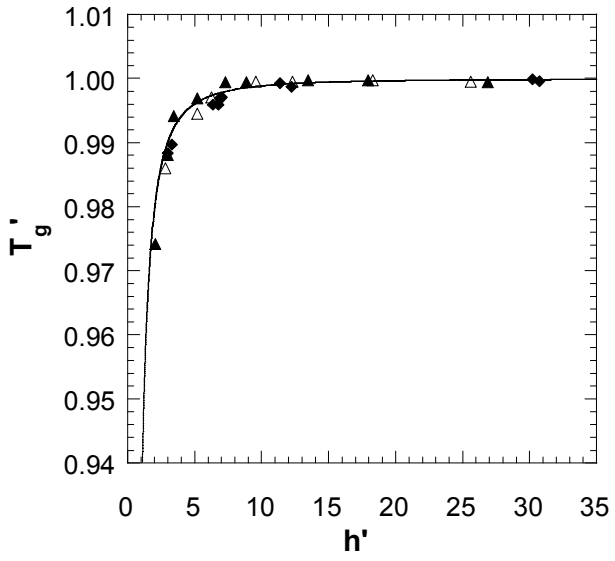

Figure 2.12. Master curve for dependence of T_g on film thickness using reduced glass transition temperature (T_g') and reduced film thickness (h') for PS on native silicon oxide. ▲ M_w=212,400, Δ M_w=560,900, ♦ M_w=1,571,000.

Using these results, it is possible to obtain one single empirical model that can be used to predict the glass transition temperature for polystyrene thin films on silicon native oxide surfaces as a function of both molecular weight and film thickness. Combining the molecular weight dependence of the bulk glass transition temperature from equation (2.2) with the scaled dependence on film thickness from equation (2.6) yields equation (2.7), which is a general empirical model that accounts for the dependence of T_g on both molecular weight and film thickness for polystyrene on silicon native oxide surfaces.

$$T_g = \left(366 - \frac{113000}{M_w}\right)\left(1 - \frac{1}{14.4}\left(\frac{\left\langle s^2 \right\rangle^{1/2}}{h}\right)^{1.78}\right). \qquad (2.7)$$

While Equation (2.7) was fit to poly(styrene) data, we believe the basic form of this equation is more generally applicable to other amorphous polymer films. In other words, if the scaling used in generating Figure 2.12 and equation 2.7 is universal for amorphous polymers, then an equation composed of two functions of the following form,

$$T_g = f(M_w) \cdot f\left(\frac{h}{\left\langle s^2 \right\rangle^{1/2}}\right), \qquad (2.8)$$

should describe the influence of molecular weight and film thickness on the glass transition temperature. The first term in this product accounts for bulk T_g variations, while the second term accounts for confinement effects in the thin film that scale with the radius of gyration. In the case of substrate interaction work, the general functional form used to describe the confinement effect,

$$f\left(\frac{h}{\left\langle s^2 \right\rangle^{1/2}}\right) = \left[1 - \beta\left(\frac{\left\langle s^2 \right\rangle^{1/2}}{h}\right)^{\delta}\right], \qquad (2.9)$$

can capture the reported substrate interaction behavior. The magnitude of the δ coefficient and the magnitude and sign of the β coefficient allow the function to capture both increases and decreases in T_g with decreasing film thickness, and the function

produces the correct functional shape as observed in experimental data. In particular, the coefficients (β=0.07 and δ=1.78) found in this case are expected to work for any polymer-substrate system with the same random coil conformational behavior as polystyrene and a comparable level of surface interaction as in the polystyrene-native oxide case studied in this work. In order to test these ideas additional polymers and substrate surfaces were used.

Figure 2.13 shows this reduced glass transition temperature (T_g') plotted versus the reduced thickness (h') for PMMA films on HMDS covered substrate. It can be observed that using such a scaling reduces the various T_g versus film thickness curves into a single master curve regardless of molecular weight. Equation (2.10) can be obtained as an empirical fit to this master curve if one fits the reduced data to the same empirical form used by Keddie et. al. [2.5]

$$T_g' = 1 - \frac{1}{1.9h'^{2.32}}. \qquad (2.10)$$

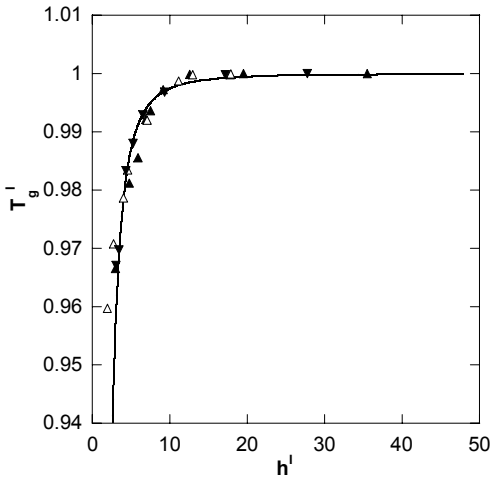

Figure 2.13. Master curve for dependence of T_g on film thickness using reduced glass transition temperature (T_g') and reduced film thickness (h′) for PMMA on HMDS covered silicon substrate. ▲ M_w=298,000, Δ M_w=838,300, ▼ M_w=1,554,000.

Using these results, it is possible to obtain one single empirical model that can be used to predict the glass transition temperature for PMMA thin films on HMDS covered silicon substrate as a function of both molecular weight and film thickness. Combining the molecular weight dependence of the bulk glass transition temperature with the scaled dependence on film thickness from equation (2.10) yields equation (2.11), which is a general empirical model that accounts for dependence of T_g on both molecular weight and film thickness for this polymer-substrate combination.

$$T_g = \left(394 - \frac{147500}{M_w}\right)\left(1 - \frac{1}{1.9}\left(\frac{\langle s^2 \rangle^{1/2}}{h}\right)^{2.32}\right). \qquad (2.11)$$

Using same reduced quantities, we plotted data for PMMA thin films on silicon native oxide substrate. Figure 2.14 shows this reduced glass transition temperature (T_g')

plotted versus the reduced thickness (h') for PMMA films on silicon native oxide substrate.

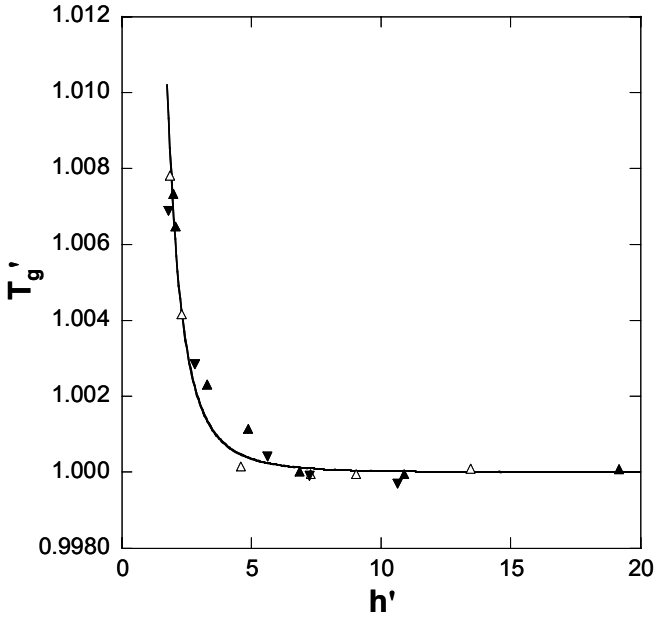

Figure 2.14. Master curve for dependence of T_g on film thickness using reduced glass transition temperature (T_g') and reduced film thickness (h') for PMMA on silicon native oxide substrate. ▲ M_w=298,000, Δ M_w=838,300, ▼ M_w=1,554,000.

Using same functional form as above, one single empirical model is obtained that can be used to predict the glass transition temperature for PMMA thin films on silicon native oxide substrate as a function of both molecular weight and film thickness.

$$T_g = \left(394 - \frac{147500}{M_w}\right)\left(1 + \frac{1}{16.4}\left(\frac{\langle s^2 \rangle^{1/2}}{h}\right)^{3.19}\right) \tag{2.12}$$

Actual resists are on the order of molecular weight ranging from 20,000-30,000, if we use this molecular weight range and attractive polymer-substrate equation (2.12) to predict film thickness value at which T_g start increasing, it predicts value of around 20-25 nm. According to ITRS, film thickness below 50 nm will be required in another 10

years, this means that if we use attractive substrate for our resists, the problem of T_g change with film thickness can be avoided for another 10 years. To test the prediction of equation (2.12), we performed experiment on low M_w PMMA-1 (M_w=52,700, M_w/M_n=1.08) on native silicon oxide substrate and as seen from Figure 2.15, there was no appreciable change in T_g value down to film thickness of around 30 nm.

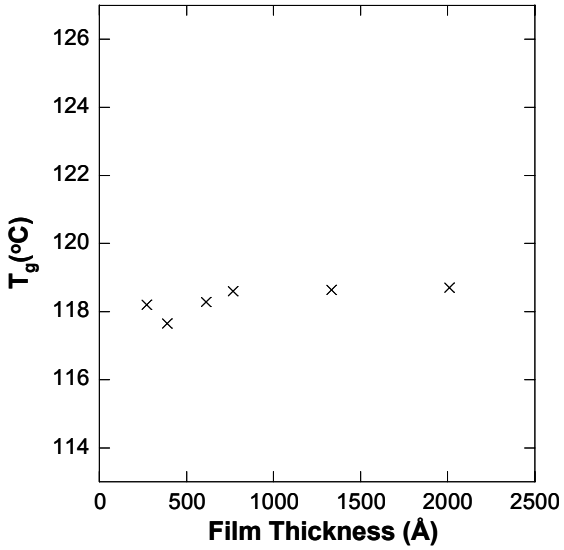

Figure 2.15. Effect of film thickness on T_g for PMMA-1 (M_w=52,700, M_w/M_n=1.08) on silicon native oxide substrate.

This work indicates that the film thickness where properties deviate from those of the bulk material scales with the dimensions of the polymer. We believe that this change in T_g in thin films is created by the difference between chain dynamics in a bulk polymer environment as compared to dynamics of chains near an interface. Depending on the nature of the interaction of the polymer with the surface, the local chain mobility near an interface may be increased (weak or unfavorable interactions) or decreased (strong interactions). This would imply that the polymer dynamics, for which T_g is a measure,

must have some spatial variation in a polymer film, with potentially large deviations from the bulk environment near an interface. As the film thickness decreases, the observed T_g for the film begins to deviate at a point where the contribution to the particular property being measured as a probe of the film T_g begins to be significantly influenced by the contributions of these surface regions. This concept of changes in the polymer structure and dynamics near interfaces is supported by other work in the literature. Kumar and co-workers have observed variations in the properties of linear polymer chains near a weakly interacting surface [2.19]. In particular, a dependence was observed in the compression of the chain dimensions in the direction normal to the surface near the polymer-substrate interface. However, this compression of the chain penetrated only 2 to 3 $\left\langle s^2 \right\rangle^{1/2}$ into the polymer from the surface. This compression of chains was also observed experimentally [2.20]. Similar penetration of deviations from bulk properties near an interface were observed in atomically detailed simulations of poly(propylene) by Mansfield and Theodorou [2.21]. These simulations indicate that the surface layer, in which the local chain structure and dynamics deviate from the bulk, is approximately 3 $\left\langle s^2 \right\rangle^{1/2}$ thick. As the film thickness approaches this surface layer thickness, an appreciable fraction of the polymer chains are contained within this surface layer. At this point, the contribution from this surface region to the property being measured as an indicator for T_g is large enough to affect the overall measurement and the measured film properties begin to change with film thickness.

Based on these ideas, stronger interactions with the substrate would be expected to decrease the rate at which T_g decreases or even increase T_g for sufficiently attractive

interactions, since chain mobility near the interface would be restricted. For the opposite case, the free interface of an unsupported film would likely exhibit a decrease in T_g even more rapidly with decreasing film thickness. Such behavior was seen in the simulations of De Pablo and co-workers [2.5]. These simulations also suggested that the film thickness at which a deviation from bulk properties is observed occurs at the same film thickness regardless of the nature of polymer-surface interaction. This again would support the concept that the controlling factor is the point at which the film thickness becomes on the order of some small multiple of the radius of gyration of the polymer, regardless of the substrate. Our work would indeed indicate that this transition point will scale with the radius of gyration of the polymer, and thus depends on the polymer molecular weight and other structural or architectural factors for the polymer. Investigations of different polymers on various substrates are currently underway to verify these speculations.

2.5 Conclusions

The influence of film thickness, molecular weight and substrate on the glass transition temperature for supported polymer thin films have been studied in detail. It was observed that T_g decreases for polystyrene on native silicon dioxide substrate as film thickness decreases below a critical thickness. This critical thickness is found to be approximately 10 times the radius of gyration of polymer. The T_g of PMMA films on HMDS coated silicon surfaces decrease with decreasing film thickness below a critical film thickness of approximately 13 times the radius of gyration of the polymer. The T_g of

PMMA films on silicon native oxide surfaces increases with decreasing film thickness below a critical film thickness of approximately 6 times the radius of gyration of the polymer. This study supports the idea that there are spatially dependent polymer thermophysical properties within the ultrathin film, with deviations from bulk behavior occurring near the film interfaces. Further, the data suggests that the length scales over which these deviations occur are proportional to polymer chain dimensions as is shown in the ability to uniformly describe the thin film behavior when the film thickness is rescaled by the polymer radius of gyration. It was found that the T_g of supported polymer thin films can be modeled using a "master" curve based on reduced thickness and reduced T_g, and a single equations have been generated that describes the dependence of T_g on molecular weight and film thickness for variety of systems.

2.6 References

[2.1] J.A. Forrest, R.A.L. Jones, Polymer Surface, Interfaces and Thin Films, A. Karim, S. Kumar, editors. World Scientific, Singapore, 2000.

[2.2] J.L. Keddie, R.A.L. Jones, R.A. Cory, Europhys. Lett. 27 (1994) 59.

[2.3] K. Dalnoki-Veress, J. A. Forrest, C. Murray, C. Gigault, J.R. Dutcher, Phys. Rev. E 63 (2001) 031801.

[2.4] D.S. Fryer, P. F. Nealey, J.J. de Pablo, Macromolecules 33 (2000) 6439-6447.

[2.5] J.A. Torres J, P.F. Nealey, J.J. de Pablo, Phys. Rev. Lett. 85 (2000) 3221-3224.

[2.6] D.S. Fryer, R.D. Peters, E.J. Kim, J.E. Tomaszewski, J.J de Pablo, P.F. Nealey, C.C. White, W.L. Wu, Macromolecules 34 (2001) 5627-5634.

[2.7] J.A. Forrest, K. Dalnoki – Veress, J.R. Stevens, J.R. Dutcher, Phys. Rev. Lett. 77 (1996) 2002.

[2.8] W.E. Wallace, J.H. van Zanten, W. Wu , Phys. Rev. E. 52 (1995) R3329.

[2.9] G.B. DeMaggio, W.E. Frieze, D.W. Gidley, M. Zhu, H.A. Hristov, A.F. Yee, Phys. Rev. Lett. 78 (1997) 1524.

[2.10] D.S. Fryer, J.J. dePablo, P.F. Nealey, SPIE 3333 (1998) 1031-1039.

[2.11] G. Beaucage, R. Composto, R.S. Stein, J. Polym. Sci. Part B: Polym. Phys. Ed. 31 (1993) 319-326.

[2.12] K. Fukao, Y. Miyamoto, Europhys. Lett. 46 (1999) 649-654.

[2.13] O.K.C. Tsui, H.F. Zhang, Macromolecules 34 (2001) 9139-9142.

[2.14] G. Strobl, The Physics of Polymers: Concepts for Understanding their Structure Behaviour, Second Edition, Springer-Verlag, Berlin, 1997.

[2.15] L. Hartmann, W. Gorbatschow, J. Hauwede, F. Kremer, Eur. Phys. J. E. 8 (2002) 145-154.

[2.16] F.P. Reding, J.A. Faucher, R.D. Whitman, J. Polym. Sci. 57 (1962) 483.

[2.17] P.J. Flory, Statistical Mechanics of Chain Molecules, Hanser Publishers, 1989, pp. 11.

[2.18] J. Brandrup, E.H. Immergut, Polymer Handbook, Wiley and Sons Inc., 1989, pp.VII/38.

[2.19] S.K. Kumar, M. Vacatello, D.Y. Yoon, Macromolecules 23 (1990) 2189-2197.

[2.20] R.L. Jones, S.K. Kumar, D.L. Ho, R.M. Briber, T.P. Russell, Macromolecules 34 (2001) 559-567.

[2.21] K.F. Mansfield, D.N. Theodorou, Macromolecules 24 (1991) 6283-6294.

[2.22] O. Kahle, U. Wielsch, H. Metzner, J. Bauer, C. Uhlig, C. Zawatzki, Thin Solid Films 313 (1998) 803.

[2.23] Keddie J. L.; Jones R. A. L.; Cory R. A. *Faraday Discuss.*1994, *98*, 219.

[2.24] Prucker, O.; Christian, S.; Bock, H.; Ruhe, J.; Frank, C. W.; Knoll, W. *Macromol. Chem. Phys.* 1998, *199*, 1435.

[2.25] Chow, T. S. *J. Phys.: Condens. Matter* 2002, *14*, L333.

CHAPTER 3

COEFFICIENT OF THERMAL EXPANSION BEHAVIOR OF POLYMER THIN FILMS

3.1 Introduction

The coefficient of thermal expansion (α or CTE) for thin films is extremely important in a variety of applications such as in the field of microelectronics, where CTE mismatches in multilayer stacks can create problems with de-lamination and device failure. In the interlayer dielectric application, polymer thin films exhibit lower dielectric constants than do inorganic glasses for separation of lines of metallization and thus could potentially provide faster circuitry with less cross-talk. However, there are often severe problems with mismatch in the coefficients of thermal expansion that cause de-lamination of the polymer from the metal or from a ceramic substrate. Reduction of this mismatch requires understanding of the relationship between the film thickness of the polymer and its CTE value. Hence, direct measurement of CTE values for ultrathin polymer films is also important. Therefore, the influence of film thickness, polymer molecular weight and substrate on the coefficient of thermal expansion (α or CTE) for supported ultrathin polymer films has been investigated in this work.

The coefficient of thermal expansion (α) is generally defined as the fractional increase in volume per unit rise in temperature for a material at constant stress or pressure. Thermal expansion, or more widely thermal deformation, is characterized by the changes of the dimensions of a body resulting from temperature changes. Any formulations concerning the thermal expansivity of solids are closely related to the main ideas of an equation of state for solids. According to the original Gruneisen assumption, the internal energy of a solid can be divided into a static and a thermal contribution. This assumption leads to an equation of state for the pressure which contains two terms: one of the terms corresponds to the static interaction (internal pressure) and the other represents the thermal pressure due to the expansivity of lattice vibrations [3.1]. Thus, the most widely used form of the equation of state for solids is:

$$P = P_i + \gamma P_T \tag{3.1}$$

which corresponds to the usual Mie-Gruneisen approximation. In this equation $P_i = -dU_L/dV$ is the internal pressure, γ is the Gruneisen parameter, $P_T = U_T/V$ is the thermal pressure, and U_T is the thermal energy. Differentiation of Eq. with respect to temperature at constant volume yields:

$$\left(\frac{\partial P}{\partial T}\right)_V = \alpha K_T = \gamma \frac{C_V}{V} \tag{3.2}$$

where α is thermal expansion coefficient, and K_T is the isothermal bulk modulus. In principle, the thermal expansion of simple solids is well understood. Polymeric materials

are however a case that presents formidable problems for the theorist due to their long chain structure and the consequent need for an accurate representation of the interplay of both the weak intermolecular and strong intermolecular forces. In addition, many polymeric materials are semicrystalline, making it difficult, if not impossible, to obtain reliable estimates of ideal crystalline or amorphous behavior from experiment [3.1].

Beaucage and co-workers were the first to use single wavelength ellipsometry to measure the thermal expansion coefficients of thin (~300 nm) polystyrene (120,000 M_n) films cast on silicon wafers [3.2]. The change in film thickness with temperature was used to calculate the linear and bulk thermal expansion coefficients of the material. The coefficient of thermal expansion at ambient pressure of the polystyrene films was found to be in reasonable agreement with values reported for bulk polystyrene. Orts and co-workers first demonstrated the use of x-ray reflectivity to measure thermal expansion in thin polymer films. In this case the samples were poly(2-vinyl pyridine) films on clean native oxide covered silicon substrate [3.3]. This system was expected to exhibit a strong polymer-substrate attraction. Thermal expansion data were acquired for films with 77 Å $< h <$ 885 Å. In this case, the expansivities both above and below the T_g are thickness dependent, and the degree of thermal expansion below the transition temperature decreases with decreasing film thickness. So far, researchers have ignored the influence of molecular weight on coefficient of thermal expansion of ultra-thin films. It is objective of this chapter to study and to develop a comprehensive model to account for influence of film thickness, polymer molecular weight and substrate effect on thin film CTE value.

3.2. Experimental Section

3.2.1 Materials

Five different polystyrene samples that vary in both molecular weight and polydispersity index (M_w/M_n) were used to investigate the variation in coefficient of thermal expansion with film thickness and molecular weight. These polystyrene samples are hence forth referred to as samples PS-1 through PS-5. PS-5 (M_w=239,700; M_w/M_n=2.00) and PS-2 (M_w=212,400; M_w/M_n=1.05) were purchased from Aldrich Chemical Co., while PS-1 (M_w= 31,600 M_w/M_n=1.09), PS-4 (M_w=1,571,000 M_w/M_n=1.03) and PS-3 (Mw=560,900 M_w/M_n=1.04) were purchased from Scientific Polymers. Four different poly(methyl methacrylate) samples that vary in molecular weight were also used to investigate the variation in coefficient of themal expansion with film thickness and molecular weight. These samples are hence forth referred to as samples PMMA-1 through PMMA-4. PMMA-1 (M_w=52,700; M_w/M_n=1.08), PMMA-2 (M_w=298,000; M_w/M_n=1.02), PMMA-3 (M_w=838,300; M_w/M_n=1.04) and PMMA-4 (M_w=1,554,000; M_w/M_n=1.05) were purchased from Scientific Polymers. Toluene (99.9% pure, Fisher Scientific Chemicals) was used as a casting solvent in these experiments. 1, 1, 1, 3, 3, 3 – Hexamethyl – disilazane (99.9 % pure, Aldrich Chemical Co. Inc., termed as HMDS henceforth) was used to modify nature of substrate used in experiments. Single side polished silicon <100> test grade wafers purchased from Nova

Electronic Materials were used as substrates for film preparation. All polymer materials and solvents were used as received.

3.2.2 Sample Preparation

Polystyrene thin films were cast from toluene solutions onto cleaned native oxide coated silicon wafers using a CEE 100 CB spin coat and bake system from Brewer Science (Rolla, MO). The water contact angle on the silicon substrates was measured as a test of the substrate surface condition using a VCA 2500 XE contact angle system (AST Products, Inc.). In all cases, the water contact angle was measured to be approximately 15º which supports the presence of a hydrophilic native oxide surface. Spectroscopic ellipsometry measurements also indicated a silicon native oxide thickness of approximately 25 Å. Spin speeds (1000 rpm to 5000 rpm) and polymer concentrations (0.1% to 8% polymer by weight) were tightly controlled to achieve polymer film thicknesses ranging from approximately 20 nm to 700 nm. All polystyrene films were baked at 90°C for 4 minutes using the CEE Model 100 CB hot plate to remove the majority of the casting solvent, and then transferred into a vacuum oven at 135°C (above the measured T_g for all films used in this study) and 20 inches Hg vacuum for 20-48 hrs, depending on polymer weight, to anneal the films and remove additional residual casting solvent.

Nonpolar surfaces were prepared by coating HMDS on silicon wafers using a CEE 100 CB spin coat and bake system from Brewer Science (Rolla, MO) using spin

speed of 3000 rpm and baking 4 minutes at 90°C. . The water contact angle on HMDS covered surface was approximately 69-70°. Poly(methyl methacrylate) thin films, thicknesses ranging from approximately 30 nm to 650 nm, were cast from toluene solutions onto these HMDS covered surfaces using spin speeds of 1000 rpm to 5000 rpm and polymer concentrations of 0.1% to 6% polymer by weight. All PMMA films were baked at 90°C for 4 minutes using the CEE Model 100 CB hot plate to remove the majority of the casting solvent, and then transferred into a vacuum oven at 150°C (above the measured T_g for all films used in this study) and 20 inches Hg vacuum for 15-40 hrs, depending on polymer weight, to anneal the films and remove other residual casting solvent.

3.2.3 Film Surface Roughness Measurements and Defect Metrology

Atomic force microscopy (AFM) using a Digital Instruments (Santa Barbara, CA) Dimension 3100 system with a Nanoscope III controller was used to quantify film roughness and to inspect for film defects. The RMS roughness for the films was found not to exceed approximately 1 nanometer for any of the films used in this study. Any films with observed defects were discarded and recast.

3.2.4 Determination of α from Ellipsometry Data

Coefficient of thermal expansion of each sample was determined using the ellipsometry data obtained for T_g experiments in chapter 2. Once the film thickness

versus temperature plot was generated for each sample, slope was determined both in glassy and melt state, this slope was used to determine α value in both glassy and melt state. Coefficient of thermal expansion values reported here are corrected both for temperature dependent optical properties of the substrate as well as Poisson's ratio correction [3.4].

3.3. Results

3.3.1 Effect of Film Thickness on CTE

Thickness versus temperature data was used to extract the one-dimensional coefficient of thermal expansion (α) of both the glass and melt state for the polymer films as a function of film thickness. Figure 3.1 shows the variation of CTE (glass) with film thickness for PS-2 (Mw=212,400; M_w/M_n=1.05) on native silicon oxide substrate, as seen from Figure 3.1, CTE increases below some critical thickness value and remains constant above that critical thickness. Similar results were obtained for CTE value in melt state. Figure 3.2 shows CTE (melt) variation with film thickness.

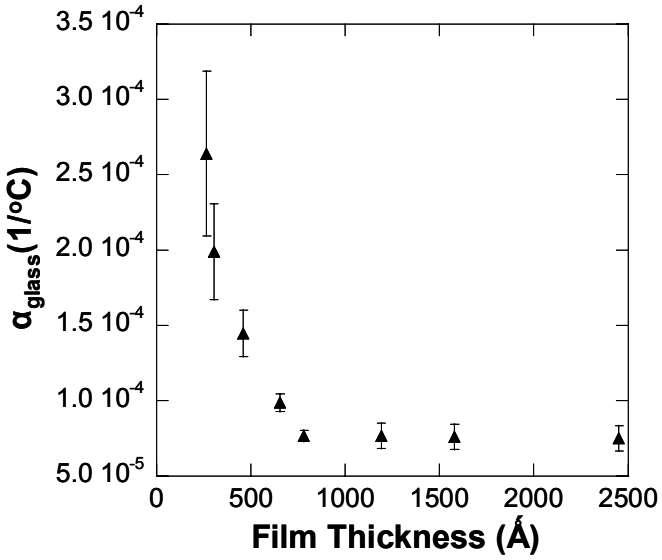

Figure 3.1 Effect of film thickness on CTE (glass) for PS-2 on native silicon oxide.

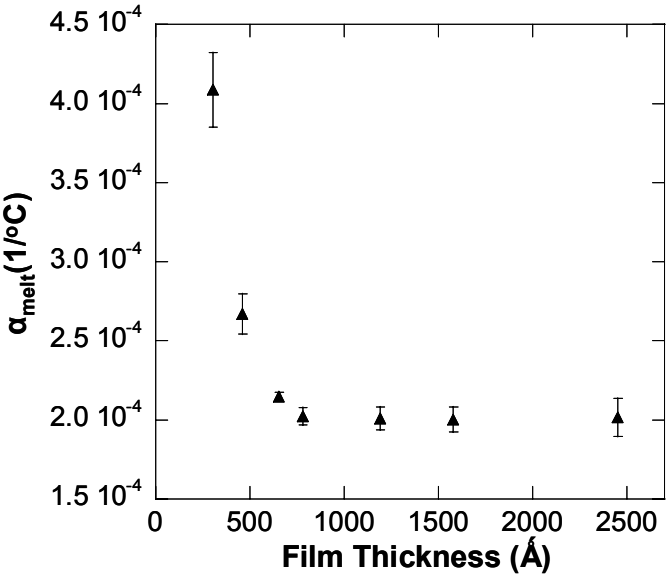

Figure 3.2 Effect of film thickness on CTE(melt) for PS-2 on native silicon oxide substrate.

3.3.2 Effect of Molecular Weight and film thickness on CTE

Since a series of narrow polydispersity samples of different molecular weights were measured, it is possible to determine effect of both film thickness and molecular weight on CTE in glassy and melt state. CTE for both melt and glassy state shows weak dependence on M_w but strong dependence on film thickness. As seen from Figure 3.3 & 3.4, CTE values, both in glassy and melt state, for higher molecular weight appears to increase at higher thickness value. Error bars are somewhat bigger to make any generalize statement regarding M_w dependence on this bulk behavior deviation.

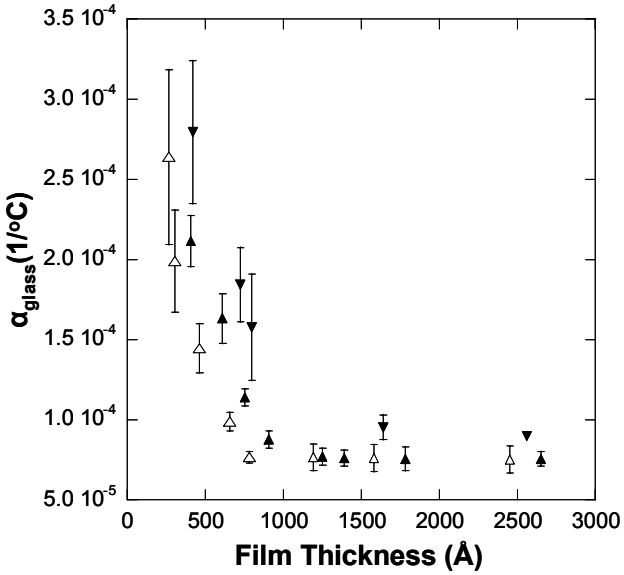

Figure 3.3 Dependence of glass α on film thickness and M_w. Δ M_w=212,400, ▲ M_w=560,900, ▼ M_w=1,571,000.

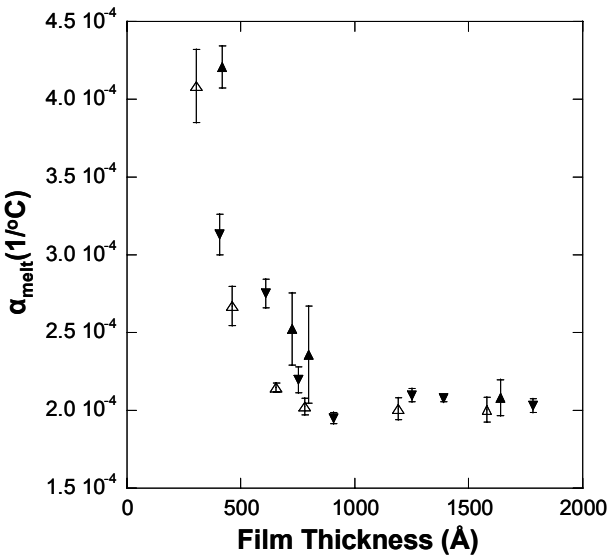

Figure 3.4 Dependence of melt α on film thickness and M_w. Δ M_w=212,400, ▼ M_w=560,900, ▲ M_w=1,571,000.

Figure 3.5a shows the α of the glassy state as a function of film thickness for three different PMMA molecular weights on HMDS primed substrate. It is observed that the α value of the glass increases as the film thickness is reduced below a critical thickness. It was observed that the film thickness at which α begins to deviate from bulk values also appears to depend on molecular weight. However, the molecular weight dependence is less clear in this data than in the case of the T_g data due to the increased scatter that is introduced by the derivative nature of such data. Similar results were obtained for the melt α. Figure 3.5b shows the dependence of the melt α with film thickness and molecular weight.

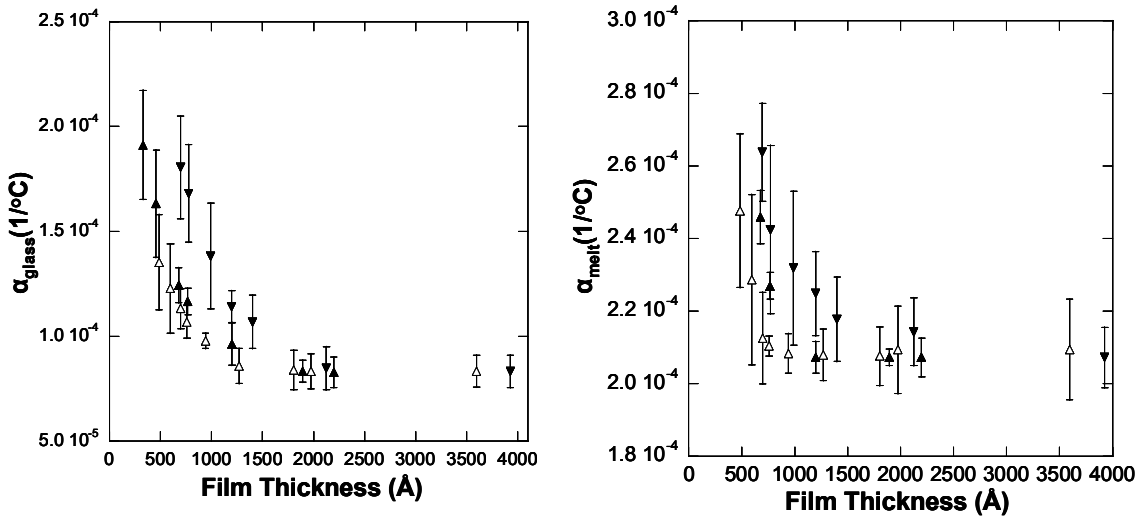

Figure 3.5. Dependence of a) glass α b) meltα on film thickness and M_w PMMA on HMDS primed substrate. Δ M_w=298,000, ▲ M_w=838,300, ▼ M_w=1,554,000.

Figure 3.6 shows the influence of substrate on α value of glassy state for ultra-thin polymer films. We compared results of PMMA films prepared on HMDS coated silicon wafers and on silicon native oxide surfaces, it was observed that for both PMMA on silicon native oxide surfaces and on HMDS coated surface α_{glass} starts increasing below the critical thickness value. α_{glass} for silicon native oxide surface was suppressed as compared with HMDS coated surface due to more attractive nature of native silicon oxide substrate.

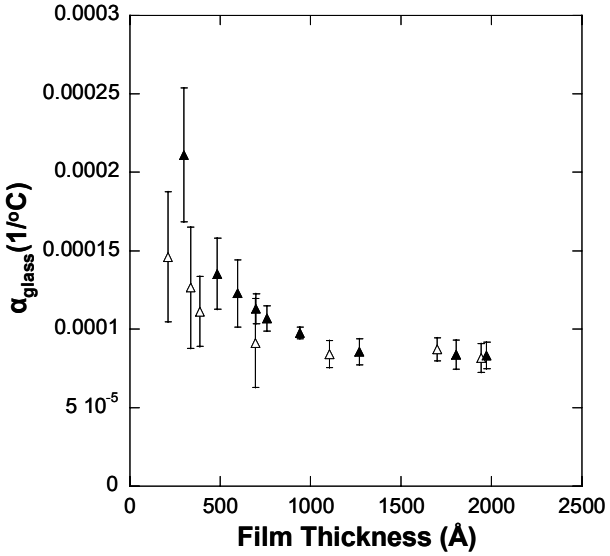

Figure 3.6 Effect of substrate on α_{glass} as a function of film thickness M_w=298,000. Δ PMMA on SiO_2/Si, ▲ PMMA on HMDS/Si.

3.4 Discussion

Forrest et al. proposed a multilayer model to describe the effect of film thickness on T_g in polymer films [3.5]. The model is based on incorporating the ideas of a length scale for cooperative dynamics by representing the polymer film with interfacial layers of higher or lower mobility and assigning an effective glass transition temperature to each layer. The model qualitatively explains most of the thin film T_g results reported in the literature, including an increase in T_g with film thickness. We tried to extend same model to define composite α for thin films, which is given by equation 3.3.

$$\alpha_{composite} = \frac{\alpha_S h_S + \alpha_B h_B + \alpha_I h_I}{h}. \qquad (3.3)$$

where α_S, α_B and α_I are surface (air-polymer), bulk and interface (polymer-substrate) expansivities with h_S, h_B and h_I their respective thickness values. Writing equation 3.3 in reduced form, we obtain equation 3.4.

$$\alpha'_{composite} = \frac{h'_S\left(\alpha'_S - 1\right) + h'_I\left(\alpha'_I - 1\right) + h'}{h'}. \tag{3.4}$$

where $\alpha'_{composite} = \alpha_{composite}/\alpha_B$, $\alpha'_S = \alpha_S/\alpha_B$, $\alpha'_I = \alpha_I/\alpha_B$, $h'_s = h_s/\langle s^2\rangle^{1/2}$ and $h'_I = h_I/\langle s^2\rangle^{1/2}$.

Figure 3.7 shows reduced $\alpha_{composite,glass}$ plotted versus the reduced thickness (h') for PS on native silicon oxide substrate. It can be observed that using such a scaling reduces the various α_{glass} versus film thickness curves into a single master curve regardless of molecular weight. We then fitted reduced data to same functional form as equation 3.4 to obtain equation 3.5.

$$\alpha'_{composite} = \frac{k_{1,glass} + k_{2,glass}h'}{h'} \tag{3.5}$$

where $k_{1,glass} = 3.333 \pm 0.8623$ and $k_{2,glass} = 0.9595 \pm 0.0705$.

When equation 3.5 is compared with equation 3.4, we get equation 3.6.

$$h'_{S,glass}\left(\alpha'_{S,glass} - 1\right) + h'_{I,glass}\left(\alpha'_{I,glass} - 1\right) = 3.333 \pm 0.8623 \tag{3.6}$$

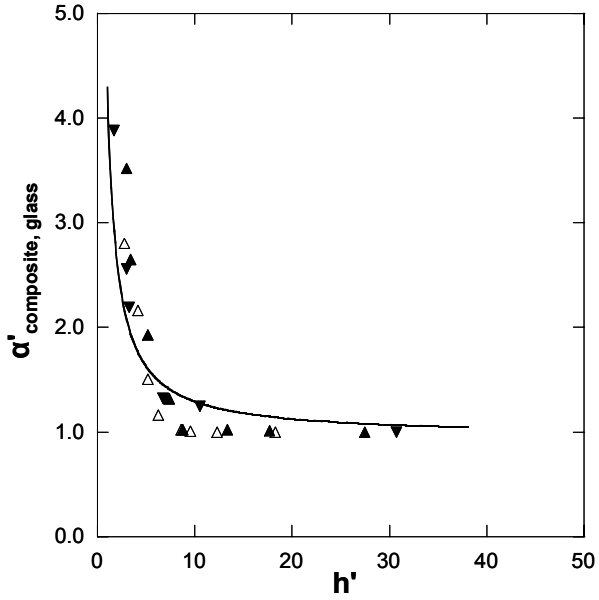

Figure 3.7 Reduced $\alpha'_{composite,\ glass}$ plotted versus the reduced thickness (h'). ▲ M_w=212,400, Δ M_w=560,900, ▼ M_w=1,571,000, curve is fit to equation (3.4).

At this stage we have no idea what values of these 4 parameters in equation 3.6 are, Keddie et al. [3.6] assumed surface layer to be in melt state which means taking $\alpha'_{s,glass}$~2.9. If we want to talk in qualitative terms and make two assumptions, the first one is that the thickness of surface layer is the same as the thickness of interface layer, and the second assumption is that α'_I~2.0, i.e. the mean of the bulk and surface expansivities, since we expect weak interaction between PS and native silicon oxide substrate. We obtain $h'_s = h'_I \sim 1.14$, which means surface and interface layers are on the order of one polymer radius of gyration. Although this analysis is rather crude, the experimental data and this analysis provides the initial desired guidance in terms of the

length scales over which such CTE variations may be expected and the order of magnitude of such effects.

3.5 Conclusions

The influence of film thickness, molecular weight and substrate on the coefficient of thermal expansion for supported polymer thin films has been studied in detail. It was observed that α increases for polystyrene on native silicon oxide substrate as film thickness decreases below a critical thickness. This critical thickness is found to be approximately 10 times the radius of gyration of polymer. α for PMMA films on HMDS coated silicon surfaces increases with decreasing film thickness below a critical film thickness of approximately 13 times the radius of gyration of the polymer. α for PMMA films on silicon native oxide surfaces shows a lower degree of increase as compared with PMMA on HMDS surface, indicating that the more attractive nature of native silicon oxide surface most likely reduces the expansivity of the interfacial polymer region near the substrate. It was found that α of supported polymer thin films can be modeled using a "master" curve based on reduced thickness and reduced α. This behavior and the length scales over which it occurs is consistent with the behavior observed in the apparent glass transition behavior of the polymer thin films as reported in Chapter 2.

3.6 References

[3.1] I. M. Ward, D. W. Hadley, " An Introduction to the Mechanical Properties of Solid Polymers, John Wiley & Sons (1998).

[3.2] G. Beaucage, R. Composto, and R. S. Stein, J. Polym. Sci., Polym. Phys. Ed., 30 (1993) 131.

[3.3] W. J. Orts, J. H. van Zanten, W. Wu, S. K. Satija, Phys. Rev. Lett., 71, 867 (1993).

[3.4] O. Kahle, U. Wielsch, H. Metzner, J. Bauer, C. Uhlig, C. Zawatzki, Thin Solid Films 313 (1998) 803.

[3.5] Forrest, J. A.; Mattsson, J. *Phys. Rev. E.*, 2000, *61*, R53.

[3.6] Keddie J. L.; Jones R. A. L.; Cory R. A. *Europhys. Lett.* 1994, *27*, 59.

CHAPTER 4

DISSOLUTION RATE BEHAVIOR OF MODEL PHOTORESIST POLYMER THIN FILMS

Fabrication of future nanoscale electronic devices will likely require the use of ultra-thin resist films. It was observed in Chapter 2 and 3 that film thickness, molecular weight, and substrate interactions can significantly affect the thermophysical properties of polymer thin films such as the glass transition temperature and coefficient of thermal expansion. The changes in polymer film thermophysical properties can potentially have an impact of the lithographic performance of polymer thin film photoresists. Hence, it is desirable to understand the influence of film thickness on a variety of other lithographically important polymer properties.

Dissolution rate is one such important physical property for photoresist polymer thin films that is of particular importance to the microelectronics industry. Simulation of lithographic processes relies to a great extent on knowledge of the dissolution or development behavior of photoresist thin films. Resist contrast is also known to be strongly affected by the dissolution behavior of the resist matrix polymer. So far, the possibility of film thickness significantly affecting the dissolution behavior of thin photoresist films has generally been ignored. This chapter reports on work focused on determining the effect of film thickness on the dissolution behavior of a variety of resist polymers including novolac, polyhydroxystyrene (PHOST), and bis-trifluoromethyl

carbinol substitute polynorbornene (HFAPNB). In addition, effect of substrate on dissolution rate behavior is also investigated for PHOST thin films.

4.1 Introduction

As mentioned previously, as feature sizes have diminished in the semicodncutor industry and lithographic exposure wavelengths have decreased, the thickness of the photoresist films used in lithography processes have also decreased [4.1-4.2]. This movement towards thinner resist films creates larger surface to volume ratios, and hence thin films can exhibit thermodynamic, structural, and dynamic properties that are different from those of the bulk material. The previous chapters have already demonstrated such effects for the glass transition and thermal expansion behavior of polymer thin films. In other words, it is possible that polymeric photoresists may behave differently simply when applied and used as thinner films. Thus, understanding the behavior of polymer ultra-thin films may be critical to the successful design of future photoresist materials and processes. The thermophysical properties and mass transfer behavior of polymer ultra-thin films have already been studied in some detail, and these investigations have shown that such properties show a strong dependence on polymer film thickness [4.3-4.7]. Based on this initial work, the goal of the work described in this chapter was to provide a comprehensive understanding of the influence of film thickness and other polymer characteristics on the dissolution behavior of photoresist polymer resin ultra-thin films.

Traditionally, most polymer film dissolution rate studies have utilized optical Development Rate Monitor (DRM) systems based on either monochromatic interferometry [4.8] or polychromatic reflectometry [4.9-4.11]. These techniques have worked well for characterizing resist materials with initial thicknesses in the 400 nm – 2500 nm range. However, both methods have difficulty with measuring the dissolution rate of ultrathin films. Recently, Robertson and coworkers proposed a polychromatic measurement technique based on depositing insoluble transparent thin film, such as a silicon dioxide layer between the resist and the silicon, for determining the dissolution rate of ultra-thin resist films [4.12]. Researchers have also demonstrated that ellipsometry is a useful technique for studying thin film dissolution rates for systems such as PMMA in organic solvents using single wavelength ellipsometers [4.13-4.14]. Burns and coworkers have also used spectroscopic ellipsometry to determine the dissolution rate of ultra-thin novolac films [4.15]. In their work, Burns and coworkers observed that the dissolution rate of novolac films decreases significantly at thicknesses below approximately 100 nm while Robertson and coworkers reported opposite behavior for an ESCAP type polymer. While these results indicate that there is some dependence of polymer dissolution rate on film thickness, the contradictory nature of the results and the limited data sets available clearly indicate that a more systematic and comprehensive study of such behavior would be useful. Therefore, the present chapter has focused on investigating the film thickness dependent dissolution behavior of a variety of model photoresist polymers in aqueous alkaline solutions.

4.2 Experimental Section

4.2.1 Materials

Three different types of polymers were studied in the present work. Novolac (M_w=22,000, PDI=25) was obtained from AZ Electronic Materials, PHOST (M_w = 11,800, PDI=1.641) was obtained from Electronic Polymers, part of Dupont Electronic Technologies (formerly TriQuest, LP), HFAPNB-1 (M_w = 19,590; PDI= 2.38 for dissolution rate studies) and HFAPNB-2 (M_w = 10,425 ; PDI = 1.72 for hydrogen bonding studies) were obtained from Promerus Electronic Materials. Novolac is the polymer resin used for positive-tone I-line photoresists while PHOST is the polymer resin commonly used for formulation of deep-UV (DUV) photoresists. HFAPNB is a fluorinated alicyclic polymer that serves a model polymer similar to resins that may be used for the development of 193 nm or 157 nm photoresists. Propylene glycol methyl ether acetate (PGMEA) (99%) was purchased from Aldrich Chemical Co. and used as the casting solvent for all of the polymers. The polymers and solvent were used as received. Novolac, PHOST, and HFAPNB all were dissolved in PGMEA to create polymer solutions containing approximately 4 to 30 wt.% solids depending on the polymer type and the viscosity needed to obtain the desired target thickness. The solution was then filtered through 0.45 micron teflon filters and spin-coated at 1000-5000 rpm for 30 seconds onto QCM crystals using a CEE Model 100 CB spin coat and bake system. Film thicknesses ranging from approximately 100 nm to 1.5 μm in thickness were created and used in this work. A soft bake of 90ºC for 2 minutes was performed to remove the

majority of residual casting solvent left in the film after spin coating. The tetramethyl ammonium hydroxide (TMAH) developer solutions used in this work were prepared by appropriate dilution of AZ 300 MIF (0.26 N TMAH) developer provided by AZ Electronic Materials (Clariant Corporation).

4.2.2. Film Thickness Measurement

A V-VASE variable angle spectroscopic ellipsometer (J.A. Woollam Inc.) was used to measure the thickness of the cast polymer films. The ellipsometry parameters, Ψ and Δ, were collected over the wavelength range from 500 nm to 1000 nm at angles of 65º, 70º, and 75º. The Ψ and Δ data were analyzed using the WVASE-32 analysis software (J.A. Woollam Inc.) by fitting the ellipsometry data using a film stack model composed of a Cauchy model for the polymer film and a semi-infinite gold film for the substrate (i.e. representing the gold electrode coated QCM crystal).

4.2.3 Fourier Transform Infrared Spectroscopy.

Fourier Transform Infrared Spectroscopy was performed in transmission mode using a Bruker KLS/088 FTIR. The optics and sample chamber were maintained under vacuum throughout the measurement.

4.2.4 Determination of Dissolution Rate from QCM

The dissolution rate of a polymer film can be determined by a direct measurement of either the weight or the film thickness as a function of time when the film is immersed in a solvent. Although optical reflectometry methods for measuring film thickness during dissolution have been most commonly used, utilizing mass loss measurements obtained via a quartz crystal microbalance has several advantages. The advantages of the QCM method include (1) simpler data analysis, (2) no sensitivity to developer liquid surface disturbances, and (3) more facile measurement of ultra-thin films as compared to reflectometry methods. Maxtek quartz crystal microbalance (PLO-10 Phase Lock Oscillator, 5MHz gold plated quartz crystals model # SC-501-1) and Q-sense corporation (QCM-D) were used in present work. The QCM system works on the principle that the resonant frequency of a quartz crystal is directly dependent on the mass of the crystal, including the mass of any film coated onto the crystal surface. In order to monitor the mass of films residing on the crystal surface, all that is required is a knowledge of the natural frequency of the clean QCM crystal. In this work, the natural frequency of each QCM crystal was measured in each experiment before being coated with the polymer film. The mass of material on the crystal can then be calculated using equation (1) which is simply a variation of the Sauerbrey equation [4.16]. Blank crystal experiments were performed as control experiments to account for any frequency shifts due to immersion in liquid.

$$m_{added} = \frac{\left(f_{uncoated} - f_{measured}\right)}{C_f} \tag{4.1}$$

In this equation, m_{added} is the mass added to the crystal per unit area, $f_{uncoated}$ is the natural frequency of the clean crystal, $f_{measured}$ is the frequency of the crystal after some mass is added to the crystal, and C_f is a constant calculated using equation (2) [4.16].

$$C_f = \frac{2f_q^2}{\left(\rho_q v_q\right)} \tag{4.2}$$

Here f_q is the resonant frequency of the bare crystal (nominally 5.0 MHz), ρ_q is the density of the quartz crystal (2.649 g/cm^3), and υ_q is the shear wave velocity of the AT cut quartz crystals used in this study (332,200 cm/s). By monitoring the QCM oscillator frequency as a function of time as the film coated crystal is immersed in solution, the film mass as a function of time can be calculated using equations (4.1) and (4.2). By measuring the starting thickness of the film via ellipsometry or other similar methods and using the starting mass of the film found from the QCM measurement, it is possible to calculate the density of the film. The average film thickness as a function of time can then be calculated by dividing the mass as a function of time data set by the film density.

Figure 4.1 shows a typical QCM data set of frequency change versus time for a novolac film dissolving in 0.26N TMAH developer. As soon as developer is introduced into QCM crystal chamber, there was an immediate small decrease in frequency due to the contact of the liquid with the film surface. The liquid acts as a medium with a higher acoustic loss than an air, and this results in a shift in crystal frequency. After the initial

decrease in frequency, the frequency increased indicating a loss in mass from the crystal as the film dissolved. After the film was completely dissolved, the crystal frequency reached and maintained a constant value. This frequency versus time data was then converted to mass versus time data using equations (4.1) and (4.2). This data was finally converted to thickness versus time data using the film density, and the dissolution rate versus time or film thickness was calculated by numerically evaluating the derivative of the data. Figure 4.2 shows the thickness versus time profile obtained from the data shown in Figure 4.1, along with the resulting dissolution rate versus time profile calculated from this same data.

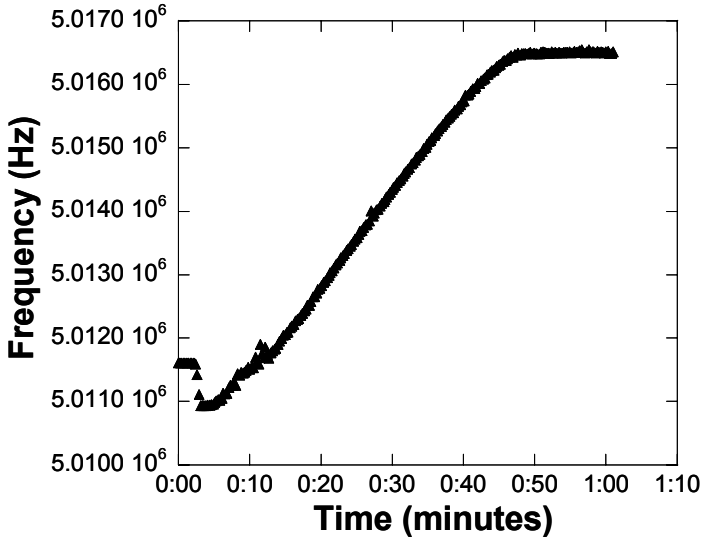

Figure 4.1. Typical data obtained from QCM for dissolution of 820 nm novolac film in 0.26 N TMAH at 25°C.

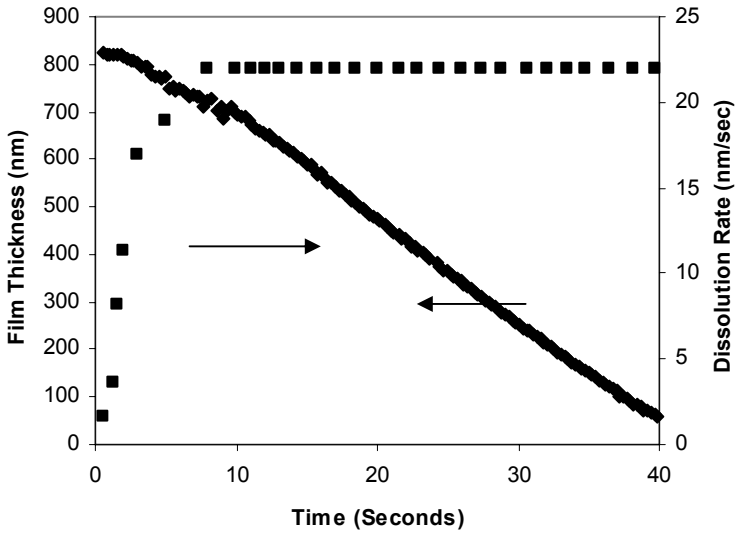

Figure 4.2. Dissolution rate profile for 820 nm in 0.26 N TMAH at 25°C. ♦ Film Thickness ■ Dissolution Rate

4.3 Results

4.3.1 Surface Dissolution Rate Inhibition versus Surface Dissolution Rate Enhancement

One distinct advantage of QCM based methods is that they allow for measurement of film thickness and dissolution rate from the moment the film is exposed to the developer solution. This is particularly useful for studying the dissolution behavior of the polymer film near its top surface. Figure 4.2 shows the dissolution rate profile for a novolac film that is approximately 820 nm thick. It is observed that approximately the top 100 nm of the film exhibits a non-linear dissolution rate as compared to the rather linear and constant dissolution rate behavior of the bulk of the film. This retardation in the dissolution rate of novolac films near their top surface is commonly known as

"surface inhibition". In contrast, Figure 4.3 shows the dissolution rate profile of an 1100 nm thick PHOST film. As can be seen from this figure, PHOST films are observed to also exhibit a non-linear dissolution rate near their top surface, and the dissolution rate near the top surface is faster than that of the bulk of the film. Thus, PHOST films exhibit "surface acceleration". Another interesting characteristic that can be seen in Figure 4.3 is that non-linear, surface enhanced dissolution rate in the case of PHOST extends approximately 300 nm into the film as compared to the 100 nm range typically cited for surface inhibition in novolacs. Figure 4.4 shows the dissolution rate profile for a 900 nm thick HFAPNB film. This material behaves in a manner similar to PHOST in that it also exhibits surface acceleration, and in this case the higher dissolution rates observed near the surface (e.g. as compared to the remaining bulk of the film) appear to extend even farther into the film, perhaps to a depth of approximately 400 nm.

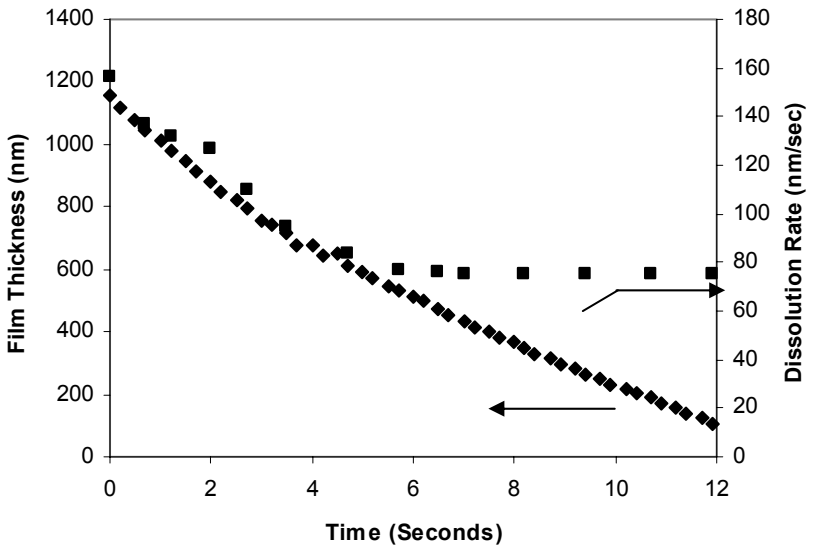

Figure 4.3. Dissolution rate profile for 1100 nm PHOST thick film in 0.165 N TMAH at 25°C. (♦ Film Thickness ■ Dissolution Rate)

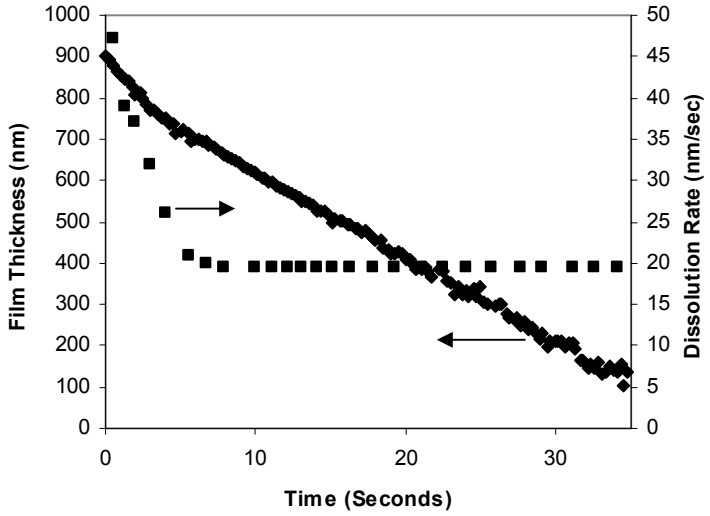

Figure 4.4. Dissolution rate profile for 900 nm HFAPNB thick film in 0.165 N TMAH at 25°C. (♦ Film Thickness ■ Dissolution Rate)

4.3.2 Effect of Film Thickness on the Polymer Dissolution Behavior

Figure 4.5 shows film thickness versus time behavior for novolac films of different initial film thickness. Figure 4.6 shows effect of film thickness on the dissolution rate of the novolac polymer in 0.26 N TMAH developer. In Figure 4.6, the "bulk" dissolution rate for each initial film thickness has been plotted, where the bulk rate is characterized as the constant dissolution rate region observed for the 50% remaining film thickness and below region in all films. There is a slight decrease in dissolution rate as a function of film thickness observed over the thickness range from approximately 900 nm to 100 nm. However, the effect is relatively minor.

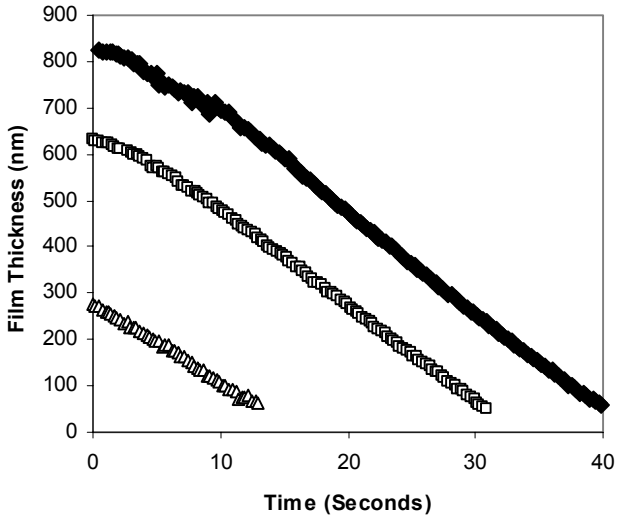

Figure 4.5. Film thickness versus time behavior for novolac films of different initial thicknesses in 0.26 N TMAH at 25°C. Initial novolac film thicknesses were: ♦ 820 nm, □ 630 nm, and Δ 270 nm.

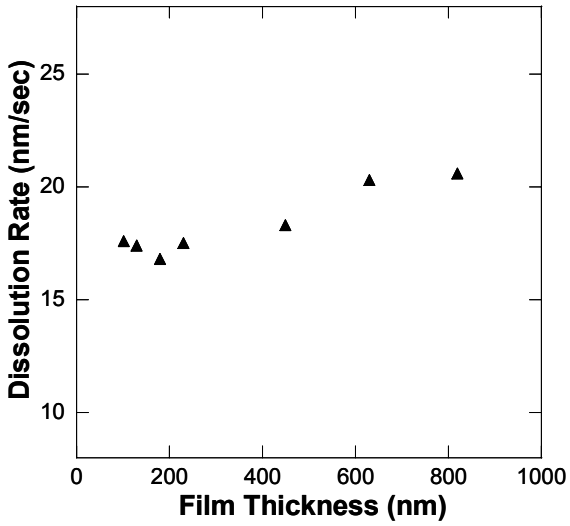

Figure 4.6. Effect of initial film thickness on novolac dissolution rate in 0.26 N TMAH at 25°C.

Figures 4.7 and 4.8 shows the effect of initial polymer film thickness on the dissolution behavior of PHOST. As can be seen from Figure 4.8, decreasing the film thickness results in faster bulk dissolution rates for PHOST. In fact, for the thinner films, the appearance of two different "surface" and "bulk" development regimes is not observed. However, the difference in dissolution rate as a function of initial film thickness does not appear to be due solely to the fact that the thinner films reflect the higher dissolution rates found in the "near surface" regions of thicker PHOST films. If this were the case, one might expect the thinner films to exhibit the same high dissolution rate, but this is not what is observed. Figure 4.9 shows the dissolution rate as a function of initial film thickness for PHOST films ranging in initial film thickness from approximately 900 nm to 200 nm in two developers of different normalities. It appears that changing the developer normality only changes the over magnitude of the dissolution rate, but not the basic behavior of the system. In generating Figure 4.9, the "bulk" dissolution rate for each initial film thickness has been plotted, where the bulk rate is characterized as the constant dissolution rate region observed for the 50% remaining film thickness and below region in all films. Below a critical thickness of approximately 700 nm, the bulk dissolution rate of PHOST is observed to be a strong function of initial film thickness.

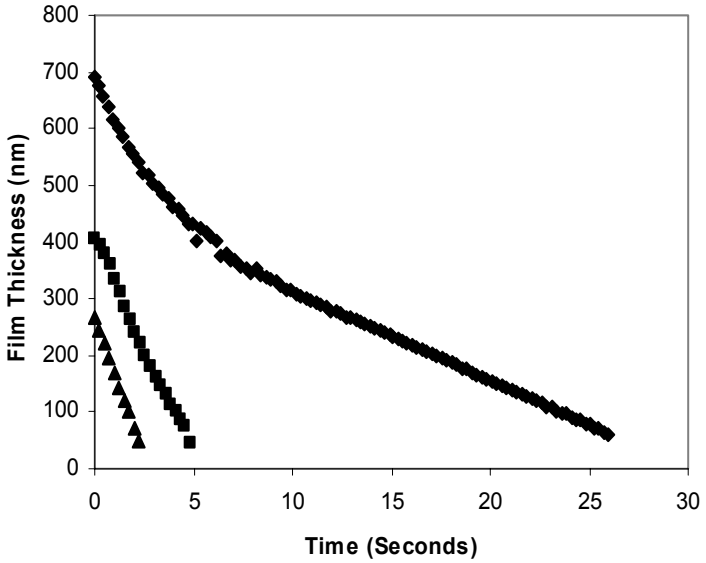

Figure 4.7. Film thickness versus time behavior for PHOST films of different initial thicknesses in 0.12 N TMAH at 25°C. Initial PHOST film thicknesses were: ♦ 690 nm, ■ 400 nm, and ▲ 270 nm.

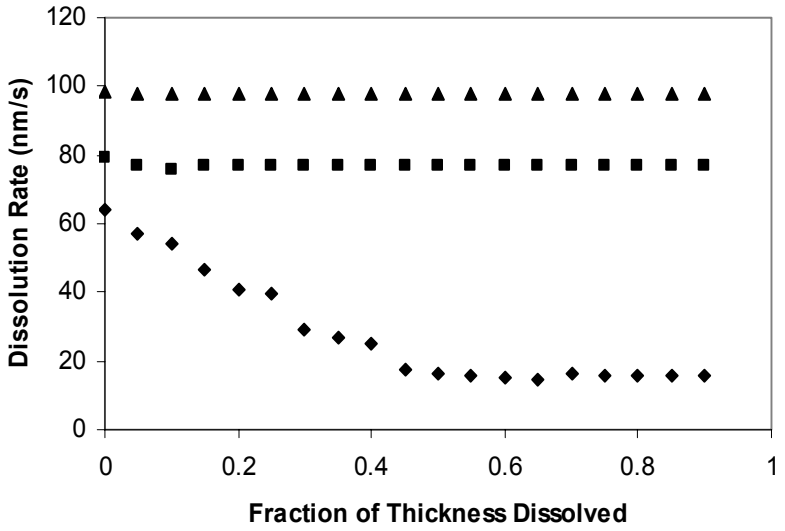

Figure 4.8. Dissolution rate profiles for PHOST films of different initial thicknesses in 0.12 N TMAH at 25°C. Initial PHOST film thicknesses were:♦ 690 nm, ■ 400 nm, and ▲ 270 nm.

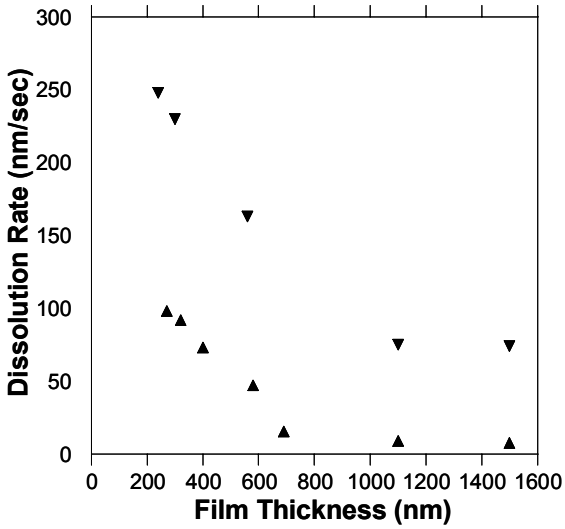

Figure 4.9. Effect of initial film thickness on the dissolution rate of PHOST (M_w = 11,800, PDI=1.641). Developers used were (1) ▲ 0.12 N TMAH and (2) ▼ 0.165 N TMAH at 25°C.

Behavior similar to that observed in the case of PHOST was also seen in the case of the dissolution behavior of HFAPNB. Figure 4.10 shows a plot of the dissolution rate of HFAPNB as a function of initial polymer film thickness. Again, below a certain critical thickness, there is a dramatic dependence of dissolution rate on the initial polymer film thickness.

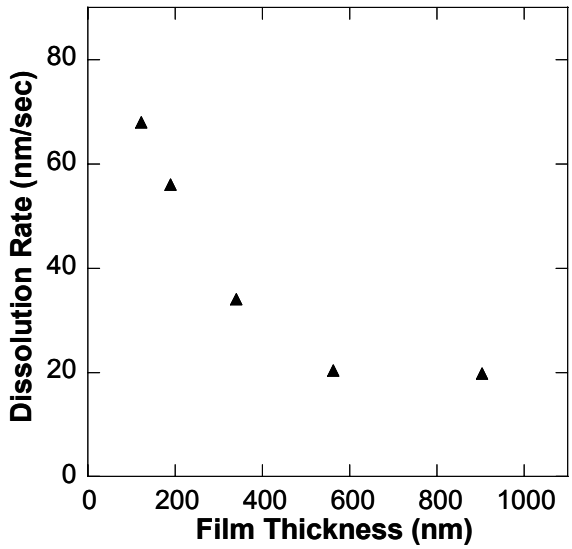

Figure 4.10. Effect of initial polymer film thickness on the dissolution rate of HFAPNB (M_w = 19,590; PDI= 2.38) in 0.165 N TMAH at 25°C.

4.3.3 Effect of Substrate on the Polymer Dissolution Behavior

All the results reported so far were on gold coated QCM substrates. There is potentially the question of whether the observed effect is influenced by or only a result of the nature of substrate surface. In order to investigate the effect of the substrate on dissolution rate, silicon dioxide coated substrate surfaces were also used for dissolution rate studies. These silicon dioxide surfaces would be expected to have a much stronger interaction with the hydroxyl containing polymer resins than the golad QCM surfaces. As seen from Figure 4.11, the dissolution rate of the polymer resin is found to be independent of substrate above film thicknesses of around 100nm. As we further decrease film thickness, it was found that dissolution rate was a strong function of both film thickness and substrate type. For silicon dioxide substrate surfaces, the dissolution rate starts decreasing with decreasing film thickness below 100 nm while for the gold

substrate surfaces the dissolution rate continues to increase with decreasing film thickness. It is well known in the literature that PHOST has strong tendency to form covalent bonds with native silicon dioxide substrates when thermally treated [4.17]. Such covalent bond formation between the polymer and the substrate would thus naturally be expected to decrease the dissolution rate for the polymers within a few polymer radius of gyrations of the substrate surface. So this may partially explain the observed decrease in dissolution rate for PHOST on the silicon dioxide surface. However, this effect persists up to length scales of approximately 100 nm, which would be on the order of 30 times the polymer radius of gyration. Such long range effects from covalent bonding of the polymer nearest the substrate surface on the dissolution rate of polymer chains well removed from the substrate surface are hard to rationalize at this point.

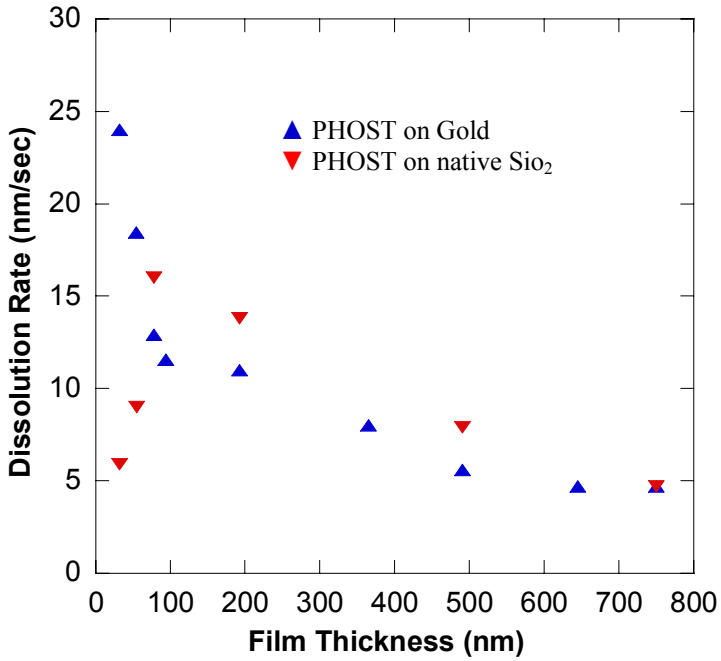

Figure 4.11. Effect of substrate on ultra-thin polymer film dissolution rate behavior in 0.1 N TMAH at 25°C.

Burns and coworkers investigated the possible causes of surface inhibition in novolac polymers and concluded that the critical ionization model for phenolic polymer dissolution best describes the surface inhibition phenomena [4.18]. While the critical ionization model can capture the surface inhibition observed in novolac, it can not explain the surface dissolution rate enhancement observed here for PHOST and HFAPNB. Simulations based on the critical ionization model by Burns and coworkers predict that there will be little surface inhibition in case of PHOST but do not predict any enhancement of dissolution rate near the polymer film surface. Currently, the cause of the surface acceleration observed in the PHOST and HFAPNB polymers is not well understood.

4.4 Discussion

It is known from prior work on photoresist polymers that the ability to form hydrogen bonds can significantly impact the dissolution rate of polymer resins. Dissolution inhibition through hydrogen bonding has been relatively well established in the case of diazonaphthoquinone (DNQ)-novolac resists [4.19-4.20]. The combination of DNQ and novolac polymers is believed to create extensive hydrogen bonding networks in the polymer which serve to retard the dissolution rate of the material. Inductive cluster polarization is one of the more popular interpretations of the mechanism by which the dissolution inhibition occurs in these materials. The mechanism postulates that the DNQ molecule starts a small string or cluster of hydrogen bonds within the novolac chain and

potentially between neighboring chains. The cluster originates with the formation of a hydrogen bond between a DNQ molecule and a novolac segment in the polymer chain. The initial hydroxyl group that is hydrogen bonded then forms hydrogen bonds with the next closest hydroxyl group in the polymer matrix. This process repeats itself to extend the hydrogen bonding network down the polymer chain or through the polymer matrix some number of repeat units. Dissolution inhibition is then hypothesized to be the result of the increase in pKa of the phenolic hydrogen while it participates in the hydrogen bonding network [4.21]. We observed that dissolution rate behavior is a strong function of film thickness, and this observation in conjunction with the prior studies of hydrogen bonding as a means to influence polymer dissolution motivated a study of the influence of polymer film thickness on hydrogen bonding in ultra-thin polymer films.

4.4.1 Effect of film thickness on hydrogen bonding in PHOST films

Figure 4.12 shows FTIR spectra for PHOST films at three different film thicknesses. The two peaks of interest in this spectrum occur at approximately 3532 cm^{-1} and 3380 cm^{-1}. The 3532 cm^{-1} peak corresponds to the position observed for hydroxyl peaks and represents the "free" (non-hydrogen bonded) OH peak. The 3380 cm^{-1} peak corresponds to hydrogen bonded OH peak [4.22]. Figure 4.13 shows a plot of the ratio of the FTIR peak area of the "free" OH peak to the peak area of the "bonded" OH peak as a function of film thickness. As seen from figure 4.13, the ratio of free peak area to bonded peak area was found to be strong function of film thickness and the ratio of the non-

hydrogen bonded or free OH groups increases with decreasing film thickness below a critical thickness value of around 600 nm.

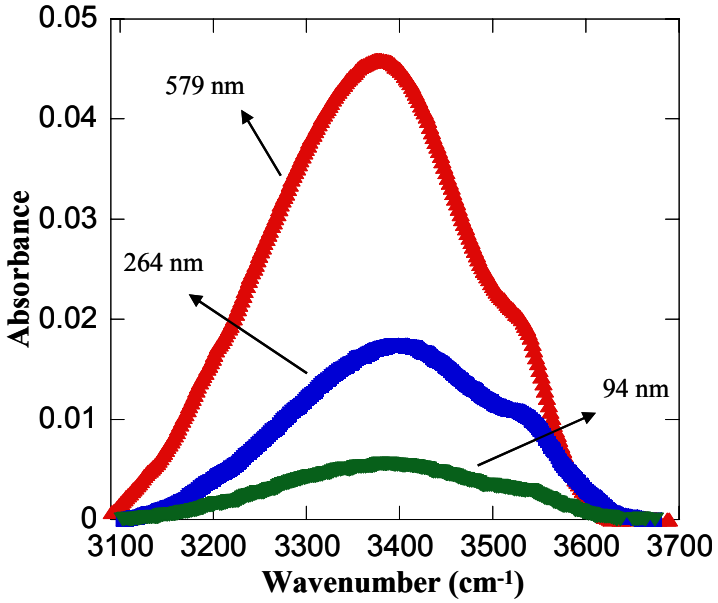

Figure 4.12. FTIR spectrum for PHOST films showing three different film thicknesses. Film thickness ▲579 nm ■ 264 nm ▼ 94 nm.

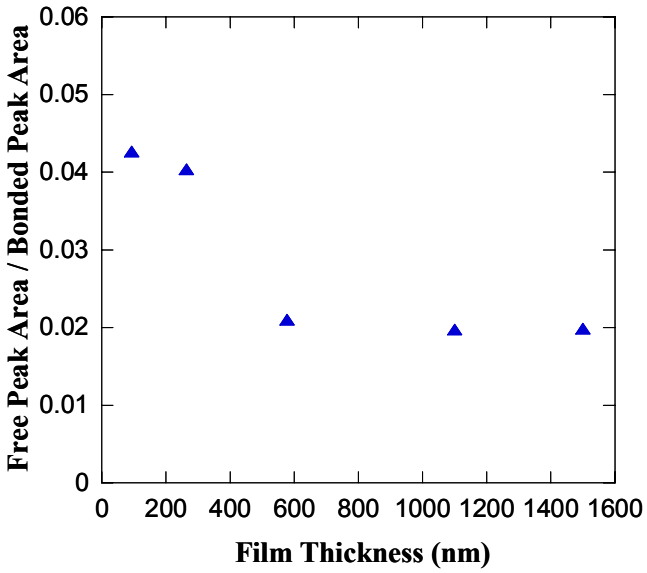

Figure 4.13. Ratio of deconvoluted free OH peak area to hydrogen bonded OH peak area ratio as a function of film thickness for PHOST.

4.4.2 Effect of film thickness on hydrogen bonding in HFAPNB films

In order to further generalize our results, we performed FTIR experiments on HFAPNB films. Figure 4.14 shows FTIR spectra for three different film thicknesses HFAPNB films. The two peaks of interest in this spectrum occur at approximately 3600 cm^{-1} and 3500 cm^{-1}. The 3600 cm^{-1} peak corresponds to the normal position observed for hydroxyl peaks and represents the "free" (non-hydrogen bonded) OH peak [4.23-4.24]. Hydrogen bonding would be expected to result in a spectroscopic shift in the OH peak to lower wavenumbers, and the presence of such a shift in bis-trifluoromethyl carbinol substituted polystyrenes has previously been demonstrated in the literature [4.24]. In the case of HFAPNB materials, it is clear that such a hydrogen bonded OH peak at approximately 3500 cm^{-1} is present. This hydrogen bonding in the polymer must occur between bis-trifluoromethyl carbinol substituted on adjacent HFAPNB polymer chains. The steric hinderance caused by the fluorines in the bis-trifluoromethyl carbinol group and the large distances between neighboring carbinol groups on the same polymer chain due to its rigid extended secondary structure make intramolecular hydrogen bonding difficult or impossible.

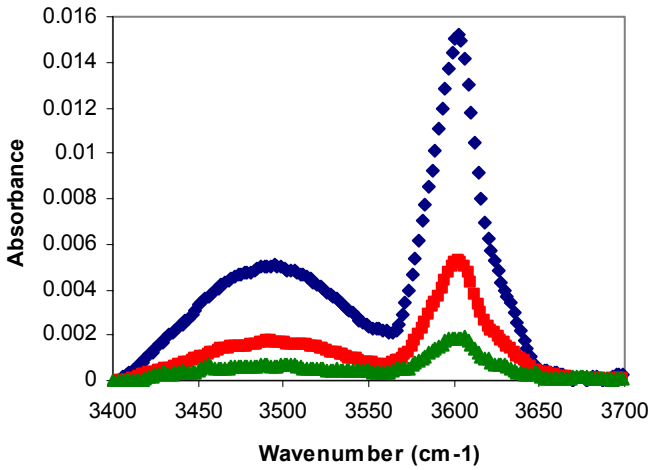

Figure 4.14. FTIR spectrum for HFAPNB films showing three different film thicknesses. Film thickness ♦ 422 nm ■ 205 nm ▲82 nm.

Figure 4.15 shows a plot of the ratio of the FTIR peak area of the "free" OH peak to the peak area of the "bonded" OH peak as a function of film thickness. As seen from figure 4.15, the ratio of free peak area to bonded peak area was found to be strong function of film thickness and the ratio of the non-hydrogen bonded or free OH groups increases with decreasing film thickness below a critical thickness value of around 500 nm.

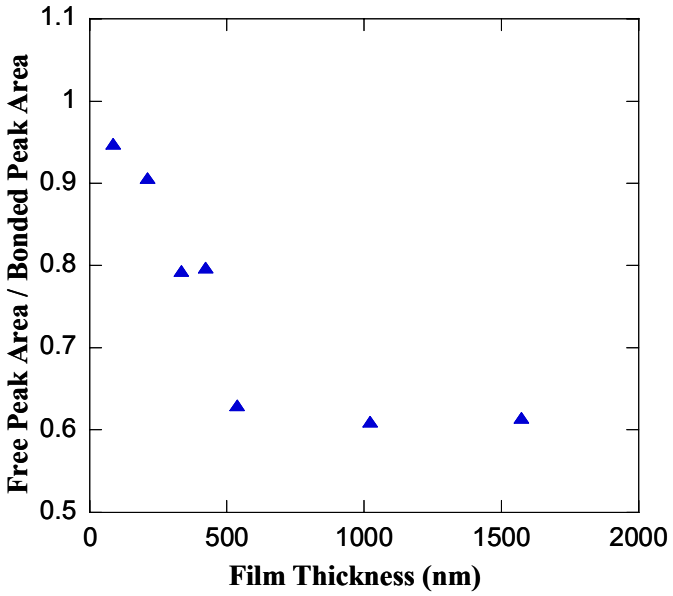

Figure 4.15. Ratio of deconvoluted free OH peak area to hydrogen bonded OH peak area ratio as a function of film thickness for HFAPNB.

4.4.3 Effect of film thickness on hydrogen bonding in Novolac films

In our previous work, we observed that there was no change in dissolution rate with initial film thickness for novolac resin. We performed FTIR experiments on novolac films to determine effect of film thickness on hydrogen bonding on this resin. Figure 4.16 shows FTIR spectra of three films for novolac resin. The 3525 cm^{-1} peak corresponds to the position observed for hydroxyl peaks and represents the "free" (non-hydrogen bonded) OH peak. The 3380 cm^{-1} peak corresponds to hydrogen bonded OH peak. Figure 4.17 shows ratio of free peak area to bonded peak area for novolac resin. As seen from figure 4.17, there was no change in hydrogen bonding as film thickness is decreased for

this particular resin. This result correlates well with our dissolution rate studies performed on same resin.

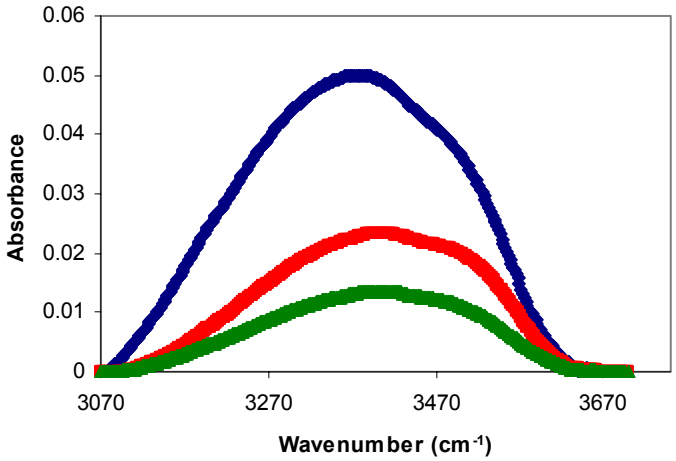

Figure 4.16. FTIR spectrum for Novolac films showing three different film thicknesses. Film thickness ♦ 853 nm ■ 372 nm ▲ 72 nm.

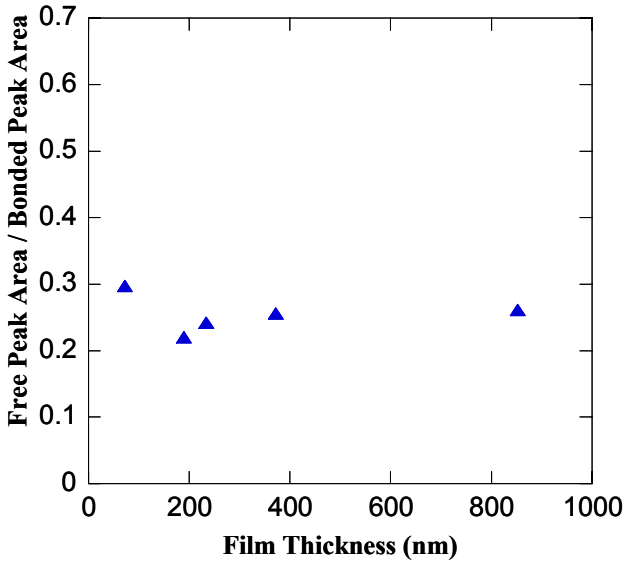

Figure 4.17. Ratio of deconvoluted free OH peak area to hydrogen bonded OH peak area ratio as a function of film thickness for Novolac.

4.4.4 Effect of casting solvent on hydrogen bonding of ultra-thin films

PGMEA, the casting solvent normally used for spin casting of photoresist polymer films, has a moderate affinity to hydrogen bond with PHOST. In an effort to understand the potential effect of casting solvent on the hydrogen bonding behavior of ultra-thin films, experiments were also performed PHOST using cyclohexanone as casting solvent. As seen from figure 4.18, PHOST films cast out of cyclohexanone also shows similar increasing free peak area versus bonded peak area ratio with decreasing film thickness. Here again critical thickness found to be around 600 nm. Figure 4.18 also shows that decreasing hydrogen bonding with decreasing film is independent of solvent used in casting films.

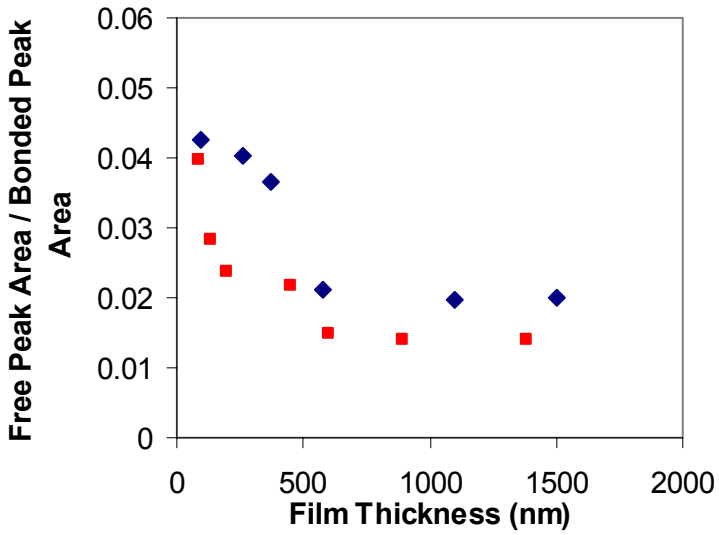

Figure 4.18 Effect of casting solvent on hydrogen bonding of PHOST thin films. ♦ PHOST/PGMEA ■ PHOST/Cyclohexanone

4.4.5 Effect of residual solvent on hydrogen bonding of ultra-thin films

In order to further investigate effect of residual solvent on hydrogen bonding of ultra-thin films, we performed FTIR experiments on films exposed to different baking conditions. Figure 4.19 shows FTIR spectra of 371 nm PHOST film baked for different time at 90^{o}C. As seen from figure 4.19, as baking time is increased bonded OH peak decreases while free OH peak remains same. Figure 4.20 shows FTIR spectra for same film baked at temperatures around and above glass transition temperature of film for around 15 mins ($T_g \sim 160^{o}$C). It was observed that after baking at 180^{o}C (20^{o}C above T_g) for 15 mins bonded OH peak stays at constant height and does not change further. This is situation where majority of residual solvent is taken out of the film. We made similar measurements for thin and thick films, figure 4.21 shows ratio of free peak area to bonded peak area versus film thickness for films baked at 90^{o}C for 2 mins and 180^{o}C for 15 mins. As seen from figure 4.21, it was found that hydrogen bonding decreases in ultra-thin film irrespective of amount of solvent present in the films.

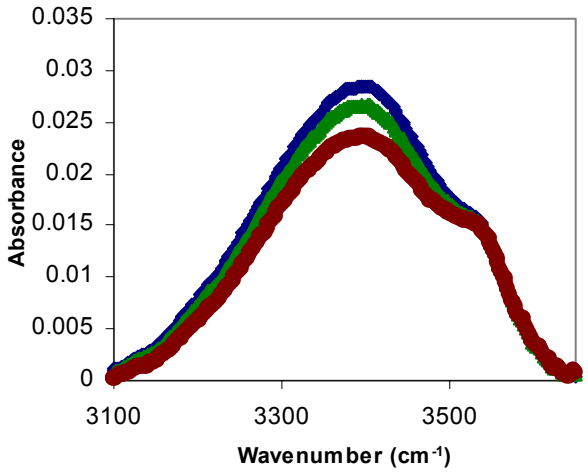

Figure 4.19. Effect of annealing time at 90°C on FTIR spectrum of 371 nm PHOST film. Baking time ♦ 2 mins ▲ 17 mins ● 244 mins.

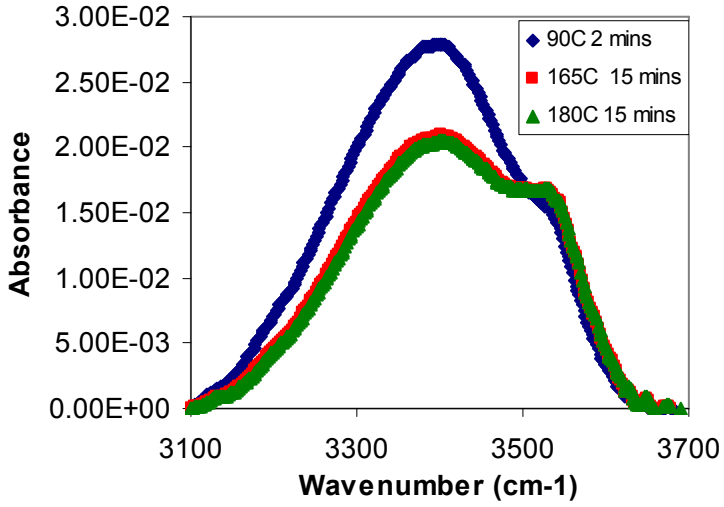

Figure 4.20. Effect of annealing temperature on FTIR spectrum of 371 nm PHOST film.

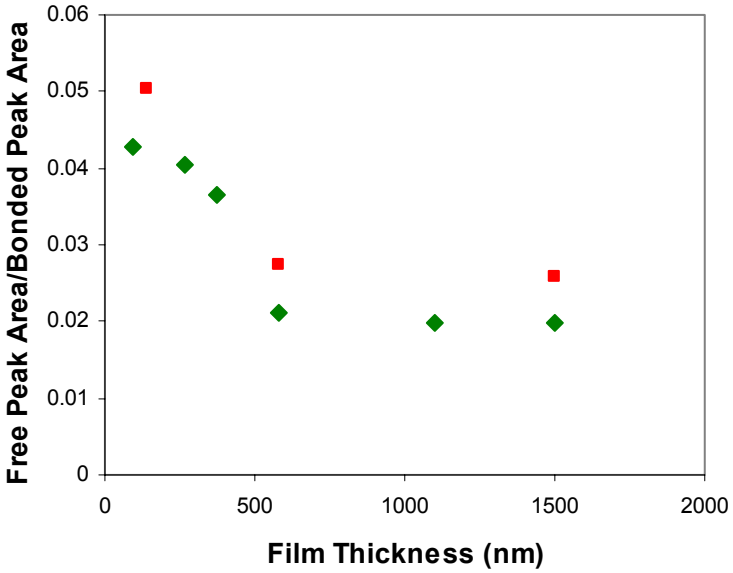

Figure 4.21. Effect of annealing on hydrogen bonding of PHOST thin films. Baking conditions ♦ 90°C 2 mins ■ 180°C 15 mins.

4.5 Conclusions

The influence of initial polymer film thickness on the dissolution behavior of three photoresist polymers, novolac, PHOST, and HFAPNB, was studied in detail using quartz crystal microbalance methods. In addition, the effect of substrate type on dissolution rate behavior was also determined for PHOST films. Novolac polymers displayed a slight dependence of dissolution rate on initial film thickness. In the case of novolac, the dissolution rate was observed to decrease slightly with decreasing film thickness. In contrast, the dissolution rate of both PHOST and HFAPNB films exhibited a strong dependence on the initial film thickness of the polymer film below a critical

initial film thickness. For these two polymers, the dissolution rate increased dramatically as initial film thickness was decreased below a critical thickness value that was in the range of 500 to 700 nm. Surface rate enhancement or surface acceleration of the dissolution rate was observed for both PHOST and HFAPNB as compared to the well known surface inhibition observed for novolac resins. Novolac polymers displayed a slight dependence of hydrogen bonding on initial film thickness. In contrast, the hydrogen bonding of both PHOST and HFAPNB films exhibited a strong dependence on the initial film thickness of the polymer film below a critical initial film thickness. Hydrogen bonding was observed to decrease as film thickness is decreased below approximately 600 nm. For these two polymers, the dissolution rate also increased dramatically as initial film thickness was decreased below a critical thickness value that was in the range of 500 to 700 nm. Results indicate that hydrogen bonding can be responsible for changing dissolution rate in ultra-thin films. The hydrogen bonding and dissolution rate behavior was found to be independent of solvent used or the amount of residual solvent in the films. The nature of the substrate surface and its interaction with the polymer film was found to play an important role in changing the dissolution rate of the polymer below film thicknesses of approximately 100 nm. One possible implication of these observations is that the lithographic performance of photoresists based on polymers such as PHOST and HFAPNB may be influenced by such thickness dependent dissolution behavior.

4.6 References

[4.1] V. Rao, J. Hutchinson, S. Holl, J. Langtom, C. Henderson, D.R. Wheeler, G. Cardinale, D. O' Connell, J. Goldsmith, J. Bohland, G. Taylor, R. Sinta, *J. Vac. Sci. Technol. B* **16**, 3722, 1988.

[4.2] Solak, H. H.; He, D.; Li, W.; Cerrina, F. *J. Vac. Sci. Technol. B* **17**, 3052, 1999.

[4.3] L. Singh, P. Ludovice, C. L. Henderson *Thin Solid Films,* **449/1-2**, 231, 2004.

[4.4] L. Singh, P. Ludovice, C.L. Henderson, *Proc. SPIE*, **5039**, 1008, 2003.

[4.5] L. Singh, P. Ludovice, C.L. Henderson, *Proc. SPIE*, **5376**, Paper 38, 2004.

[4.6] D. L. Goldfarb, M. Angelopoulos, E. K. Lin, R. L. Jones, C. L. Soles, J. L. Lenhart, W. Wu, *J. Vac. Sci. Technol. B* **19**, 2699, 2001.

[4.7] L. Singh, P. Ludovice, C.L. Henderson, *Proc. MRS Annual Meeting,* 2003.

[4.8] Perkin-Elmer Development Rate Monitor 5900.

[4.9] C.L. Henderson, S. A. Scheer, P.C. Tsiartas, B.M. Rathsack, J.P. Sagan, R.R. Dammel, A. Erdmann, and C.G. Willson, *Proc. SPIE* **3333**, 256-267, 1998.

[4.10] S.A. Scheer, C. Brodsky, S.A. Robertson, D. Kang, *Proc. SPIE* **4689**, Paper 113, 2002.

[4.11] A. Agrawal, C. L. Henderson. *Proc. SPIE*, **5038**, 1026-1037, 2003.

[4.12] S.A. Robertson, D. Kang, S.A. Scheer and C. Brodsky *Proc. SPIE* **4689**, 213-222, 2002.

[4.13] J.S. Papanu, D.W. Hess, A.T. Bell, D.S. Soane, *J. Electochem. Soc*. **136**, 1195-1200, 1989

[4.14] J.S. Papanu, D.W. Hess, D.S. Soane, A.T. Bell, *J Appl. Polym. Sci*. **39**, 803-823, 1990.

[4.15] S. Burns, G. Schmid, B. Trinque, J. Willson, J. Wunderlich, P. Tsiartas, J.C. Taylor, R. Burns, C.G. Willson, *Proc. SPIE*, **5039**, 1063, 2003.

[4.16] C. Lu, A. Czanderna *Applications of Piezoelectric Quartz Crystal Microbalances*, New York:Elsevier; chapter 2, 1984.

[4.17] Fryer, David S.; Nealey, Paul F.; de Pablo, Juan J. *Journal of Vacuum Science & Technology, B*, (2000), 18(6), 3376-3380.

[4.18] S. Burns, A.B. Gardiner, V.J. Krukonis, P.M. Wetmore, J. Lutkenhaus, G.M. Schmid, L.W. Flanagin, C.G. Willson, *Proc. SPIE* **4345**, 37-49, 2001.

[4.19] Ito, H. *IBM Journal of Research and Development* **2001**, *45*, 683-695.

[4.20] Honda, K.; Beauchemin, B. T., Jr.; Hurditch, R. J.; Blakeney, A. J.; Kawabe, Y.; Kokubo, T. *Proceedings of SPIE-The International Society for Optical Engineering* **1990**, *1262*, 493-500.

[4.21] McAdams, C. L.; Flanagin, L. W.; Henderson, C. L.; Pawloski, A. R.; Tsiartas, P.; Willson, C. G. *Proceedings of SPIE-The International Society for Optical Engineering* **1998**, *3333*, 1171-1179.

[4.22] D. Li, J. Brisson, Polymer 39(4), 793, 1998.

[4.23] Schaal, H.; Haeber, T.; Suhm, M. A. *Journal of Physical Chemistry A* **2000**, *104*, 265-274.

[4.24] Barlow, J. W.; Cassidy, P. E.; Lloyd, D. R.; You, C. J.; Chang, Y.; Wong, P. C.; Noriyan, J. *Polymer Engineering and Science* **1987**, *27*, 703-715.

CHAPTER 5

DIFFUSION BEHAVIOR OF POLYMER THIN FILMS

5.1 Introduction

Diffusion of small molecules in thin polymer films is an important phenomena in a wide variety of applications including membrane based separations, coatings, microelectronics, and many other fields. For example, the diffusion of photoacid within chemically amplified photoresist (CAR) polymer thin films is of critical importance in determining the ultimate resolution of CAR materials. As feature sizes in microelectronic devices decrease below 100 nanometers, the thickness of resist films used to fabricate such features also decreases rapidly. It is clear that for certain future patterning technologies, such as 157 nm lithography, Extreme Ultraviolet Lithography (EUVL), and low voltage electron beam lithography, resist film thicknesses well below 200 nm may be required [5.1-5.2]. Thinner resist films are required in order to minimize the effect of factors such as high resist absorption and limited depth of focus on the imaging performance of low wavelength lithography systems. The diffusion of a variety of species within the photoresist film can play an important part in controlling the behavior and imaging performance of a photoresist. For example, the presence of water can be required in the photoresist to enable desired chemical reactions or the removal of water can be important for applications such as 157nm lithography where the presence of

water can make the film opaque at the exposure wavelength [5.3]. In the case of CARs, which rely on the use of photochemically generated acids in the resist film to catalyze the solubility change of the resist polymer, the diffusion of photoacid in the film can lead to "diffusional blur" of the exposed image and ultimately limit the resolution of such materials. It has already been shown that thin film confinement of a polymer affects the thermal properties of ultrathin polymer films [5.4]. Goldfarb and co-workers have shown through model bilayer film diffusion experiments that the kinetics of a reaction-diffusion process decreases as the thickness of the model photoresist receiving layer is reduced [5.5]. So far, no fundamental study has been reported on isolating the effect of film thickness, polymer type, and polymer molecular weight on the diffusion coefficient of small molecules in polymer ultra-thin films. Understanding the extent and origin of any such confinement induced effects on the diffusion of small molecules in thin polymer films could impact a variety of areas such as the photoresist problems mentioned earlier.

It is the goal of this work to determine the effect of film thickness, polymer type, and polymer molecular weight on the diffusion coefficient of small molecules in polymer ultrathin films. Due to the importance of photoacid diffusion in CARs, two model photoresist polymers were studied in this work: poly(p-hydroxystyrene) (PHOST) and bis-trifluoromethyl carbinol substituted polynorbornene (HFAPNB). PHOST is the base resin for DUV (248 nm) resist materials while HFAPNB is a model homopolymer for fluorinated resist materials that may be used for 157 nm lithography. There have been many methods used to measure water sorption and calculate diffusion coefficients in polymer thin films. These include gas permeation techniques [5.6-5.9], electro-

microbalances [5.6-5.9], quartz spring microbalances [5.10-5.12], FTIR [5.13], stress analyzers [5.14-5.16] and quartz crystal microbalance (QCM) [5.17]. Due to the high accuracy and sensitivity of QCM methods, sorption experiments using a QCM have been conducted in this work to study the diffusion coefficient of small molecules in polymer ultra-thin films.

5.2 Experimental Section

5.2.1 Materials and Sample Preparation

Two different types of polymers were studied in the present work. PHOST (M_w = 11,800, PDI=1.641, R_g=2.5 nm) was obtained from Triquest Chemical Company; HFAPNB-1 (M_w =12,848; PDI=1.93, R_g= 3.5 nm) and HFAPNB-2 (M_w =71,810, PDI =2.17, R_g=10 nm) were obtained from Promerus Electronic Materials. Propylene glycol methyl ether acetate (PGMEA, 99%, Aldrich Chemical Co.) was used as the casting solvent for all polymers. The polymers and solvent were used as received. PHOST was dissolved in PGMEA to create polymer solutions containing approximately 4 to 20 wt.% solids. The HFAPNB-1 and HFAPNB-2 polymers were dissolved in PGMEA to create approximately 12 to 30 wt.% and 2 to 13 wt.% solutions respectively. The solutions were then filtered through 0.45 micron teflon filters and spin-coated at speeds ranging from 1000 to 5000 rpm for 30 seconds onto QCM crystals (CEE Model 100 CB spin coat and bake system) to create films ranging in thickness from approximately 50 nm to 1.1 μm. A soft bake of 90ºC for 4 minutes, similar to the bake conditions used in photoresist

processing, was performed to remove the majority of residual casting solvent left in the film after spin coating.

5.2.2 Film Thickness Measurement

A V-Vase variable angle spectroscopic ellipsometer (J.A. Woollam Inc.) was used to measure the thickness of the cast polymer films. The ellipsometry parameters, Ψ and Δ, were collected over the wavelength range from 500 nm to 1000 nm at angles of 65º, 70º, and 75º. The Ψ and Δ data were analyzed using the WVASE-32 analysis software (J.A. Woollam Inc.) by fitting the ellipsometry data using a film stack model composed of a Cauchy layer model for the polymer film and a semi-infinite gold film (representing the gold electrode surface of the QCM crystal) for the substrate.

5.2.3 Experimental Procedure

Two small controlled ambient chambers were custom designed and constructed for this work. Nitrogen gas was used to purge one chamber and provide a low vapor concentration (e.g. humidity) environment. A second nitrogen stream was bubbled through a liquid reservoir containing the penetrant (i.e. diffusional probe molecule) of interest and introduced into the second chamber in order to adjust the vapor phase penetrant concentration. This concentration could be controlled by adjusting the gas flow

rate passed through the bubbler. The penetrants used in these studies consisted of distilled water, benzene, and pure trifluoroacetic acid. In the case of water, a hygrometer probe (Omega, model # RH411) was inserted into the chambers near the location of the polymer coated samples and used to provide real-time monitoring of relative humidity of the chambers. This was done to ensure that the vapor concentration of the chambers was stable and remained stable during the crystal transfer process. A Maxtek quartz crystal microbalance (PLO-10 Phase Lock Oscillator, 5MHz gold plated quartz crystals model # SC-501-1) was used to measure mass uptake and loss in the polymer films during sorption/desorption cycles. One chamber was allowed to stabilize at a low penetrant concentration value (e.g. 0-10 %) while the other stabilized at a high concentration value (80-95 %). The dynamics of penetrant sorption in the various films was investigated by monitoring sorption and desorption from the films as they were transferred from one chamber to the other. The polymer coated QCM crystal was first placed inside the low concentration chamber and allowed to equilibrate. The frequency of the QCM crystal was recorded and once the crystal frequency reached a constant value, indicating that the polymer coated crystal had reached equilibrium with its environment, the crystal was transferred into the high concentration chamber and the crystal frequency was recorded. Once the frequency stabilized again, the crystal was immediately transferred back into the low concentration chamber. This process was repeated several times to investigate the reproducibility of the data. The temperature inside the chamber was held relatively constant at $23 \pm 2\ ^{o}C$ during all of these experiments.

5.3 Results and Discussions

The natural frequency of the QCM crystal used in each experiment was measured before being coated with the polymer film. The mass of material on the crystal can then be calculated using equation (5.1) which is simply a variation of the Sauerbrey equation [5.18].

$$m_{added} = \frac{\left(f_{uncoated} - f_{measured}\right)}{C_f} \tag{5.1}$$

In this equation, m_{added} is the mass added to the crystal per unit area, $f_{uncoated}$ is the natural frequency of the clean crystal, $f_{measured}$ is the frequency of the crystal after some mass is added to the crystal, and C_f is a constant calculated using equation (5.2) [5.18].

$$C_f = \frac{2f_q^2}{\left(\rho_q v_q\right)} \tag{5.2}$$

Here f_q is the resonant frequency of the bare crystal (nominally 5.0 MHz), ρ_q is the density of the quartz crystal (2.649 g/cm^3), and υ_q is the shear wave velocity of the AT cut quartz crystals used in this study (332,200 cm/s). Using equations (5.1) and (5.2) it is possible to calculate diffusion coefficient as the function of film thickness.

5.3.1. Effect of Film Thickness on Diffusion Behavior

If purely Fickian diffusion occurs during the sorption process into the polymer thin film, the diffusion behavior and uptake can be modeled using equation (5.3) [5.19-5.25].

$$\frac{M_t}{M_\infty} = 1 - \frac{8}{\pi^2}\sum_{n=0}^{\infty}\frac{1}{(2n+1)^2}\exp\left[-\frac{(2n+1)^2\pi^2 Dt}{4L^2}\right] \tag{5.3}$$

where M_t is the mass uptake at time t, M_∞ is the ultimate mass uptake at time $t = \infty$, D is the diffusion coefficient (cm^2/s), and L is the film thickness. For the initial phases of the sorption process ($M_t/M_\infty < 0.6$), the water uptake for these polymers is observed to follow a linear relationship versus the square root of time as would be expected for a Fickian diffusion process. Thus, a simplified version of equation (5.3) can be used that describes mass uptake into a thin, semi-infinite slab from one face [5.19, 5.24-5.25].

$$\frac{M_t}{M_\infty} = \frac{2}{L}\left(\frac{Dt}{\pi}\right)^{\frac{1}{2}} \tag{5.4}$$

This equation is often referred to as the "short time" equation and was used to estimate a Fickian diffusion coefficient of the various film thicknesses studied.

Fractional mass uptake (M_t/M_∞) was plotted against $t^{1/2}$ and the slope of the resulting plot was used to evaluate D.

Figure 5.1 shows a typical dynamic QCM data set for a sorption/desorption process for a 125 nm thick PHOST film. In this case, the film was initially equilibrated in a high relative humidity (RH) chamber, then immediately transferred to a low RH chamber and allowed to equilibrate, and finally transferred back to the high humidity chamber and allowed to equilibrate. The raw QCM frequency data for the sorption cycle was converted into relative or fractional mass uptake versus time (see Figure 5.2) by using equations (5.1) and (5.2). Equation (5.4) was then used to calculate the penetrant diffusion coefficient from this fractional mass uptake data. Figure 5.2 shows the fractional mass uptake of water versus time for the 125 nm thick PHOST film sorption curve shown in Figure 5.1. As seen in Figure 2, water uptake is initially linear up to fractional mass uptakes of approximately 0.7. This linear behavior for fractional mass uptakes up to approximately 0.6 to 0.7 was observed for all polymers and penetrants studied in this work. The deviation from Fickian behavior for fractional mass uptakes above approximately 0.7 is typical of so-called dual-mode sorption which is commonly observed in a variety of polymer systems.

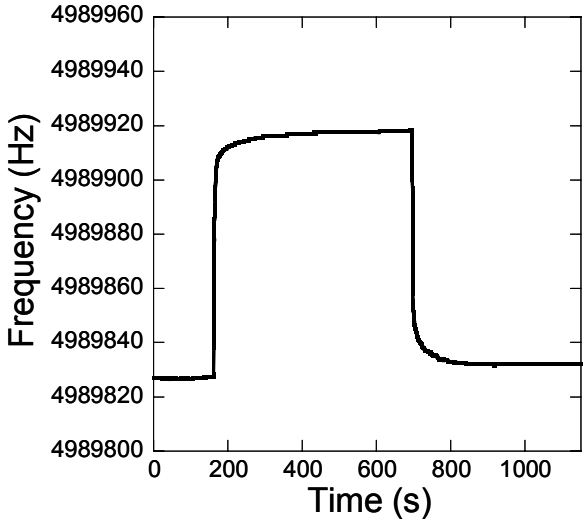

Figure 5.1. Typical dynamic QCM data for sorption/ desorption process for 125 nm thick PHOST film.

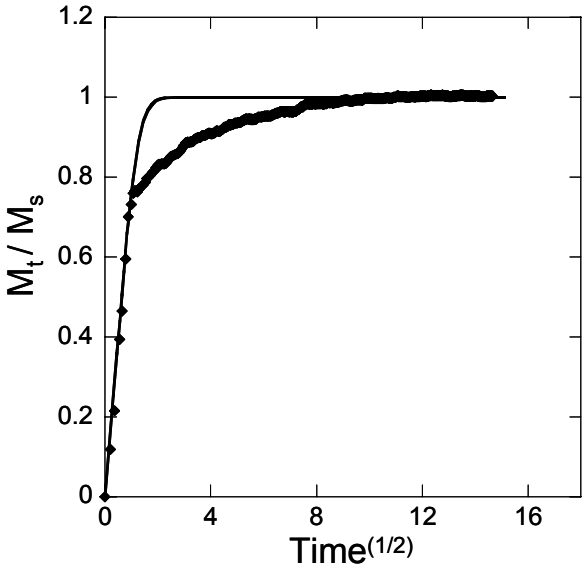

Figure 5.2. Relative mass uptake versus the square root of time for 125 nm thick PHOST film.♦ **Experimental** —— **Theoretical.**

Figure 5.3 compares sorption and desorption behavior for the same film used to generate the data shown in Figures 5.1 and 5.2. As seen in Figure 5.3, the short time

behavior during both sorption and desorption exactly overlap each other as would be predicted for Fickian diffusion. Diffusion coefficient values predicted for both the sorption and desorption experiments are $8.9 \times 10^{-11} \pm 2.1 \times 10^{-11}$ cm^2/sec and $7.8 \times 10^{-11} \pm 1.9 \times 10^{-11}$ cm^2/sec respectively. In figure 5.3, M_t/M_s defines relative mass uptake as a function of time for the sorption curve and defines mass lost as a function of time for the desorption curve.

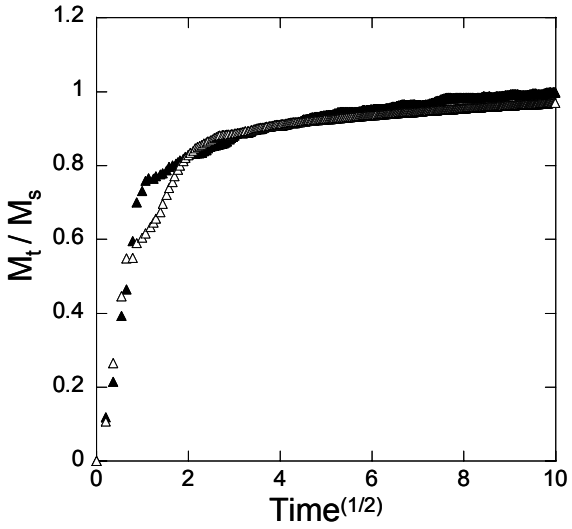

Figure 5.3. Sorption and desorption behavior for 125 nm PHOST thick film. ▲ Sorption Δ Desorption.

Figure 5.4 shows the measured diffusion coefficient for water in PHOST as a function of polymer film thickness. It was observed that as the PHOST film thickness was decreased, the diffusion coefficient for water in the films decreased rapidly with decreasing film thickness for films thicknesses below approximately 260 nm. Similar results were obtained for the HFAPNB-1 and HFAPNB-2 materials as shown in Figure 5.5. In the case of the HFAPNB materials, there appears to be some dependence of the critical thickness value (i.e. the thickness below which the diffusion coefficient changes depends strongly on film thickness) on the molecular weight of the polymer. Bulk values

reported here for water diffusion coefficients in these polymers are consistent with values reported previously by Berger and co-workers [5.17].

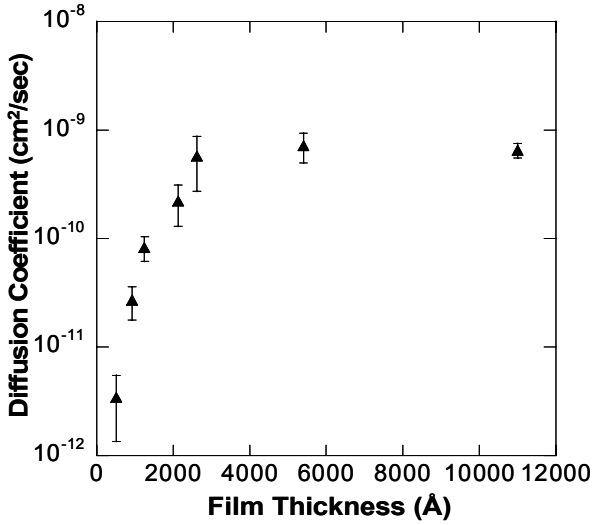

Figure 5.4. Water diffusion coefficient versus initial film thickness for PHOST. Error bars represent 90% confidence interval.

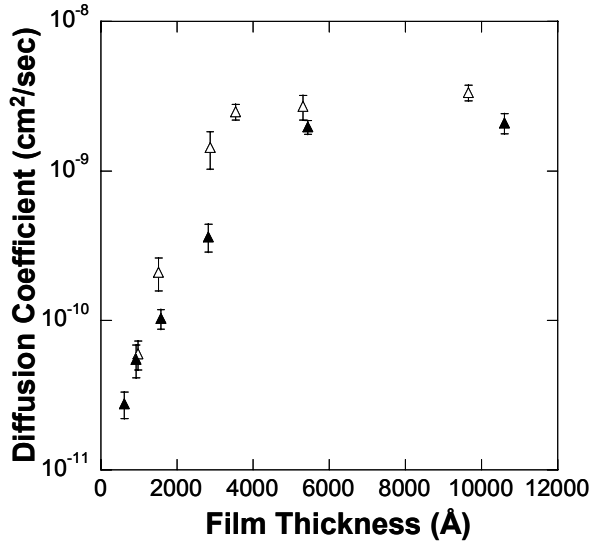

Figure 5.5. Water diffusion coefficient versus initial film thickness for HFAPNB. Δ Mw =12,848; PDI=1.93▲ **Mw =71,810, PDI =2.17. Error bars represent 90% confidence interval.**

In order to further generalize the effect of film thickness on the diffusion coefficient of small molecules in ultra-thin polymer films, the diffusion of benzene and trifluoroacetic acid into the PHOST model resist polymer was also studied. Benzene was selected as a generic representative of solvents that should not display a strong hydrogen bonding interaction with the polymer as might be exhibited by water and other relatively polar solvents. Trifluoroacetic acid was chosen as a model compound to investigate the diffusion of acidic species such as photoacids in resist thin films. It was specifically selected due to its high volatility which makes the vapor sorption studies rather straightforward. The diffusion coefficients extracted from these experiments are shown in Figures 5.6 and 5.7. It is evident from these figures that the diffusion coefficients for benzene and trifluoroacetic acid also decrease rapidly with decreasing film thickness for film thicknesses below the 260 nm critical thickness determined earlier for the water data.

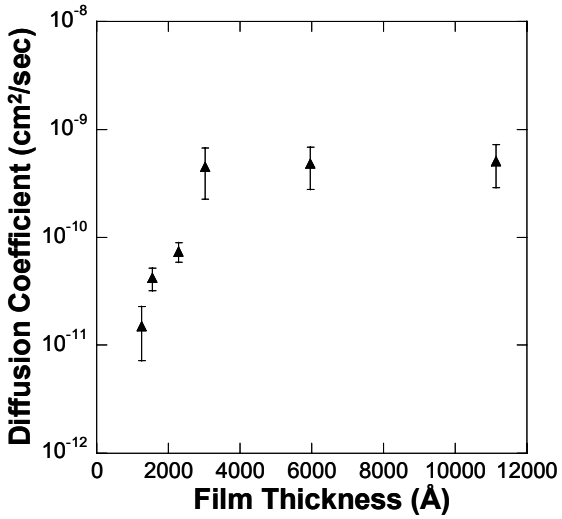

Figure 5.6. Benzene diffusion coefficient versus initial film thickness for PHOST. Error bars represent 90% confidence limits.

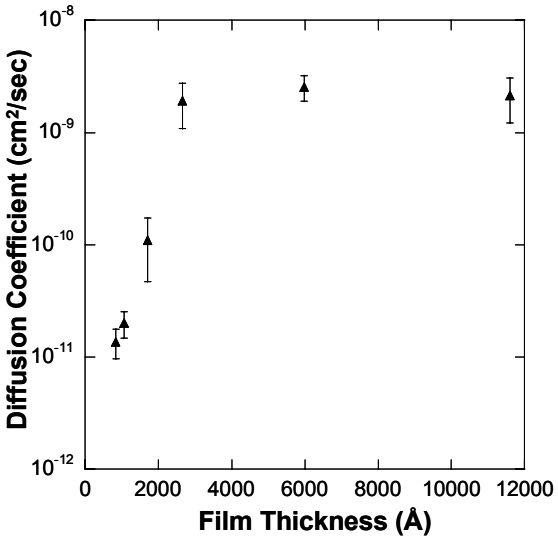

Figure 5.7. Trifluoroacetic acid diffusion coefficient versus initial film thickness for PHOST. Error bars represent 90% confidence interval.

5.3.2 Effect of Substrate on Diffusion behavior of ultra-thin polymer films

In order to investigate effect of substrate on diffusion coefficient of small species in ultra-thin films, we compared results for film spin coated on gold as well as on silicon oxide substrate. Results reported so far were on gold substrate. Figure 5.8 shows diffusion coefficient of water molecule in PHOST film spin coated on both gold substrate and silicon oxide substrate. As seen from figure 5.8, film thickness dependent diffusion behavior was found to be independent of substrate. It is known from our thermal properties work that substrate plays important role only around thickness of one time radius of gyration, for diffusion coefficient measurements minimum film thickness for which measurement was made was around 20 times radius of gyrations. This thickness is

much higher than the thickness expected to observe any substrate effects; hence the results we obtained are independent of substrate.

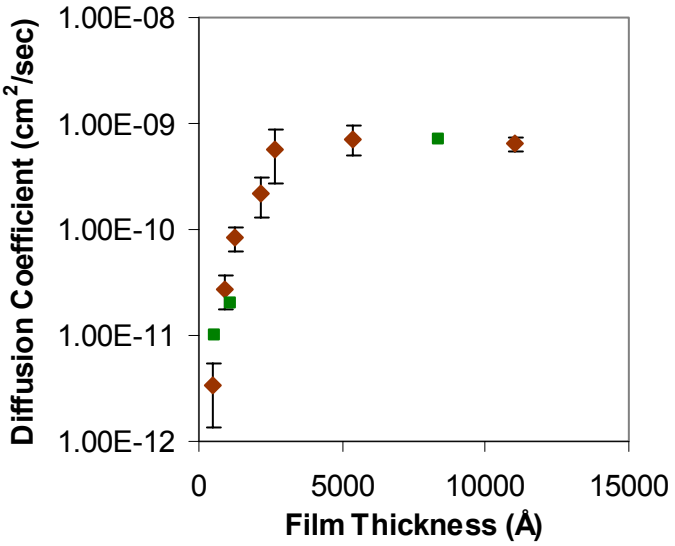

Figure 5.8. Effect of substrate on water diffusion coefficient in PHOST films. ♦ PHOST on gold substrate ■ PHOST on silicon oxide substrate.

Fick's law indicates that the calculated diffusion coefficient will be independent of the concentration gradient in imposed on the film. To verify this, experiments were conducted to measure the diffusion coefficient in polymer films using different magnitudes of the ambient relative humidity change (21% - 80%). In addition, this serves to confirm that there are no artifacts of condensation present in the data when relative humidities approaching 97 % were used. Table 5.1 shows results for two PHOST film thicknesses and the error terms represent a 90% confidence interval. It was

observed that changing the relative humidity gradient makes no statistically significant change in the diffusion coefficient value obtained.

Table 5.1. Effect of RH gradient change on water diffusion coefficient.

Film Thickness	D (RH 6-97%) (cm^2/sec)	D (RH 21-80%) (cm^2/sec)
91 nm	$2.7* 10^{-11} \pm 9.2*10^{-12}$	$3.47 * 10^{-11} \pm 7.3* 10^{-12}$
540 nm	$7.2 * 10^{-10} \pm 2.2*10^{-10}$	$9.7 * 10^{-10} \pm 1.8*10^{-10}$

5.4 Conclusions

Vapor sorption and desorption studies using quartz crystal microbalance methods have been used to study the effect of film thickness, polymer type, and polymer molecular weight on the diffusion coefficients of water, benzene, and trifluoroacetic acid in two model photoresist polymers. It was observed that the diffusion coefficient for small molecules decreases dramatically with decreasing film thickness below a critical thickness value. A decrease in the diffusion coefficient of approximately two orders of magnitude was observed for films ranging in thickness from their critical thickness value (~260 nm for the PHOST sample, ~350 nm for the HFAPNB-1 sample, and ~550 nm for the HFAPNB-2 sample) to approximately 50 nm in thickness. Film thickness dependent diffusion behavior was found to be independent of substrate in the film thickness regime studied (>20R_g). One possible implication of this phenomena though is that the latent

image formation of photoresists based on polymers such as PHOST and HFAPNB may be influenced by such thickness dependent diffusion behavior.

5.5 References

[5.1] V. Rao, J. Hutchinson, S. Holl, J. Langtom, C. Henderson, D.R. Wheeler, G. Cardinale, D. O' Connell, J. Goldsmith, J. Bohland, G. Taylor, R. Sinta, *J. Vac. Sci. Technol. B* **16,** 3722, 1988.

[5.2] H.H. Solak, D. He, W. Li, F. Cerrina*, J. Vac. Sci. Technol. B* **17,** 3052, 1999.

[5.3] E. Palik *Handbook of optical constants of solids II. San Diego*: Academic Press; p. 1059-77, 1998.

[5.4] J.A. Forrest, R.A.L. Jones, *Polymer Surface, Interfaces and Thin Films,* A. Karim, S. Kumar, editors. World Scientific, Singapore, 2000.

[5.5] D.L. Goldfarb, M. Angelopoulos, E.K. Lin, R. L. Jones, C. L. Soles, J. L. Lenhart, W. Wu*, J. Vac. Sci. Technol. B* 19, 2699 (2001).

[5.6] W. Hubbell, H. Brandt, Z. Munir *J. Polym. Sci., Part B: Polym Phys* **13**, 493-507, 1975.

[5.7] E. Sacher, J. Susko *J. Appl. Polym. Sci* **26**, 679-686, 1981.

[5.8] S. Numata, K. Fujisaki, N. Kinjo *Polymer* **28**, 2282-2288, 1987.

[5.9] Sykes G, Clair A. *J. Appl. Polym. Sci.* 1986; 32:3725-3735.

[5.10] D. Yang, W.J. Koros, H. Hopfenberg, V. Stannett *J. Appl. Polym. Sci.* **30**, 1035-1047, 1985.

[5.11] D. Yang , W.J. Koros, H. Hopfenberg, V. Stannet *J. Appl. Polym. Sci.* **31,** 1619-1624, 1986.

[5.12] K. Okamoto, N. Tanihara, H. Watanabe, K. Tanaka, H. Kita, A. Nakamura, Y. Kusuki, K. Nakagawa *J. Polym. Sci, Part B: Polym Phys* **30**, 1223-1231, 1992.

[5.13] K. Ichikawa, T. Mori, H. Kitano, M. Fukuda, A. Mochizuki, M. Tanaka *J. Polym. Sci, Part B: Polym Phys* **39**, 2175-2182, 2001.

[5.14] M. Ree, S. Swanson, W. Volksen *Polymer* **34**, 1423-1439, 1993.

[5.15] J. Jou, R. Huang, P. Huang, W. Shen *J. Appl. Polym. Sci.* **43**, 857-875, 1991.

[5.16] J. Jou, P. Huang *Polymer* **33**, 1218-1222, 1992.

[5.17] C.M. Berger, C.L. Henderson *Polymer* **44**, 2101-2108, 2003.

[5.18] C. Lu, A. Czanderna *Applications of Piezoelectric Quartz Crystal Microbalances*, New York:Elsevier; chapter 2, 1984.

[5.19] H. Han, J. Seo, M. Ree, S. Pyo, C. Gryte *Polymer* **39(13)**, 2963-2972, 1998.

[5.20] S. Despond, E. Espuche, A. Domard *J Polym Sci , Part B: Polym. Phys.* **39**, 3114-3127, 2001.

[5.21] J. Seo, K. Cho, H. Han *Polym. Degrad. Stab* **74**, 133-137, 2001.

[5.22] K. Mueller, W.J. Koros, Y. Wang, C.G. Willson *Proc SPIE* **3049**, 871-878, 1997.

[5.23] A.L. Hines, R.N. Maddox *Mass Transfer: Fundamentals and Applications,* Englewood Cliffs:Prentice-Hall; chapter 4, 1985.

[5.24] J. Comyn *Polymer Permeability*, New York:Elsevier, pp. 7, 345-350, 1985.

[5.25] W. Vieth *Diffusion In and Through Polymers: Principles and Applications*, New York:Hanser, pp. 19–47, 1991.

[5.26] S. Ahmed, P.J. Ludovice, P. Kohl *J. Comput. Theor. Polym. Sci* **10**, 221-233, 2000.

CHAPTER 6

SIMULATIONS – ULTRA-THIN POLYMER FILMS

6.1. Introduction

The behavior of polymeric systems confined into thin films is a situation that has numerous practical consequences. In previous chapters, experimental nano-characterization techniques were used to get physical properties of ultra-thin films. In present chapter molecular dynamics simulation will be performed to explain and understand experimental results. The objective of this chapter is to carry out molecular dynamics simulations to investigate the variation of local properties as a function of depth in ultrathin films. This information will help to elucidate the origin of the change in properties with film thickness. The multilayer model proposed by Forrest and co-workers qualitatively explains the variation of T_g and the coefficient of thermal expansion (α) [6.1]. Previous simulations of films have shown a variation in polymer mobility throughout the film profile. Theodorou and co-workers simulated molecular mobility, which is characterized by mean square displacements of atoms and chain centers of mass, at various regions in ultrathin glassy atactic polypropylene [6.2-6.3]. The model system they used is a film of polymer (polypropylene) exposed to two semi-infinite nonpolymeric (gaseous or solid) phases on either side. The thickness of the film, h, was large in comparison to the chain dimensions. They found that the region near free surface or vacuum has more mobility as compared to bulk region. Kumar and co-workers

performed Monte Carlo simulations on polymer melts confined between hard walls (substrate) [6.4-6.5]. They found that the single-chain statistics are perturbed by the substrate, and this effect is screened out only after one proceeds to a distance comparable to twice the unperturbed radius of gyration of the polymer chains. They also observed that the chains near the surface are flattened into nearly two-dimensional structures. To our knowledge no one has reported anisotropic nature of thermal and mass transfer properties for ultra-thin polymer films. Hence, it is objective of this chapter to simulate variety of spatial physical properties like coefficient of thermal expansion, glass transition temperature, and fractional free volume near interfaces and compare them with their respective bulk values. It was observed in our experiment work that thermal properties and mass transfer properties start deviating from their bulk behavior at different length scales. Hence, it is also objective of this chapter to understand why different physical properties change at different length scales.

6.2 Simulation Approach

6.2.1 Model

We studied atactic polypropylene (a-PP, w_m=0.48) film at - 40^{o}C on an attractive substrate. Two models of film thickness around 3.5 times radius of gyration (Model-1) and 7.5 times radius of gyration (Model-2) (M_w= 4300; R_g= 20.5 Å) were generated using the Material Studio software by Accelrys [6.6]. Models were initially equilibrated through molecular mechanics by Cerius^2 for 5000 steps. After molecular mechanics,

around 300 picoseconds of NPT molecular dynamics simulations were performed. Figure 6.1 shows equilibrated model structure of thin atactic polypropylene film on attractive substrate. As seen from figure 6.1, space larger than energy cut-off was created in z-direction to effectively convert 3D periodicity to 2D periodicity.

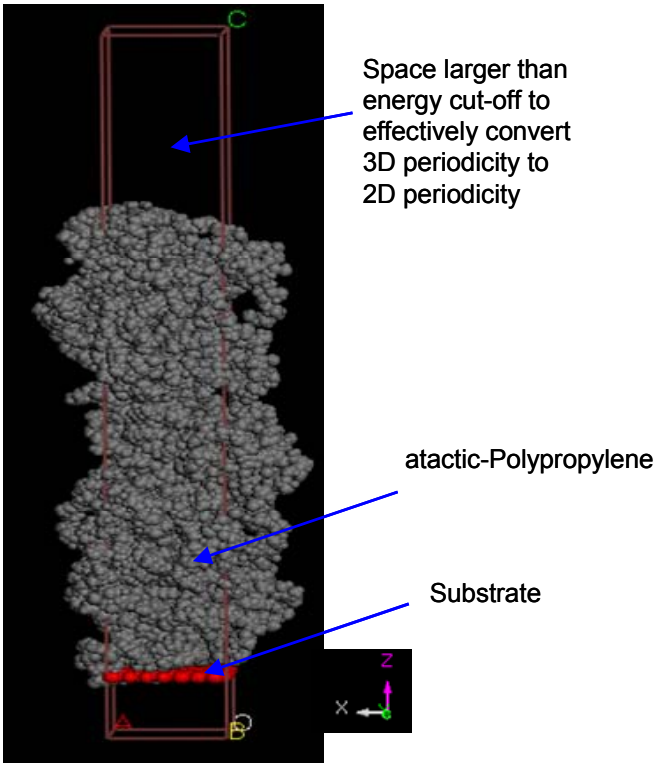

Figure 6.1 Equilibrated model structure of thin atactic polypropylene film on substrate.

Molecular dynamics (MD) is the numerical integration of Newton's equation of motion shown in Equation 6.1 and the potential energy function is the same as the one used in molecular mechanics. MD samples phase space more efficiently compared to molecular mechanics by adding energy to the system in the form of temperature. MD

provides microscopic information and statistical mechanics allows it to be converted into macroscopic quantities such as temperature, pressure, and internal energy [6.7].

$$F = -\frac{dU}{dR} = m\frac{d^2R}{dt^2} \tag{6.1}$$

Newton's equation of motion is integrated to determine those atomic positions and its velocities over the time of the simulation. This method samples greater phase space than the molecular mechanics method because of the added thermal motion which allows the system to sample other local minimas by overcoming energy barriers.

MD ensembles include the following: constant number, volume and energy (NVE), constant number, pressure, and temperature (NPT), constant number, pressure, and enthalpy (NPH), and constant number, volume, and temperature (NVT). The NPT MD simulations were performed in this research. Pressure in these simulations was approximately zero (P~ 0), which makes these simulation NVT with 1-D volume variation. Cerius^2 software by Accelrys was used in this research to perform MD simulations [6.6] A more detailed and complete discussion on molecular dynamics can be found in Allen and Tindesley [6.7].

NPT MD

The equation of motion for the positions, q and the momenta, p in NPT MD are

$$\frac{dq}{dt} = \frac{p}{m} + \frac{\rho_\varepsilon q}{W} \tag{6.2}$$

$$\frac{dp}{dt} = F(q) - \left(1 + \frac{d}{dN}\right)\frac{\rho_{\varepsilon}}{W} p - \frac{\rho_{\varepsilon_1}}{Q_1} p \tag{6.3}$$

In these equations of motions a thermostat is introduced via the variable $\rho_{\varepsilon 1}$ and Q_1. A barostat is introduced via the variables ρ_{ε} and W. The equation of motion (6.2) and (6.3) are complemented with an equation of motion for the volume,

$$\frac{dV}{dt} = \frac{dV\rho_{\varepsilon}}{W} \tag{6.4}$$

$$\frac{d\rho_{\varepsilon}}{dt} = dV(P_{\text{int}} - P_{ext}) + \frac{1}{N}\sum_i \frac{p^2}{m} - \frac{\rho_{\varepsilon_1}}{Q_1}\rho_{\varepsilon} \tag{6.5}$$

In these equations P_{ext} is the external pressure, which is imposed. P_{int} is the internal pressure, which can be calculated during the simulation

$$P_{\text{int}} = \frac{1}{dV}\left[\sum_i \left(\frac{p^2}{m} + q.F\right) - dV\frac{\partial U(V)}{\partial V}\right] \tag{6.6}$$

Where U is the potential. A more detailed and complete discussion on molecular dynamics can be found in Frenkel and Smit [6.8]. We employed the Paranello Rahman pressure controller [6.9] and Nosé temperature controller [6.10] in these simulations.

6.2.2 Force Field

A force field is a set of equations that describe the potential energy of a molecular system in the effort to approximate the behavior of the system. The selection of an appropriate force field that accurately describes the system is very crucial to any molecular mechanics, MD simulations, and Monte Carlo (MC) simulations [6.11].

The potential energy is divided into two groups of interactions given by the following

$$E = E_{Bonded} + E_{Nonbonded} \tag{6.7}$$

where E_{Bonded} is the bonded interactions and $E_{Nonbonded}$ is the nonbonded interactions.

6.2.2.1 Bonded Energy Terms

The bonded interactions are comprised of bond stretch, bond angle, and bond torsion terms.

$$E_{Bonded} = E_{Bond} + E_{Angle} + E_{Torsion} \tag{6.8}$$

Where E_{Bond} is the bond stretching, E_{Angle} is the angle bending, and $E_{Torsion}$ is the intrinsic torsion potential energy terms. The bond stretching and angle bending

components are quadratic functions. The harmonic potential function for the bond stretching and angle bending is given by the following

$$E_{Bond} = \tfrac{1}{2} K_b (r-r_o)^2 \quad (6.9)$$

$$E_{Angle} = \tfrac{1}{2} K_\theta (\theta-\theta_o)^2 \quad (6.10)$$

where r_o is the equilibrium bond distance, θ_o is the equilibrium bond angle, K_b is the bond stretching constant, and K_θ is the angle bending force constant.

Torsion angle is defined as the dihedral angle created between two different bonds connected to a common bond. The torsion interaction for two bonds *IJ* and *KL* connected via a common bond *JK* is taken of the form

$$E_{IJKL} = \tfrac{1}{2} V_{JK} \{1-\cos[n_{JK} (\varphi - \varphi^o_{JK})]\} \quad (6.11)$$

Where φ is the dihedral angle (angle between *IJK* and *JKL* planes), n_{JK} is the periodicity (an integer), V_{JK} is the barrier to rotation (always positive), and φ^o_{JK} is the equilibrium angle.

6.2.2.2 Nonbonded Energy Terms

The nonbonded interactions include only the van der Waals interactions.

$$E_{Nonbonded} = E_{van\ der\ Waals} \tag{6.12}$$

The van der Waals potential is represented by 12-6 Lennard-Jones potential function

$$E_{van\ der\ Waals} = \Sigma\ D_o\ [(\sigma^o/r_{ij})^{12} - 2\ (\sigma^o/r_{ij})^6] \tag{6.13}$$

where r_{ij} is the distance between atoms i and j, σ^o is the distance at maximum attraction or distance at lowest energy, and D_o is the energy at maximum attraction. The parameters, σ^o and D_o , are obtained from molecular crystals of pure compounds. The arithmetic combination rule was used for the off-diagonal van der Waals parameters for interactions between two different atomic species is given by

$$\sigma^0_{ij} = ½\ (\sigma^0_{ii} + \sigma^0_{jj}) \tag{6.14}$$

The nonbonded potential is determined from the sum of pairwise interactions including every permutation of atomic pairs. The computational requirements for such calculations scale quadratically with the number of atoms in the system. In order to reduce the number of pairwise interactions and increase the speed of the simulations, a cutoff in the interatomic distance of 9.0 Å is used in this research. Force field parameters used in this work were taken from literature reported on atactic polypropylene by Theodorou and co-workers [6.12].

6.3 Results

It was found that at end of 300 picoseconds total energy fluctuations of less than 1 % were obtained, which was used as criteria to reach equilibrium structure in this research. The resultant low energy structure was used to extract local physical properties. Results obtained from this analysis will be discussed in following sections.

6.3.1 Density Profile in Ultra-thin films

Figure 6.2 shows the mass density distribution across the film for model-1. As seen from figure 6.2, density displays a strong maximum next to the substrate. Similar results were obtained by Kumar, Theodorou and co-workers [6.2-6.5]. In the middle of film, density assumes bulk value. Near free surface there is decrease in density and this region is around one time radius of gyration of polymer. This result indicates anisotropic nature of density in ultra-thin films. Similar results were obtained for model-2, figure 6.3 shows mass density profile for 30 Å near substrate. Error bars calculated by averaging structure co-ordinates from 300 to 310 picoseconds.

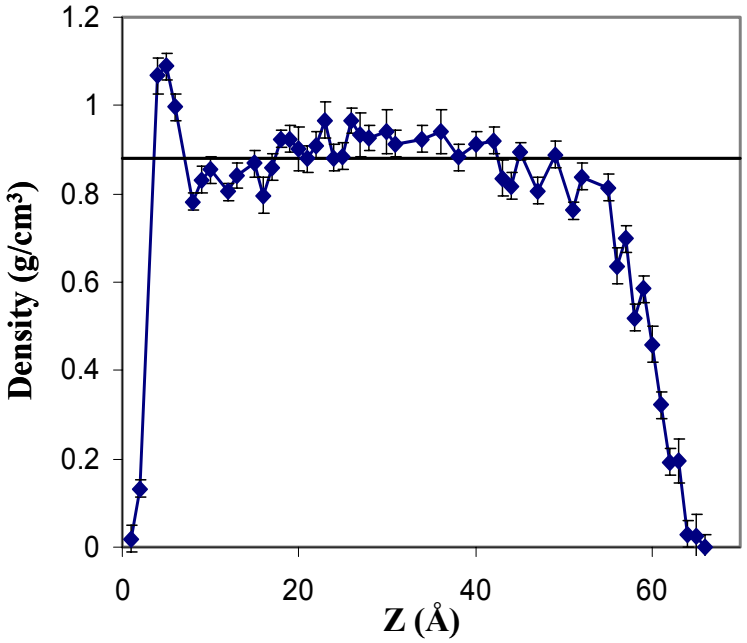

Figure 6.2 Mass density profile for Model-1 (Film Thickness 66 Å). Error bars represent 90 % confidence interval.

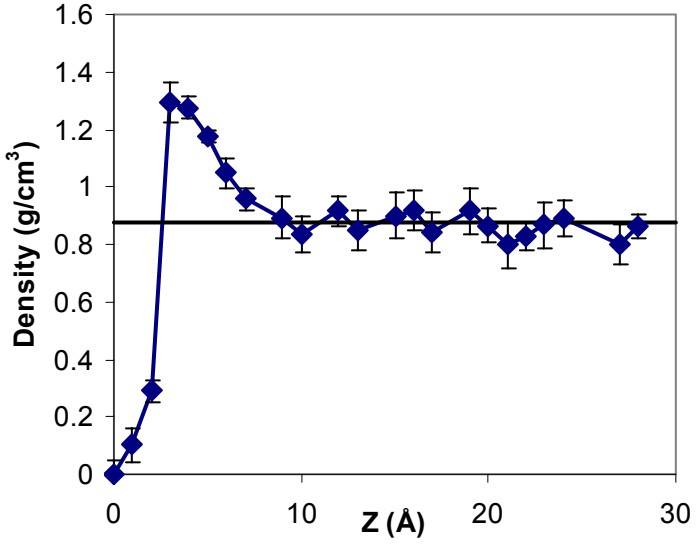

Figure 6.3 Mass density profile for 30 Angstroms near substrate for Model-2 (155 Å). Error bars represent 90 % confidence interval.

6.3.2 Local Bond order Parameter

Local orientational tendencies of C-C bond is shown in figure 6.4. A bond order parameter is defined as

$$S_B=0.5[3<\cos^2\theta>-1] \qquad (6.15)$$

in terms of the angle θ formed between a bond and the direction normal to the surface. S_B would assume a value of -0.5, 0.0, or 1.0, respectively, for bonds characterized by perfectly parallel, random, and perpendicular orientation with respect to the surface. As seen from figure 6.4, near substrate C-C bond has tendency to orient parallel to substrate, this region is around 0.5 times radius of gyration of polymer. Similar results were obtained for 155 Å thick film. In bulk region C-C skeleton bonds are random in nature. At free surface skeleton bonds have a weak tendency to lie parallel to the surface. Similar results were obtained by Kumar, Theodorou and co-workers [6.2-6.5]

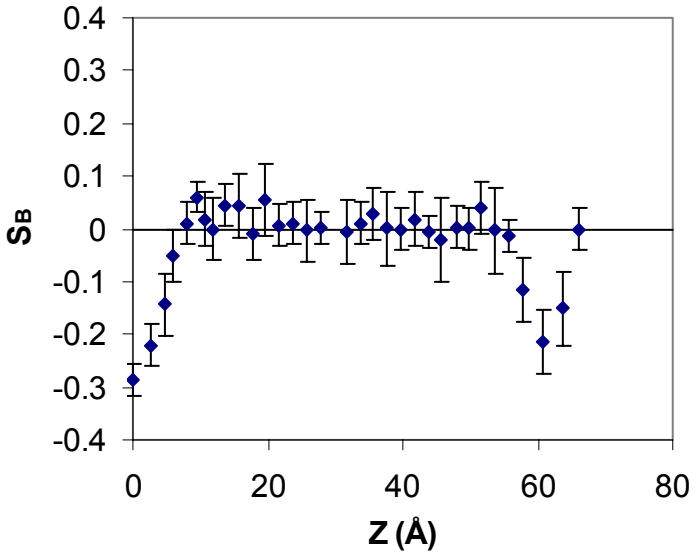

Figure 6.4 Local order parameter for C-C bond as a function of distance from substrate. Error bars represent 90 % confidence interval.

6.3.3 Mean Square Displacement

Figure 6.5 shows mean square displacements (MSD) of atoms (from 300 to 310 picoseconds) as a function of location in film. MSD value is related to amount of mobility in particular region. As seen from figure 6.5, atoms near attractive substrate have lesser value of MSD compared to the bulk value in the middle of film. Atoms in region near free surface exhibits higher value of MSD, indicating more mobility near free surface. We believe that this anisotropic nature of mobility gives rise to anisotropic thermal properties in ultra-thin polymer films. Similar results were obtained for 155 Å thick film.

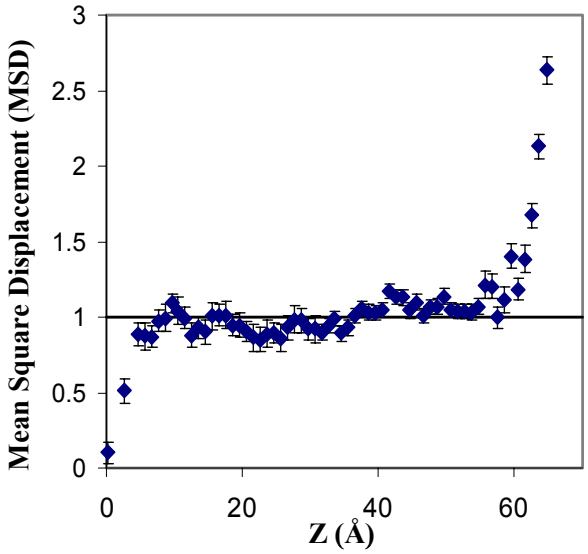

Figure 6.5 Distribution of Mean square displacement (MSD) of atoms in Model-1. Error bars represent 90 % confidence interval. Error bars calculated by averaging from 300 to 310 picoseconds.

6.3.4 CTE distribution

To avoid the delay in relaying the structure for various values of temperature, we use the fluctuations for only one temperature simulations. We took advantage of the relationship between the volume (V) - enthalpy (H) fluctuations for the NPT ensemble to α [6.7],

$$kT^2V\alpha = \langle \delta V \delta H \rangle_{NPT} \tag{6.16}$$

where k and T are Boltzmann's constant and the absolute temperature respectively. Use of equation 6.16 allows the efficient simulation to determine α value with only one equilibrium NPT simulation in the glass state. Table 6.1 shows the results of spatial and

composite coefficient of thermal expansion values in glassy state obtained for two models.

Table 6.1. Spatial α values for two Models.

	Model -1 (Film Thickness 66 Å)	Model – 2 (Film Thickness 155 Å)
$\alpha^{surface}$ (ppm/^{o}C)	648 ± 23	521 ± 16
α^{bulk} (ppm/^{o}C)	240 ± 15	234 ± 11
$\alpha^{substrate}$ (ppm/^{o}C)	138 ± 11	128 ± 13
$\alpha^{composite}$ (ppm/^{o}C)	296 ± 16	251 ± 12

It was found out that α value is strong function of Z-direction, as seen from table 1, α value close to surface is around 2.7 times higher than the bulk value and α value near substrate found to be lower than the bulk value, indicating attractive nature of substrate. Here surface region is defined as region close to free surface with thickness approximately 1 times radius of gyration, likewise the substrate region is region close to substrate with thickness around 1 times radius of gyration. Similar results were obtained for model -2. Composite α value was also determined for two models and as seen from

table 1, composite α value increases as film thickness is decreased for this polymer-substrate combination.

In addition to CTE distribution, equations (6.17) and (6.18) were used to determine distribution of heat capacity (C_p) and isothermal compressibility (β_T).

$$kT^2 C_p = \left\langle \delta H^2 \right\rangle_{NPT} \tag{6.17}$$

$$VkT\beta_T = \left\langle \delta V^2 \right\rangle_{NPT} \tag{6.18}$$

Table 6.2 shows spatial distribution of specific heat capacity for both models. It was found out that region near free surface has higher specific heat capacity compared with bulk and region near substrate has lower specific heat capacity compared with bulk. Table 6.3 shows spatial distribution of isothermal compressibility for both models. As seen from table 6.3, free surface has higher value of isothermal compressibility compared with bulk region and substrate. Isothermal compressibility in bulk and substrate region found to be approximately same in both models. Table 6.4 and 6.5 shows enthalpy - height fluctuations for two models.

Table 6.2. Spatial C_p values for two Models.

	Model -1 (Film Thickness 66 Å)	Model – 2 (Film Thickness 155 Å)
$C_p^{surface}$(J/kg/K)	33765	29636
C_p^{bulk}(J/kg/K)	12621	9744
$C_p^{Substrate}$(J/kg/K)	6690	4196

Table 6.3. Spatial β_T values for two Models.

	Model -1 (Film Thickness 66 Å)	Model – 2 (Film Thickness 155 Å)
$\beta_T^{surface}$ ($Pa^{-1)}$	$1.866x10^{-09}$	$1.735x10^{-09}$
β_T^{bulk}(Pa^{-1})	$8.54x10^{-10}$	$4.24x10^{-10}$
$\beta_T^{Substrate}$(Pa^{-1})	$9.33x10^{-10}$	$7.837x10^{-10}$

Table 6.4. Fluctuations for Model-1 (Film Thickness 66 Å) .

	$\delta H \delta h$	δH^2	δh^2
Surface	5.822×10^{-21}	2.069×10^{-19}	0.100
Bulk	7.353×10^{-21}	1.255×10^{-18}	0.113
Substrate	1.241×10^{-21}	2.91×10^{-19}	0.050

Table 6.5. Fluctuations for Model-2 (Film Thickness 155 Å) .

	$\delta H \delta h$	δH^2	δh^2
Surface	5.82×10^{-21}	1.92×10^{-19}	0.093
Bulk	7.35×10^{-21}	2.92×10^{-18}	0.182
Substrate	1.24×10^{-21}	2.29×10^{-19}	0.042

6.3.5 T_g distribution

Free volume theory is used to extract spatial T_g distribution from spatial CTE values. The Free volume theory first developed by Eyring and others [6.13], molecular motion in the bulk state depends on the presence of holes, or places where there are vacancies or void (Figure 6.6). When a molecule moves into a hole, the hole, of course, exchanges places with the molecules, as illustrated by the motion indicated in Figure 6.6. With real materials, Figure 6.6 must be imagined in three dimensions.

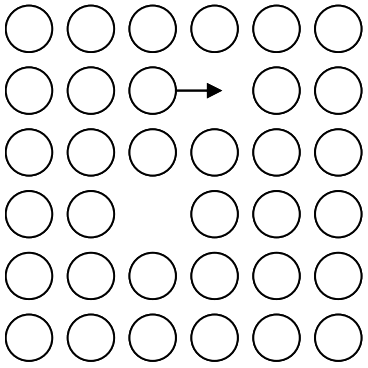

Figure 6.6 A quasicrystalline lattice exhibiting vacancies, or holes. Circles represent molecules; arrow indicates molecular motion.

Although Figure 6.6 suggests small molecules, a similar model can be constructed for the motion of polymer chains, the main difference being that more than one "hole" may be required to be in the same locality, as cooperative motions are required. Thus, for

a polymeric segment to move from its present position to an adjacent site, a critical void volume must first exist before the segment can jump.

The important point is that molecular motion cannot take place without the presence of holes. These holes, collectively, are called free volume. One of the most important considerations of the theory discussed below involves the quantitative development of the exact free-volume fraction in a polymeric system.

In 1950, Fox and Flory studied the glass transition and free volume of polystyrene as a function of molecular weight and relaxation time [6.14]. For infinite molecular weight, the found that the specific free volume, v_f, could be expressed above T_g as

$$v_f = K + (\alpha_{melt} - \alpha_{glass})\, T \tag{6.19}$$

where K was related to the free volume at 0^o K, and α_{melt} and α_{glass} represented the cubic (volume) expansion coefficients in the melt and glassy states respectively. Fox and Flory found that below T_g the same specific volume-temperature relationships help for all of the polystyrenes, independent of molecular weight. From this study, they concluded that (1) below T_g the local conformational arrangement of the polymer segments was independent of both molecular weight and temperature, and (2) the glass transition temperature was an iso-free-volume state.

Simha and Boyer [6.15] then postulated that the free volume at $T = T_g$ should be defined as

$$v - (v_{0,melt} + \alpha_{glass}T) = v_f \qquad (6.20)$$

Figure 6.7 illustrates these quantities.

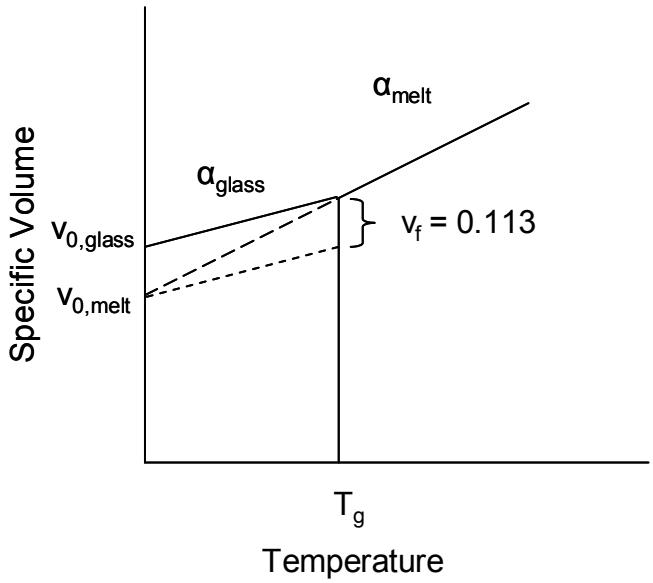

Figure 6.7 A schematic diagram illustrating free volume.

Substitution of the quantity

$$v = v_{0,melt} + \alpha_{melt}T \qquad (6.21)$$

leads to the relation

$$(\alpha_{melt} - \alpha_{glass})\, T_g = K_1 \qquad (6.22)$$

In the above, v is the specific volume, and $v_{0,glass}$ and $v_{0,melt}$ are the volumes extrapolated to 0^oK using α_{melt} and α_{glass} as the coefficients of expansion, respectively. Based on the data present in literature, Simha and Boyer concluded that

$$(\alpha_{melt} - \alpha_{glass})\, T_g = 0.113 \qquad (6.23)$$

Using data in literature they also found following relationships

$$\alpha_{melt} T_g = K_2 = 0.164 \qquad (6.24)$$

$$\alpha_{glass} T_g = K_3 = 0.051 \qquad (6.25)$$

Using Table 1 and equation (6.25), table 6.6 was generated. Table 6.6 shows T_g values obtained as a function of space. As seen from table 6.6, in surface region we obtained lower value of T_g indicating higher mobility and in region near substrate T_g is higher than bulk value indicating less mobility due to attractive nature of substrate. Table 6.6 also shows composite T_g value for two film thickness, it was found that for this polymer-substrate combination T_g decreases with decreasing film thickness. These simulations predict that surface layers for thermal property change are approximately 1 times radius of gyration, and property values are such in these layers that they can start affecting the overall thermal properties at around 10 times radius of gyration, similar to our experimental results.

Table 6.6. Spatial T_g values for two Models.

	Model -1 (Film Thickness 66 Å)	Model – 2 (Film Thickness 155 Å)
$T_g^{surface}$ (K)	78.8 ± 2.8	97.8 ± 2.9
T_g^{bulk} (K)	213.1 ± 13.4	218.3 ± 9.6
$T_g^{substrate}$ (K)	369.2 ± 26.7	397.0 ± 41.1
$T_g^{composite}$ (K)	172.3 ± 9.8	203.1 ± 9.05

6.3.6 FFV Distribution Profile

The fractional free volume of polymers can be experimentally characterized by gas permeation and positron annihilation lifetime spectroscopy (PALS) experiments; it is difficult to characterize subtle changes in free volume distributions. For this reason, molecular simulation was used to characterize the fractional free volume distribution using an accurate Delaunay Tessellation algorithm that corrects for triple overlap of adjacent atoms [6.11,6.16]. The simulations showed that the total fractional free volume

did not change while the distribution of free volume elements of the approximate size of the small molecule species used in the diffusivity measurements decreased with decreasing film thickness (see figure 6.8). In figure 6.8 and 6.9, x-axis represents the radius of circle that fits in the largest tetrahedral defined by Delaunay Tessellation algorithm. This decrease in fractional free volume available to the diffusing molecules appears to be responsible for the observed decrease in diffusion coefficient. However, the same simulations showed increased mobility near the polymer surface consistent with the observed decrease in the glass transition temperature. As seen from figure 6.9, fractional free volume distribution is same for surface and bulk region, indicating that surface layer for diffusion coefficient change is much higher than thermal property change. The spatial range over which the mobility increases is significantly smaller than the scale over which the free volume distribution changes occur. This is consistent with the experimental observations that show a decrease in diffusivity that occurs on a large scale compared to the decrease in glass transition temperature. The simulation results indicate that the observed decrease in diffusivity occurs because of a redistribution of fractional free volume that occurs over a relatively large length scale. These same simulations indicate that changes in glass transition and coefficient of thermal expansion are caused by a thin high mobility layer near the film surface that is much smaller in scale compared to that over which the free volume distribution changes. This explains why the diffusivity changes are observed at much larger film thicknesses than the changes in glass transition and coefficient of thermal expansion.

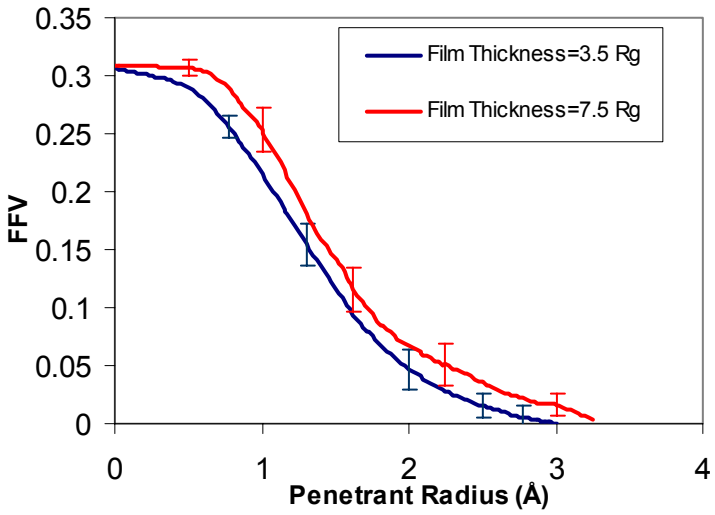

Figure 6.8 Fractional Free Volume distribution as a function of film thickness. Curves represent average from 300 to 315 picoseconds.

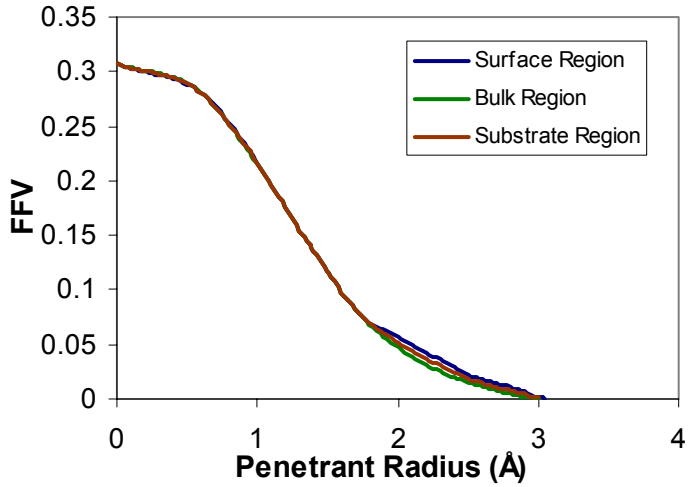

Figure 6.9 Fractional Free Volume distribution as a function of space (Z direction). Curves represent average from 300 to 310 picoseconds. (Film Thickness 3.5R_g)

6.4 Conclusions

Molecular dynamics was used to determine spatial physical properties of ultra-thin polymer films on attractive substrate. It was found out the density decreases near free surface and increases near attractive substrate. Mobility characterized by MSD value of atoms increases near free surface and decreases near attractive substrate. Coefficient of thermal expansion was simulated using novel fluctuation technique. It was observed that α was strong function of space, increases near free surface and decreases near substrate. Composite α was found to be function of film thickness and increases as film thickness is decreased for this polymer-substrate combination. Free volume theory was used to determine spatial T_g, it was found out that near free surface T_g decreases and increases near attractive substrate. Composite T_g found to be function of film thickness and decreases as film thickness is decreased. Fractional free volume distribution was characterized using an accurate Delaunay Tessellation algorithm that corrects for triple overlap of adjacent atoms. The simulations showed that the total fractional free volume did not change while the distribution of free volume elements of the approximate size of the small molecule species used in the diffusivity measurements decreased with decreasing film thickness. This decrease in fractional free volume available to the diffusing molecules appears to be responsible for the observed decrease in diffusion coefficient observed in experimental work.

6.5 References

[6.1] Forrest, J. A.; Mattsson, J. *Phys. Rev. E.*, 2000, *61*, R53.

[6.2] K. F. Mansfield and D. N. Theodorou Macromolecules 24, 6283 (1991).

[6.3] K. F. Mansfield and D. N. Theodorou Macromolecules 24, 4295 (1991).

[6.4] S. K. Kumar; M. Vacatello; D. Y. Yoon, J. Chem. Phys. 89 (8), 5206 (1988).

[6.5] S. K. Kumar; M. Vacatello; D. Y. Yoon, Macromolecules 23, 2189 (1990).

[6.6] Material Studio, Molecular Simulations, Inc., San Diego (1997)

[6.7] M. P. Allen and D. J. Tildesley. Computer Simulaions of Liquids. Clarendon Press: Oxford,(1987)

[6.8] D. Frenkel; B. Smit, Understanding Molecular simulation From Algorithms to Applications, Academic Press (1996).

[6.9] Parrinello, M.; Rahman, A. Physical Review Letters **45**, 1196 (1980).

[6.10] Nosé, S. J.; *Journal of Chemical Physics*. 81, 511 (1984).

[6.11] W. J. Chung; *Molecular Modeling of Structure-Property Relationship for Palladium Catalyzed Poly(Norbornene) and Its Derivatives* in *Chemical Engineering: PhD Dissertation*. Atlanta: Georgia Institute of Technology (2003).

[6.12] J. S. Antoniadis, C. T. Samara, D. N. Theodorou, Macromolecules (1998), 31(22), 7944-7952.

[6.13] H. Eyring, J. Chem. Phys., 4, 283 (1936).

[6.14] T. G. Fox and P. J. Flory, J. Appl. Phys., 21, 581 (1950); T. G. Fox and P. J. Flory, J. Polym. Sci., 14, 315 (1954).

[6.15] R. Simha and R. F. Boyer, J. Chem. Phys., 37, 1003 (1962).

[6.16] Tanemura, M.; Ogawa, T.; Ogita, N.; *Journal of Computational Physics.* **51**, 191 (1983).

CHAPTER 7

SUMMARY AND RECOMMENDATIONS FOR FUTURE WORK

7.1 Major Findings

The major findings in this work can be summarized as follows:

1. The critical film thickness length scale at which deviations in the glass transition temperature of polymer thin films occur relative to bulk polymer behavior is dependent on polymer molecular weight (or effectively overall polymer dimensions) and the nature of the interaction between the polymer and the substrate.

2. The apparent glass transition temperature for polymer thin films on weakly interacting substrates deviates from the bulk polymer T_g at a critical film thickness length scale on the order of 10 to 15 times the polymer radius of gyration.

3. The apparent glass transition temperature for polymer thin films on strongly interacting substrates deviates from the bulk polymer T_g at a critical film thickness length scale on the order of 5 to 10 times the polymer radius of gyration.

4. The apparent thin film glass transition temperature behavior for a particular type of polymer can be described using a single "master curve" which relates the reduced glass transition temperature (i.e. $T_g/T_{g,bulk}$) to the reduced film thickness (i.e. film thickness divided by the polymer radius of gyration).

5. The coefficient of thermal expansion for polymer thin films deviates from bulk polymer behavior at length scales that are consistent with the trends observed in the polymer film glass transition temperature.

6. The dissolution rates of polyhydroxystyrene and bis trifluoromethyl carbinol substituted polynorbornene polymer thin films was observed to deviate from bulk behavior at film thickness length scales which are significantly larger than the length scales for the observed glass transition and coefficient of thermal expansion deviations. It was found that the observed dissolution rate deviations relative to bulk dissolution behavior can be correlated to changes observed in the extent of hydrogen bonding of the hydroxyl groups in the polymer thin film as a function of film thickness. The origin of this influence of film thickness on the extent of hydrogen bonding in thin polymer films is not well understood at this time.

7. The diffusion coefficient of small molecule penetrants in polymer thin films was found to be a strong function of film thickness. The diffusion coefficient decreased rapidly with decreasing film thickness below a critical film thickness in

both polyhhydroxystyrene and polynorbornene systems which is on the order of several hundred times the polymer radius of gyration.

8. Simulations were performed for a polymer thin film on an attractive substrate. These simulations were able to qualitatively reproduce the observed glass transition and coefficient of thermal expansion behavior. Most importantly, the simulations revealed a possible explanation for the observed thin film diffusion behavior. As the film thickness is decreased for a polymer film, the simulation showed that the total amount of free volume in the polymer film does not change substantially (i.e. the density does not change), but that the distribution of free volume element sizes shifts strongly to smaller elements. This decrease in the number of larger free volume sites in the polymer film may be responsible for observed strong reduction in diffusion coefficient for small molecules in the polymer films as function of decreasing film thickness.

7.2 Summary

In this thesis, the effect of thin film and nanoscale confinement on the physical properties of polymer thin films was studied using a combination of molecular dynamics simulations and experimental characterization techniques. It was shown that the confinement of polymers into thin films influences a number of their bulk physical properties including glass transition temperature, coefficient of thermal expansion, dissolution rate, and diffusion behavior. This study supports the idea that there are

spatially dependent polymer thermophysical properties within the ultrathin film in the case of glass transition temperature and coefficient of thermal expansion, with deviations from bulk behavior occurring near the film interfaces. Further, the data suggests that the length scales over which these deviations occur in T_g and α are proportional to polymer chain dimensions as is shown in the ability to uniformly describe the thin film behavior when the film thickness is rescaled by the polymer radius of gyration. It was observed that T_g decreases for polystyrene on native silicon dioxide substrate as film thickness decreases below a critical thickness. This critical thickness is found to be approximately 10 times the radius of gyration of polymer. The T_g of PMMA films on HMDS coated silicon surfaces decrease with decreasing film thickness below a critical film thickness of approximately 13 times the radius of gyration of the polymer. The T_g of PMMA films on silicon native oxide surfaces increases with decreasing film thickness below a critical film thickness of approximately 6 times the radius of gyration of the polymer. It was found that the T_g of supported polymer thin films can be modeled using a "master" curve based on reduced thickness and reduced T_g, and a single equations have been generated that describes the dependence of T_g on molecular weight and film thickness for variety of systems.

It was observed that α increases for polystyrene films on native silicon oxide substrate as film thickness decreases below a critical thickness. This critical thickness is found to be approximately 10 times the radius of gyration of polymer. α for PMMA films on HMDS coated silicon surfaces increases with decreasing film thickness below a critical film thickness of approximately 13 times the radius of gyration of the polymer. α

for PMMA films on silicon native oxide surfaces shows depressed increase compared with PMMA on HMDS surface, indicating more attractive nature of native silicon oxide surface. It was found that α of supported polymer thin films can be modeled using a "master" curve based on reduced thickness and reduced α.

The influence of initial polymer film thickness on the dissolution behavior of three photoresist polymers, novolac, PHOST, and HFAPNB, was studied using quartz crystal microbalance methods. Effect of substrate on dissolution rate behavior was determined for PHOST films. Novolac polymers displayed a slight dependence of dissolution rate on initial film thickness. In the case of novolac, the dissolution rate was observed to decrease slightly with decreasing film thickness. In contrast, the dissolution rate of both PHOST and HFAPNB films exhibited a strong dependence on the initial film thickness of the polymer film below a critical initial film thickness. For these two polymers, the dissolution rate increased dramatically as initial film thickness was decreased below a critical thickness value that was in the range of 500 to 700 nm. Surface rate enhancement or surface acceleration of the dissolution rate was observed for both PHOST and HFAPNB as compared to the well known surface inhibition observed for novolac resins. Novolac polymers displayed a slight dependence of hydrogen bonding on initial film thickness. In contrast, the hydrogen bonding of both PHOST and HFAPNB films exhibited a strong dependence on the initial film thickness of the polymer film below a critical initial film thickness. Hydrogen bonding start decreasing as film thickness is decreased below around 600 nm. For these two polymers, the dissolution rate also increased dramatically as initial film thickness was decreased below a critical thickness value that was in the range of 500 to 700 nm. Results indicate that hydrogen

bonding can be responsible for changing dissolution rate in ultra-thin films. Behavior was found to be independent of solvent used, amount of residual solvent in films. Substrate plays important role in changing dissolution rate below film thicknesses around 100 nm. One possible implication of this phenomena though is that the lithographic performance of photoresists based on polymers such as PHOST and HFAPNB may be influenced by such thickness dependent dissolution behavior.

Vapor sorption and desorption studies using quartz crystal microbalance methods have been used to study the effect of film thickness, polymer type, substrate and polymer molecular weight on the diffusion coefficients of water, benzene,, and trifluoroacetic acid in two model photoresist polymers. It was observed that the diffusion coefficient for small molecules decreases dramatically with decreasing film thickness below a critical thickness value. A decrease in the diffusion coefficient of approximately two orders of magnitude was observed for films ranging in thickness from their critical thickness value (~260 nm for the PHOST sample, ~350 nm for the HFAPNB-1 sample, and ~550 nm for the HFAPNB-2 sample) to approximately 50 nm in thickness. Film thickness dependent diffusion behavior was found to be independent of substrate used in film thickness regime studied ($>20R_g$). One possible implication of this phenomena though is that the latent image formation of photoresists based on polymers such as PHOST and HFAPNB may be influenced by such thickness dependent diffusion behavior.

Molecular dynamics was used to determine the spatially dependent physical properties of ultra-thin polymer films on an attractive substrate. It was found that the polymer density decreases near the free surface and increases near the attractive

substrate. Polymer mobility, as characterized by the mean squared displacement (MSD) value of atoms, increases near the free surface and decreases near the attractive substrate. The coefficient of thermal expansion for the polymer was simulated using a novel fluctuation technique. It was observed that α was a strong function of spatial position within the resist film, increasing near the free surface and decreasing near the attractive substrate. The composite α for the film was found to be a function of film thickness and increases as film thickness is decreased for this polymer-substrate combination. Free volume theory was used to determine the spatially dependent local T_g. It was found that near the free surface, the local polymer T_g decreases and while the local polymer T_g increases near attractive substrate. The composite T_g for the film was found to be a function of film thickness and decreases as film thickness is decreased. The fractional free volume distribution in the polymer film was characterized using an accurate Delaunay Tessellation algorithm that corrects for triple overlap of adjacent atoms. The simulations showed that the total fractional free volume did not change as a function of polymer film thickness, but the distribution of free volume elements of the approximate size of the small molecule species used in the diffusivity measurements decreased with decreasing film thickness. This decrease in fractional free volume sites of appropriate size which are available to the diffusing molecules appears to be responsible for the observed decrease in diffusion coefficient observed in experimental work.

7.3 Recommendations for Future Work

It was observed in present work that the interaction between a polymer and a substrate plays an important role in tailoring the effective thermal properties of ultra-thin

polymer films. Currently there are few techniques available to accurately measure the interaction between polymer thin films and their substrate. Therefore, one potential avenue of future research which could help further elucidate the origins of the observed thin film behavior would be the development of new methods for measuring such polymer surface interactions. It is proposed that there are two techniques that could be developed which would be useful for this purpose, one based on high temperature contact angle measurements (i.e. high temperature goniometry) and another based on the use of AFM methods to directly measure adhesion and interaction forces. Measurements of water and other fluid contact angles on surfaces is a well established method to characterize the interaction between a fluid and a substrate. This same idea could be extended to polymers, if the polymer can be heated to its liquid or molten state and the contact angle of such a molten drop of polymer on the surface can be measured. This technique requires construction of a high temperature cell that can be used in conjunction with a conventional contact angle machine (i.e. goniometry system). This high temperature cell would be used to maintain the polymer in its liquid or molten state while the contact angle measurements are made. In a complimentary fashion, a method in which an AFM cantilever is coated with the polymer of interest and the interaction and adhesion forces between the polymer and a substrate of interest are measured would also be extremely useful. In addition to such "pulling" tests, the polymer coated tip could also be moved in a lateral mode and the frictional forces between the polymer and substrate could be measured by means of lateral deflection of the tip in a manner similar to conventional AFM lateral force microscopy. If such methods were developed, this type

of polymer-surface interaction data could be useful in formulating a more rigorous model for the observed thin film behavior.

It was mentioned in this work that the physical properties of the polymer thin films used as photoresists, such dissolution rate, diffusion coefficient, and glass transition temperature, affect the ultimate resist performance criteria such as resist resolution and contrast. In this work, essentially only pure photoresist resin films were studied. However, real photoresist systems contain numerous additional components such as photoacid generators, small molecule bases. Therefore, one natural extension of this work is to expand the present studies to include multi-component polymer films that more closely resemble real photoresist systems. In many cases, the small molecule additives used to formulate photoresist materials can act as plasticizers, and studies of such plasticized systems would be extremely relevant and interesting. Additional effects such as the possible preferential segregation of film components to one of the interfaces may significantly affect the behavior of such complex systems, and the study of such phenomena would be very useful. In a more practical and engineering sense, a different path forward would be to choose a particular set of candidate resist polymers and study the performance (i.e. resolution, contrast, image profiles, sensitivities, etc.) of these resist materials as a function of resist film thickness. By gathering experimental data on such materials as a function of film thickness through patterning experiments, and by combining this data with modern lithographic simulators, it may be possible to directly illustrate and measure the impact of thin film effects on the performance of real photoresists.

Finally this work can be extended to study other important physical properties such as the polymer film mechanical properties, since these properties are not only important for the microelectronics industry but also for variety of other applications. The mechanical modulus is an important property since it determines the ability of a polymer film or microstructure to mechanically withstand various forces to which it is subjected without deforming. Nanoindentation and AFM based techniques can be used to study the mechanical properties of polymer thin films. It should thus be possible to use these techniques to study the effect of film thickness, molecular weight, and substrate on the mechanical properties of ultra-thin polymer films.

APPENDIX

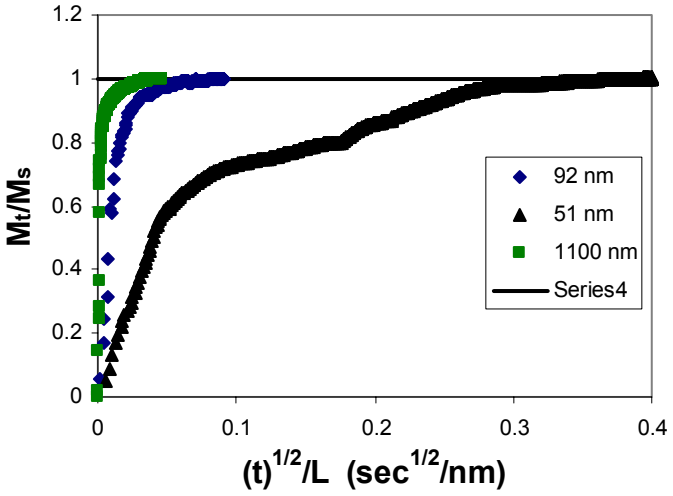

Figure A.1 Water uptake for PHOST different film thicknesses.

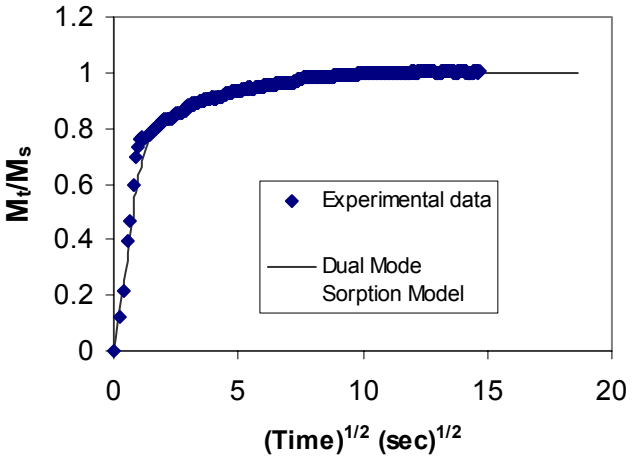

Figure A.2 Dual Mode Sorption Model fit for PHOST 125 nm thick film.

VITA

The author, Lovejeet Singh, was born on October 27, 1978 in Moradabad, India. A graduate of Wilsonia High School in Moradabad, India. Lovejeet attended University of Roorkee at Roorkee (India) from August 1996 until May of 2000 in pursuit of a B.S. in Chemical Engineering. After obtaining his bachelor's degree, Lovejeet enrolled in graduate school in August of 2000 to obtain his MS & PhD. For the last four years, Lovejeet has worked on polymer nano-characterization projects under the direction of Dr. Clifford L. Henderson & Dr. Peter J. Ludovice in the School of Chemical & Biomolecular Engineering at Georgia Tech in Atlanta, Georgia. After obtaining his PhD, Lovejeet will be joining AMD to continue his career in microelectronics as a senior production engineer.